CP VIOLATION IN A HIGH MAGNETIC FIELD

A Thesis Presented for the Degree of
Doctor of Philosophy of the University of London

by

DAVID JOSEPH ANTHONY COCKERILL

Department of Physics

Imperial College of Science and Technology

London S.W.7

August 1979

To my Mother, Father and Family

ABSTRACT

Title: CP Violation in a High Magnetic Field

Author: David J.A. Cockerill

This thesis describes an experiment which investigated the effect of a high magnetic field on $K_L^o \rightarrow \pi^+\pi^-$ decays. The decay violates CP conservation. Gauge theories with broken symmetries predict that above a certain, but hard to estimate, critical magnetic field the CP violating interaction would not operate and the above decay would not take place.

The experiment was carried out with a pulsed solenoid magnet which provided a maximum field of 250 kGauss. The K^o decays were detected with multiwire proportional chambers and drift chambers in conjunction with a spectrometer magnet. A comparison of the number of 2π decays with the pulsed field on and off revealed no evidence for the suppression of the decay by the high magnetic field. This puts the lowest value possible for the critical field at above 21 Tesla.

CONTENTS

CHAPTER I

INTRODUCTION

I.1 Theoretical Background

One of the most important developments in weak interaction theory has been that of gauge theories with spontaneously broken symmetry [1]. The four point Fermi theory of the weak interaction, together with the conserved vector current hypothesis was an incomplete and non-renormalisable theory in which higher order effects could not be calculated. Renormalising became possible by mediating the interaction with vector boson exchanges, with the techniques for making higher order calculations provided by the gauge theories. The theories, initially developed by Weinberg and Salam, also unified the weak and electromagnetic interactions, with the intermediate vector bosons $W^{\pm}$, W^{o} and the photon arising from the broken symmetry of the vacuum state and thus accounting for the experimentally observed dissimilarities between the two interactions.

The unified field theories combine two main ideas - 1) spontaneously broken symmetry, and 2) Invariance under local gauge transformations. The symmetry of the vacuum state is spontaneously broken through the Lagrangian used to describe fundamental processes which implies the existence of massless scalar bosons known as Goldstone bosons. By requiring the Lagrangian to be invariant under local gauge transformations one obtains, instead of the Goldstone bosons, the massive vector gauge mesons sought for the weak interaction.

A consequence of such a theory is the existence of a transition temperature at which the mass of the gauge boson mediating the weak interaction goes to zero with the disappearance of the corresponding asymmetry so that the weak interaction becomes long range [2,3]. The temperatures involved have been estimated at $\sim 10^{16}$ °C [3]. Salam and Strathdee have suggested that similar effects could occur in intense magnetic fields [4]. They predict that the broken symmetry giving rise to the charge asymmetry of $K_L \to \pi^{\pm} + \ell^{\pm} + \bar{\nu}(\nu)$ may disappear for fields of $\sim 8.10^{10}$ gauss and that the Cabibbo angle may be reduced to zero, leading to a suppression of certain hyperon decays, in fields of 10^{16} gauss. However the broken symmetry most easy to restore could be the CP violating interaction which gives rise to the decay $K_L^o \to \pi^+\pi^-$. The transition field needed is very hard to estimate but, on a superweak model of CP violation, fields of 10^5-10^6 gauss may be adequate.

The coupling expected between the neutral K meson and the magnetic field concerns higher order processes in the gauge theories. The situation is analogous to superconductivity where the broken symmetry or state of order is represented by the density of Cooper pairs. The Cooper pair field is charged and the magnetic field couples directly with it. For K^o fields this is not the case but the magnetic field does interact in higher order "loop graphs"[4]. For the Cooper pairs the expectation value for their density vanishes above a certain critical field. Likewise the expectation values for processes such as $K_L^o \to \pi^+\pi^-$ are expected to vanish if Salam and Strathdee are correct.

I.2 Outline of the Experiment

The Imperial College / Rutherford Laboratory experiment described in this thesis sought to test Salam and Strathdee's hypothesis concerning the restoration of CP symmetry by passing a K_L^o beam through a pulsed solenoid which produced a maximum field of 250 Kg. Fields in this region are thought to be a plausible lower limit for CP restoration. At present the highest fields produced by pulsed techniques, over reasonable volumes, have been up to 400 Kg beyond which the magnetic pressure is so great that coils quickly destroy themselves. The solenoid was originally designed to operate at this field but the requirement that the coil should have a lifetime of about 200,000 pulses meant the maximum field had to be reduced to 250 Kg. Apart from the IC/RL experiment, the highest field in which a $K_L^o \to 2\pi$ experiment has been done appears to be that of Bugadov et al. on $K_L^o \to 2\pi^o$ in the CERN heavy liquid chamber with a field of 27 Kg [5]. A fairly convincing signal was seen, though the statistics were poor. Only 15 ± 6 events were found above a background of 15 ± 3 events from $K_L^o \to 3\pi$.

Other experiments have sought to test Salam and Strathdee's hypotheses by using the intense fields generated in nuclei. Fields of up to 10^{16} gauss have been estimated from odd-even nuclei [6]. At this level the Cabibbo angle should go to zero and an experiment by E. Hagberg et al. on the superallowed decay of ^{35}Ar has reported an anomalous Cabibbo angle with $\theta_V < 0.1$ radians with a 95% confidence level [7]. The calculation of the Cabibbo angle from the experimental data is not straightforward and the result is anomalous since the Cabibbo angle is well behaved in other nuclei where similar high

fields exist. However the invariant $B^2 - E^2/c^2$ enters the theory for predicting the required field so the large values of E in nuclei make matters more confusing. The presence of the invariant also means it is not possible to effectively obtain higher magnetic fields when studying $K_L^o \to 2\pi$ by using kaons with $\gamma >> 1$.

I.3 Predicted Effect of the High Field on $K_L^o \to \pi^+\pi^-$

Above the transition field CP is no longer violated so K_1 is no longer coupled to K_2 and the decay $K_2 \to 2\pi$ is strictly forbidden. Thus a K_L entering the high field region behaves as a combination of K_2 and K_1. The small K_1 component dies away leaving almost pure K_2. On reentering the low field region, the K_2 behaves as a K_L and K_S combination giving interference effects over some two K_S^o lifetimes for $K^o \to 2\pi$ decays. The amplitude of CP = +1 in K_L^o is given by ε. Thus -

$$\left.\begin{array}{ll} K_L = K_2 + \varepsilon K_1 & K_2 = K_L - \varepsilon K_S \\ \text{and} & \\ K_S = K_1 + \varepsilon K_2 & K_1 = K_S - \varepsilon K_L \end{array}\right\} \text{ to } O(\varepsilon)$$

and $$\eta_{+-} = \frac{\langle \pi^+\pi^- | T | K_L \rangle}{\langle \pi^+\pi^- | T | K_S \rangle}$$

The high field region

State $K(t) = K_2 e^{-im_2 t} + \varepsilon K_1 e^{-im_1 t}$ where $m = M - i\Gamma/2$

Neglecting Γ_2 and dropping the phase factor $e^{-im_2 t}$ then

$$K(t) = K_2 + \varepsilon K_1 e^{i\Delta M_{21} t} e^{-\Gamma_1 t/2} \qquad (I.1)$$

giving a 2π intensity $|\varepsilon|^2 e^{-\Gamma_1 t}$ (I.2)

Beyond the high field

If the total (proper) time in the high field region is t_H then immediately beyond, using I.1, the state is -

$$K(t) = (K_L - \varepsilon K_S) + \varepsilon(K_S - \varepsilon K_L)e^{i\Delta M_{21} t_H} e^{-\Gamma_1 t_H/2}$$

$$= K_L - \varepsilon K_S R e^{i\phi}$$

where $$Re^{i\phi} = (1 - e^{i\Delta M_{21} t_H} e^{-\Gamma_1 t_H/2}) \qquad (I.3)$$

so the time developement beyond the high field is -

$$K(t) = K_L e^{-im_L t} - \varepsilon R K_S e^{-im_S t} e^{i\phi}$$

Neglecting Γ_L and removing the overall phase factor as before

$$K(t) = K_L - \varepsilon R K_S e^{i(\Delta M_{Ls} t+\phi)} e^{-\Gamma_S t/2} \qquad (I.4)$$

Therefore the 2π amplitude is

$$\eta_{+-} - \varepsilon R e^{i(\Delta M_{Ls} t+\phi)} e^{-\Gamma_S t/2} \qquad (I.5)$$

In evaluating (I.5) for the statistical analysis of the $K_L^o \to \pi^+\pi^-$ events obtained by the experiment, we assumed $\Delta M_{21} = \Delta M_{Ls} = 0.48\Gamma_S$ and $\Gamma_S = \Gamma_1$. Moreover we assumed $\eta_{+-} = \varepsilon$. Experimentally the two are consistent and equality is demanded on the superweak theory. The 2π intensity is then -

Before the high field α $|\varepsilon|^2$

In the high field α $|\varepsilon|^2 e^{-\Gamma_1 t}$

Beyond the high field α $|\varepsilon|^2 \left\{1+R^2 e^{-\Gamma_S t} - 2R\cos(\Delta M . t+\phi) . e^{-\Gamma_S t/2}\right\}$ (I.6)

These expressions are plotted in Figure I.1 with respect to the normal $K^o \to \pi^+\pi^-$ rate, assuming a high field region 100 mm. long. Most of the K_1's have died away at 1 GeV/c with interference effects persisting for up to 200mm. beyond the high field region. At higher momenta the K_1's decay more slowly though the interference effects persist for longer. The experiment observed decays over a range of about 250mm. starting at 65mm. beyond the high field region.

Using equation (I.6) we see that if the high field has an effect, the relative intensity of $K_L^o \to \pi^+\pi^-$ to the normal rate is given by

$$I(p,d) = 1 + R^2 e^{-\Gamma_s t} - 2R\cos(\Delta M.t+\phi)e^{-\Gamma_s t/2} \qquad (I.7)$$

in the downstream region, where $t = M_K d/pc$ and R and ϕ are defined in equation (I.3). Apart from the proper time, t_H, spent in the high field region, the function only depends on the momentum, p, and decay position, d, of the K^o.

PREDICTIONS FOR THE TWO PI DECAY RATE

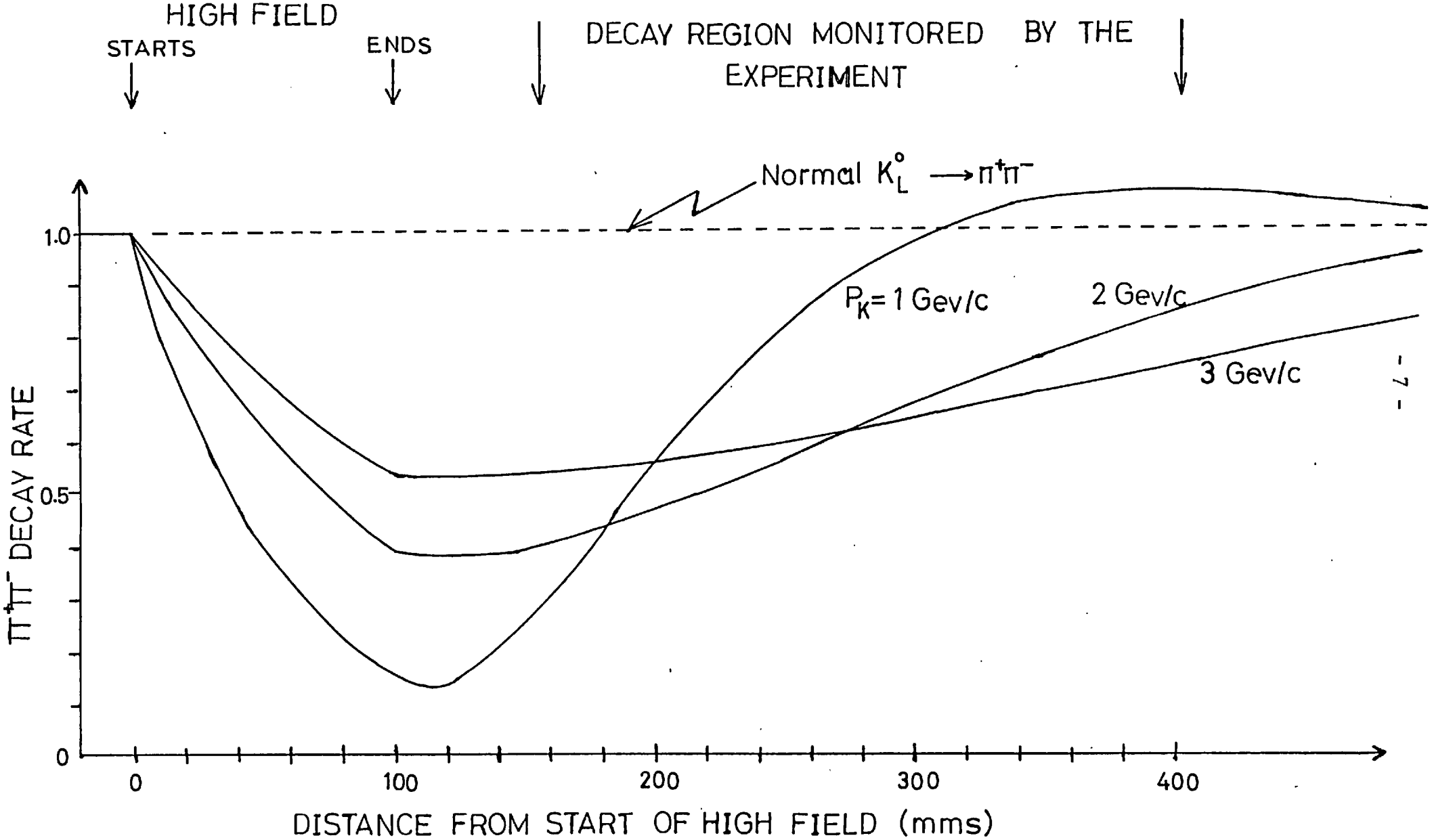

FIGURE I-1

CHAPTER II

BEAM DESIGN AND APPARATUS

II.1 Beam Line

The task of the beam line was to deliver high intensities of K_L^o while keeping the intensities of neutrons, gammas and charged particles as low as possible. The main problem was the neutron rate since it is impractical to try to physically separate K_L^o and neutrons. The only variables that could be altered to optimize the K/n ratio were the target material and the production angle of beam. Copper was chosen for the target, being considered best among the heavier elements[8]. Lighter elements such as Beryllium were considered but rejected on the grounds that, although favouring an improved K/n ratio, the absolute K_L^o flux would be low due to the small nuclear cross-section. The target was located in the extracted 7 GeV/c proton beam from Nimrod. It was 6 x 6 x 60 mm. long with its main axis along the extracted beam direction.

The production angle was chosen from estimates made by F. Atchison [9] of the intensity variation with angle for K's and neutrons. The estimates were based on the Grote-Hagedorn-Ranft thermodynamic model, using measurements at Nimrod for p and K^+ production at 0^o [8]. The thermodynamic model was normalised to these measurements and assumed n=p and $K_L^o = \frac{1}{2}K^+$. The estimates showed that the neutron flux falls very rapidly with increasing production angle while the K's fall relatively slowly (see Fig. II.1). The angle for the optimum K_L^o/neutron ratio was found to lie between 10^o and 15^o.

The beam line was constructed at 16^{o} since it was restricted on the small angle side by the X3X beam line magnets.

The beam line is shown in Fig. II.2. Collimator C1, 2 feet long with an aperture 12mm. high x 18mm. wide, removed most of the extraneous beam from the target. Charged particles were removed by the sweeping magnet M102 immediately downstream of C1. Gammas were removed by pair conversion in the lead absorber behind M102. The beam was then collimated and defined by two 6 ft. long collimators C2 and C3. Charged particles produced by neutrons hitting the collimator walls and electrons and positrons produced in the lead absorber were removed by the sweeping magnet M905 and collimator C4. The diameter of C4 (50mm.) was made greater than that of the collimated beam to avoid any further neutron interactions since charged particles produced at C4 could produce spurious tracks in the spectrometer. The two variable horizontal collimators V1 and V2 were used for beam studies. M102 and M905 were vertically deflecting sweeping magnets due to the smaller vertical dimensions of the target and the small vertical acceptance of the detecting apparatus.

After passing through C4 the beam passed through the bore of the solenoid to the K^{o} decay region, 15.5 metres from the target [10]. This lay between the solenoid and the multiwire proportional chambers in the spectrometer (see section II.3). The decays were detected and analysed by the spectrometer and associated counters. The beam traversed the spectrometer system and was dumped at the beam stop. The beam flux was measured by a special beam monitor in front of the beam stop (see section II.5).

The design of C2 and C3 was very important since any stray neutrons hitting the solenoid would have caused background problems.

Thus the neutral beam had to lie clearly within the 50mm. diameter of the solenoid bore. In fact we chose to collimate to an effective diameter of ~44mm. at the solenoid (34mm. F.W.h.m.) with a sharp radial cutoff. Fig. II.3 shows the beam profile obtained from analysis of events in slow (0.5 sec) spill. The majority of events were K_L^o leptonic decays. One can see that the beam drops quickly beyond a radius of 20mm. In fact less than 0.3% of the beam was estimated to pass outside the solenoid bore. A Monte Carlo program simulating the absorption and scattering of neutrons was used to design the collimation. The eventual design predicted less than 0.2% of the beam outside the bore radius. The solid angle accepted by the beam line was $6.7 \cdot 10^{-6}$sr and the angular divergence ± 1.3 mrad. The small solid angle greatly reduced the K_L^o flux though the removal of unwanted secondaries was made easier with gammas and neutrons generated in the lead absorber having a smaller probability of staying in the beam.

Both C2 and C3 consisted of a steel tube 75mm. in diameter and 6ft. long filled with appropriately predrilled 6" long steel cylinders of varying internal diameter so that the aperture tapered towards the target. Each tube was set in a concrete block which was carefully positioned in the shielding wall. The alignment of the tube was done with the aid of a telescope positioned behind the spectrometer magnet with which one could look along the whole beam line to the target. The collimators were positioned to within 0.25mm.

During data taking about 10^{12} protons per burst were incident on the target and the K^+ measurements discussed in the next section showed that this gave about 3000 K_L^o at the solenoid with 80mm. of lead absorber in the beam line. Using the C^{11} technique, the radiation group at Nimrod measured an absolute flux of 400,000 neutrons with energy greater than 20 MeV for the same incident beam intensity.

II.2 Measurements of K^+ Intensity

The K_L^o flux at the solenoid was estimated by measuring the K^+ spectrum in the beam. This part of the experiment was done using the short beam line with the spectrometer 10.5 metres from the target [10]. Fig. II.4 shows the experimental setup from C2. The equipment in front of C2 was as in Fig. II.2. C2 collimated the beam to about 40mm. at the spectrometer. Sweeping magnets M102 and M905 were turned off. Collimator C3 was not required but remained in the beam line.

The charged beam was detected by scintillators B1 and B2. They defined a beam with small angular divergence entering the spectrometer. B1 covered the whole beam, while B2 was a narrow finger counter. Particles deflected through 8^o by M108 were detected by B4 and B5. The momentum and momentum acceptance were calculated from the $\int B.dl$ for M108. The momentum accepted was changed by changing the current through the spectrometer.

The K^+ signal was extracted from the π^+ and protons in the beam by using the time of flight from B1 to B5. The calculated time of flight for π^+, K^+ and protons is shown in Fig. II.5 at various momenta over the 6.3 metre flight path. The plot shows that good timing resolution was crucial to separate the K^+ particularly at higher momenta where the separation between K's and protons was under 2nsecs. The timing resolution was limited by the electronics and the momentum range accepted by B4 and B5. Since this was not good enough to separate pions at higher momenta a Cerenkov counter was installed to veto the π^+ signal. The Cerenkov was filled with

Freon 13 at 185 p.s.i.g. This provided a refractive index of 1.012 giving a threshold for Č radiation of 0.9 GeV/c for π^+ and 3.2 GeV/c for K^+. Figures II.6 and II.7 show the π, K, p signals obtained at 1.0 and 2.0 GeV/c. At 2 GeV/c the f.w.h.m. for the proton peak was ∿0.6 nsecs.

To reduce the beam intensity to an acceptable value, the time of flight spectra were measured with 40mm. of lead absorber in the beam and with collimator V1 set to a gap of 5mm. Without these measures, the T.O.F. resolution was degraded due to photomultiplier droop. The ratio of K^+/protons was found at various momentum settings. The ratio was then multiplied by the absolute proton yield, determined by B1.B4 coincidences with the lead removed and V1 fully open, to give the absolute kaon yield. B4 had a momentum acceptance range of $\Delta p/p = \Delta\theta/\theta = 0.21$. Using this the kaon yield was normalised to bins of 200 MeV/c.

Corrections were made to the K^+/p ratio measurements due to coulomb scatter in the lead absorber. The scatter goes as $1/\beta p$, thus favouring kaons. The attenuation goes as the square so a correcting factor of β_p^2/β_K^2 was applied.

The K_L^o flux is given by

$$N_{K_L^o}(x_2) = \frac{A}{2} N_{K^+}(x_1) \exp\left(\frac{x_1}{\lambda_1} - \frac{x_2}{\lambda_2}\right) \quad ;$$

$$\lambda_1 = \frac{P}{M_{K^+}} \tau_{K^+} C, \quad \lambda_2 = \frac{P}{M_{K^o}} \tau_{K_L^o} C$$

where x_1 is the distance from the target to B5, 17.2m.

x_2 is the target to solenoid distance, 15.5m

A is the correction for solid angle acceptance for the 15.5 metre beam line

The rate of K_L^o production at the target was assumed to be $\frac{1}{2}K^+$. Fig. II.8 shows the expected K_L^o spectrum and the spectrum for 80mm. of lead absorber in the beam (the amount used during data taking). Losses for K^+, protons and K_L^o in the lead absorber due to the strong interaction were calculated using the same nuclear collision length (9.8cm.) throughout. In fact the nucleon cross-sections are slightly different but this affects the net results by less than ~15%. The spectra are for 10^{12} protons on the 60mm. Cu target (roughly the data taking rate). About 3000 K_L^o, with 80mm. Pb absorber in the beam, were expected at the solenoid and spectrometer per burst.

II.3 The Spectrometer System

The spectrometer system was built to detect $K^o \to \pi^+\pi^-$ decays in the interference region beyond the solenoid. The interference effects depend on K^o momenta and at 1 GeV/c extend for 200mm. and at 2,GeV/c for 400mm. beyond the end of the high field (see Fig. I.1). The most important decays are those occuring over the first 150mm. after the end of the high field, where the interference effects are strongest. These decays are lost if detection starts too far downstream, due to the geometric constraints of the spectrometer. Therefore only the first 315mm. of the interference region were chosen for study. The fringe field from the solenoid prevented study over the first 65mm. (see section III.3), leaving a decay region 250mm. long that was monitored by the experiment.

Fig. II.9 shows an outline drawing of the solenoid and $\pi^+\pi^-$ detection system. A simple compact design was chosen for the spectrometer by using a Rutherford Laboratory type 1 bending magnet, M108, which provided a field of 10.5 kgauss across a pole face gap of 10". The $\int B.dl$ was sufficient to bring the π's together again just beyond the magnet.

The 250mm. long decay region was immediately followed by three multiwire proportional chambers (MWPC's), M1, M2 and M3, and two trigger counters A1 and A2. Just forward of the magnet centre were two drift chambers DC1 and DC2. Six further drift chambers DC3-DC8 were placed beyond the magnet. DC8 was followed by a further set of trigger scintillation counters referred to as the 'T' counters. A detailed description of the detectors is given in the next section. To reduce neutron interactions, helium bags were placed between the MWPC's and DC1/2 and between DC1/2 and DC3. To reduce material in the decay region, a helium bag of 0.5 thou mylar was especially constructed to fit into the conical opening of the solenoid. Material in the chambers was kept to a minimum.

The geometrical efficiency of the spectrometer depended on the K_L^o momentum spectrum. The Grote-Hagedorn-Ranft simulation used in section II.1 predicted a K_L^o spectrum centred around 2 GeV/c (see Fig.II.8). With this in mind the experiment was initially built with the wire chambers in front of the spectrometer and DC1/2 at the centre of the magnet. However the K^+ measurements showed that most K_L^o had a momentum around 1 GeV/c. These tend to produce pions from $K_L^o \to 2\pi$ decay at about 20^o to the beam axis in the horizontal plane giving a displacement twice that for pions from 2 GeV/c K^o decays. Due to the limitations imposed by the width of the M108 pole faces, they would have failed to traverse the spectrometer, the situation getting more serious with a

long decay region between the solenoid and MWPC's. To reduce such losses the MWPC's were installed between the windings of M108 to be nearer the pole faces, DC1/2 were brought forward from magnet centre and the decay region kept to 250mm. The vertical acceptance was also improved by these alterations.

A Monte Carlo simulation of the design showed that the geometrical efficiency rose approximately linearly from 4.5% at 1 GeV/c to 18% at 3 GeV/c (see Fig. II.10). However conditions imposed by the trigger counters (see section II.6) reduced the overall efficiency to 2.8% at 1 GeV/c and to 7.5% at 3 GeV/c and this is also shown in Fig. II.10.

The resolution of the spectrometer was investigated using a Monte Carlo program. This assumed chamber resolutions of 0.5mm (std. dev.). The predicted mass resolution varied from 6.0 MeV/c^2 at 1 GeV/c to 10.0 MeV/c^2 at 3 GeV/c and the transverse momentum in the horizontal plane (P_x) from 3.5 to 7.0 MeV/c (all f.w.h.m.). The Monte Carlo predicted accuracy in decay vertex reconstruction was ±2mm. at 1 GeV/c and ±5mm. at 3 GeV/c. A good feature of the design, for the type of events selected, was that errors of π momentum and direction tend to compensate.

Almost all the 2π decays from the Monte Carlo lay within a mass range of 496 ± 8 MeV/c^2 and had a transverse momentum within 7 MeV/c of the true K^o direction. These cuts were important in reducing the background from leptonic decays. Assuming both tracks in the spectrometer to be pions, the $K_L^o \to 3\pi$ decays were entirely rejected by the mass cuts. The predicted leptonic background from $K \to \pi e \nu$ and $K \to \pi \mu \nu$ was about 12% at 1.5 GeV/c for cuts of ±6 MeV/c for horizontal (P_x) and ±8 MeV/c for vertical (P_y) transverse momentum. These were the cuts used in the analysis of the data.

The cuts in P_x and P_y were different due to the poorer resolution in the vertical.

A field map of one of the spectrometer quadrants was taken using a Hall probe scanning device, to provide data for the momentum fitting in the analysis program. An N.M.R. probe and a Hall probe were installed to monitor the field during data taking. The field was maintained to an accuracy of 0.05% throughout the experiment.

II.4 Detectors

a) MWPC's

The three MWPC planes M1, M2 and M3 were mounted as a unit to help reduce material in the beam, and were operated with a magic gas mixture of 33% Isobutane, 33% of a mixture of 99.2% Argon plus 0.8% Freon, and 33% Argon bubbled through Methylal at 0^{o}C. An exploded view of the unit is shown in Fig. II.11. M1 and M2 were built with 192 sense wires, angled at $\pm 12.3^{o}$ to the vertical, with a wire to wire separation of 1.954mm. (2mm. along the horizontal). The combined data from M1 and M2 provided both horizontal and vertical track information. Horizontal resolution was about 0.8mm. (std. dev.), and vertical resolution about 4.0mm. Angling the wire planes overcame the ambiguity of associating tracks in the horizontal plane with those in the vertical, and also helped to reduce incorrect track fitting. M3 consisted of 48 horizontal sense wires with 2mm. spacing providing vertical information with a resolution of ±0.8mm. (std. dev.). The cathode planes were of 0.5 thou. aluminium foil with common cathodes shared by M1/2 and M2/3. The assembly was made gas tight using 'O' rings and by the outer windows of 1.0 thou mylar.

The sense wire outputs were fed to passive 'mother boards' which connected the wires to 'hybrids' for preamplification and discrimination. Only the centre 160 wires from M1 and M2 were read out due to the low acceptance for 2π decays in the outer wires. This reduced the accidentals counting rate which in turn reduced the read in time required by the fast memory buffer (see section IV.1). The 50nsec. MECL pulses from the hybrids were fed along 20 metres of twisted pair cable to the multiplexers in the control room. The multiplexer provided prompt 'OR' outputs from M1 and M2 for the hardware trigger. Individual sense wire pulses from the MWPC's were delayed by the multiplexer and then gated with the event trigger. These gated channels were then scanned and wire "hits" fed to the fast memory buffer.

The MWPC unit was mounted on support bars which ran along the inner sides of the spectrometer. Plate 2.1 shows the MWPC in position together with the mother board assembly mounted on the side of M108. The unit was centred on the beam axis to within 0.25mm. in both the horizontal and vertical. During data taking the MWPC unit, sense wire outputs, mother board assembly and cables to the control room were wrapped in foil to prevent r.f. pickup from the solenoid.

b) Drift Chambers

There were two groups of chambers - DC1/2 inside the spectrometer magnet and DC3-DC8 just beyond the magnet (see Fig. II.9). The chambers were built using 'graded cathode' drift cells [11] with a field wire to field wire spacing of 48mm. (see Fig. II.12(a)) and were operated with a gas mixture of 25% Isobutane, 37.5% Argon and 37.5% Argon bubbled through Methylal at $0^{\circ}C$. The drift velocity in

each chamber was found by measuring its space-time relationship with a well-defined charged beam. The drift velocity was about 19nsecs/mm. in all chambers with position resolution to within 0.5mm.

DC1 and DC2 each contained 12 cells which measured horizontal position (vertical field and sense wires) over an active area of 576 x 100mm. Since these chambers were working in the magnetic field of M108, the cells were modified to compensate for the Lorentz force acting on the drift electrons. This was done by displacing the graded H.T. cathode planes to provide tilted electric field equipotentials as shown in Fig. II.12(b). To remove the left-right cell ambiguities in track fitting, DC2 was displaced with respect to DC1 by the drift length (24mm.).

Beyond the spectrometer DC3, 5 and 7 were used to measure horizontal position. The chambers were built with 12 cells but only the centre 8 from each were read out due to the low probability of pion tracks in the outer cells. This helped to reduce the accidental count rate and thus the digitiser load. The active area of these chambers was thus reduced from 576 x 250mm. to 384 x 250mm. Pion tracks were found by straight line fitting through DC3, 5 and 7.

DC4 and DC6 measured vertical position (field and sense wires horizontal). They were each made with 7 cells giving an active area of about 600 x 336mm. Tracks in the vertical plane were found by straight line fitting between DC4 and 6 and the MWPC's. DC8 was made with 8 cells and installed with its wires at an angle of 1 in 8 to the horizontal to solve the ambiguity of associating tracks in the horizontal and vertical planes. It was not used in the momentum fitting. The sense wire outputs from the chambers were fed to preamplification and discrimination circuits. The circuits gave 20nsec. balanced MECL pulses which were fed to the digitisers and

fast memory buffer in the control room.

Plate 2.2 shows DC3-DC7 behind the spectrometer (DC8 and the T counters removed) with DC1/2 just visible between the pole faces of M108. DC3-DC7 were mounted on guide rails and were dowelled into position by two brass pins. DC1/2 was mounted on the support bars in M108 and DC8 was suspended behind DC7 from the guide rail assembly. DC1-DC7 were positioned to within 0.2mm. in the horizontal and vertical. DC8 was positioned to within 0.4mm. During data taking DC3-DC8 were surrounded by an enclosure of aluminium foil to prevent r.f. pickup from the solenoid.

c)Scintillators

A1 and A2 were installed to provide a clean 5nsecs. trigger pulse from either one or both pion tracks at the upstream end of the apparatus. The counters were 160mm. long by 100mm. high and made 1mm. thick to minimize multiple scattering. To avoid high counting rates from neutron interactions, A1 and A2 were positioned so that there was a gap between them of 48mm. symmetric about the beam axis.

T1-T4 were made to trigger on the vertical track separation of the pions at the downstream end of the apparatus. The T counter plane is shown in Fig. II.13. Two out of the four counters were required by the hardware trigger. T2 and T3 were built to trigger on pions near the beam region after traversing M108. This region is important because K^o triggers are lost if either pion passes through the beam cutout. Monte Carlo studies showed that at the T counter plane, one of the π's was almost always within 60mm. and usually within 30mm. of the beam region at all P_K. Pions from

$K^o \to 2\pi$ decay are focussed by M108 and cross over near the beam axis. The crossover point along the beam axis depends on P_K and the K^o decay position. Care was taken to place the T counter plane away from the crossover region for P_K between 1-2 GeV/c. At 1 GeV/c the trigger losses from pions passing through the cutout were about 8% rising to 16% at 3 GeV/c. To reduce the counting rate from neutron conversions T2 and T3 were made from ½mm. thick scintillator.

II.5 Beam Monitoring

The beam intensity was monitored by measuring the rate of charged particles leaving a perspex converter placed just before the beam stop (see Fig. II.2). The charged particles were detected using two scintillators, N1 and N2, in coincidence. Care was taken to avoid accidentals between the counters in fast spill by keeping their singles rates low. The intensity was required as a function of solenoid magnetic field and therefore of time. To do this the beam intensity was monitored in 70 μsec intervals during the burst using the "bacon slicers" (see section IV.1). During summer data taking 1977 (runs 130-175) the N1N2 rate was about 60/b while for the Nov/Dec '77 data taking the rate was about 40/b (runs 176-297). A target monitor TMON based on the detection of charged particles at large angles from the target, was used during beam studies with slow spill. Its high coincidence rate made it impracticable for use during fast spill.

II.6 Hardware Trigger

The hardware trigger was required to be highly selective to K_L^o decay so that triggers from neutron interactions in the beam

should be as few as possible. A typical $K^o \to \pi^+\pi^-$ decay leads to a horizontal separation of the two tracks at the upstream end of the apparatus and a vertical separation downstream. To trigger on the horizontal separation, M1 and M2 were divided into three regions with the centre 'C' region for the beam composed of a prompt 'OR' from the middle 16 wires (32mm.) with the left and right regions on either side of 72 wires (144mm.). This is shown in Fig. II.14. The trigger required counts from two out of the three regions and a count from either A1 or A2. By requiring two charged particles at M1/2, with one outside the beam region, the triggers from neutron interactions were substantially reduced. The downstream T counter trigger required any two T counters to fire (see section II.4c).

A Monte Carlo program was run to find the overall efficiency for detecting K^o decays applying the hardware trigger conditions above. This is shown at various momenta in Fig. II.10, together with a plot of the geometric efficiency for the spectrometer and detectors. The efficiency with the trigger drops at higher momenta for two reasons. Firstly the opening angle of pions from K^o decays becomes smaller and both pions start to pass through the centre region of M1 and M2, and secondly the T counter losses mentioned in Section II.4c become more significant.

The trigger logic was formed with "NIM" electronics and is shown in Fig. II.15. Updating discriminators were used for pulses from the T and A counters to avoid losing good counts due to discriminator dead time from accidental counts coming just before genuine triggers. In the MWPC logic the linear coincidence outputs were used for the same reason. Because of the good timing resolution between the T and A counters the T.A trigger was formed first. This was then gated with the MWPC logic to provide the total trigger :-

M1 (2 out of 3) . M2 (2 out of 3) . (A1 + A2) . T (2 out of 4)
The trigger rate in fast spill was about 0.25/burst.

II.7 Beam Studies

To prepare the experiment for work in 0.3msec. fast spill, the composition of the neutral beam was examined using the slow 0.5 second spill from Nimrod. The spill was used to find the optimum length of lead absorber for the removal of slow neutrons and gammas and to estimate accidental counting rates in fast spill.

The composition of the neutral beam was found by measuring singles counting rates in M1 and M2. These rates should be mainly due to neutron conversions, in the material before the MWPC wire planes, and from charged particles from K^0 leptonic decays. By placing perspex sheets of different thickness before the wire chambers, the counting rate from neutron conversions was found per interaction length of material in the beam. Multiplying this by the amount of material estimated to be normally in front of M1 and M2 then gave the contribution from neutron conversions to the total count rate. This came to about 35-40%. Monte Carlo studies on the singles counts from leptonic decays accounted for a further 40-50%. The remaining 10-20% of the counts were unaccounted for and suggested that soft radiation, from slow neutrons or low energy gammas, was getting through the 60mm. of lead absorber used for the above study.

Counting rates in M1 and M2 were then measured with 80 and 100mm. of lead absorber. In particular, high multiplicity events (more than 7 wires) were monitored, since these were suspected to come mainly from the soft radiation. In going from 60 to 80mm. of

lead absorber, the high multiplicity event rate was attenuated by 0.55, and from 80 to 100mm. by 0.75. These results correspond to attenuation lengths in lead for the radiation producing these events, of 34cm. and 70cm. respectively. If the radiation was genuinely part of the high energy beam, with neutrons and kaons above ∿500 MeV/c, then the attenuation length in lead should be 98cm. (taken from the Particle Properties Data Booklet). This suggested that the radiation was mainly composed of low energy neutrons which have large nuclear interaction cross-sections and consequently shorter attenuation lengths.

Soft radiation in the beam contributes to higher counting rates in the chambers and higher accidental rates in fast spill. In view of the attenuation of such radiation in going from 60 to 80mm. of lead absorber, it was decided to run the experiment with 80mm. of lead in the beam. Running with 100mm. of lead would have caused an unacceptable attenuation in the K^o flux despite further attenuation of the soft radiation. Work with 100mm. of lead and perspex sheets showed that most of the remaining high multiplicity events were not from slow neutrons or gammas but came from the high energy beam.

The high multiplicity events helped to explain why the prompt 'OR' signals from M1 and M2 varied in pulse length from 50→200nsecs. A neutron conversion would be expected to lead to one or more large angle tracks and these would trigger several wires before leaving the wire chamber. The different drift distances from the track ionisation to the sense wires would then broaden the prompt 'OR' signal.

In fast spill the width of pulses used in coincidence is important since accidental coincidences go as $\frac{\tau . R_1 . R_2}{t}$ where τ is the sum of the two pulse lengths used in coincidence, R1 and R2 are the individual rates in slow spill, and t is the duration of fast spill (300 μsecs.). Initially, it was hoped to form a trigger for K decays using only the MWPC's at the upstream end and the T counter plane downstream. However the accidental rate would have been above 95% of the triggers taken. To reduce this accidental trigger rate, the A counters were installed behind the MWPC's. These provided clean 5 nsec. pulses, giving a value for τ of 10 nsecs. between the T and A counters as opposed to about 100 nsecs. had the T and MWPC counters been used together. This reduced the accidental trigger rate to about 50% of the total. A strong R.F. structure in the spill from Nimrod would have increased the accidentals rate, but studies of the beam spill showed that the structure was not serious.

In fast spill, the singles rate in M1 and M2 was about 600/burst. An accidental wire from each chamber was therefore expected in 10-15% of the events due to the 56 nsec. event gate used to read in the wire information at the multiplexer for the fast memory buffer. These accidental wires could lead to ambiguities, for example a 2π event being fitted with the wrong pair of wires thus giving an incorrect vertex. However the angling of the wire planes in M1 and M2 allowed a vertical reconstruction which could then be compared to data in M3. Using this information most accidental reconstructions were expected to be eliminated.

The accidental rate in the drift chambers suffered from neutron interactions in the material upstream and from the maximum memory time of each cell which was 480 nsecs. This was investigated by placing a 500 nsec. delay between the event trigger and drift chamber digitiser readout to obtain purely accidental digitizings. These were then displayed using a graphics routine which showed that in general the background looked manageable.

From the data taken in summer 1977, the drift chambers were found to be missing track data due to inefficiency. This was due to space charge effects around the anode wires from the high beam rates. Some of the cells were certainly operating at a rate of around 10^4 counts/sec/mm. of anode wire at which point Breskin et al. have found a fall in cell efficiency [11]. Therefore the Nov/Dec data taking was done with 30% lower beam intensity.

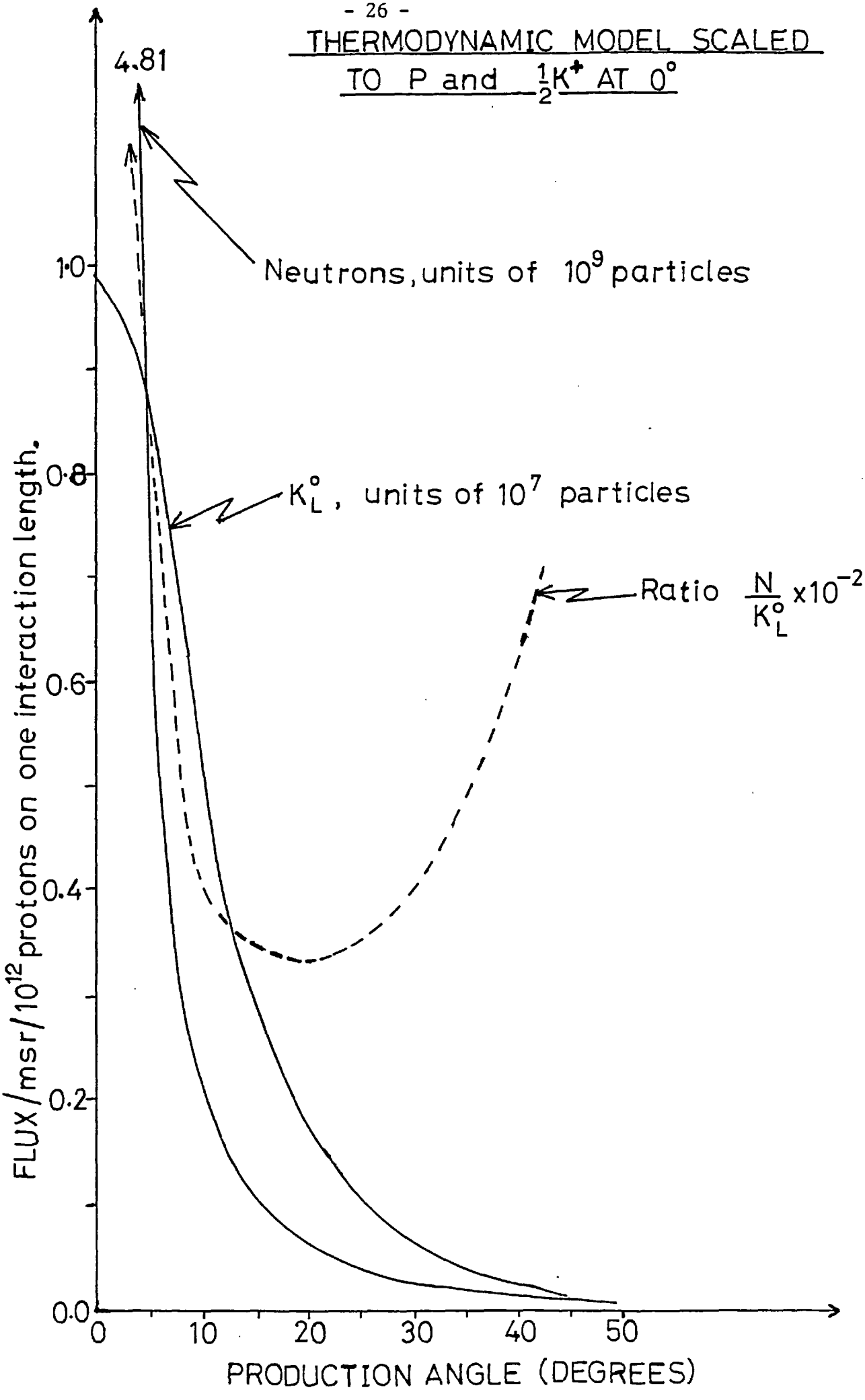
THERMODYNAMIC MODEL SCALED
TO P and $\frac{1}{2}K^+$ AT 0°
4.81
Neutrons, units of 10^9 particles
K_L^o, units of 10^7 particles
Ratio $\frac{N}{K_L^o} \times 10^{-2}$
FLUX/msr/10^{12} protons on one interaction length.
1·0
0·8
0·6
0·4
0·2
0·0
0
10
20
30
40
50
PRODUCTION ANGLE (DEGREES)

FIGURE II.1

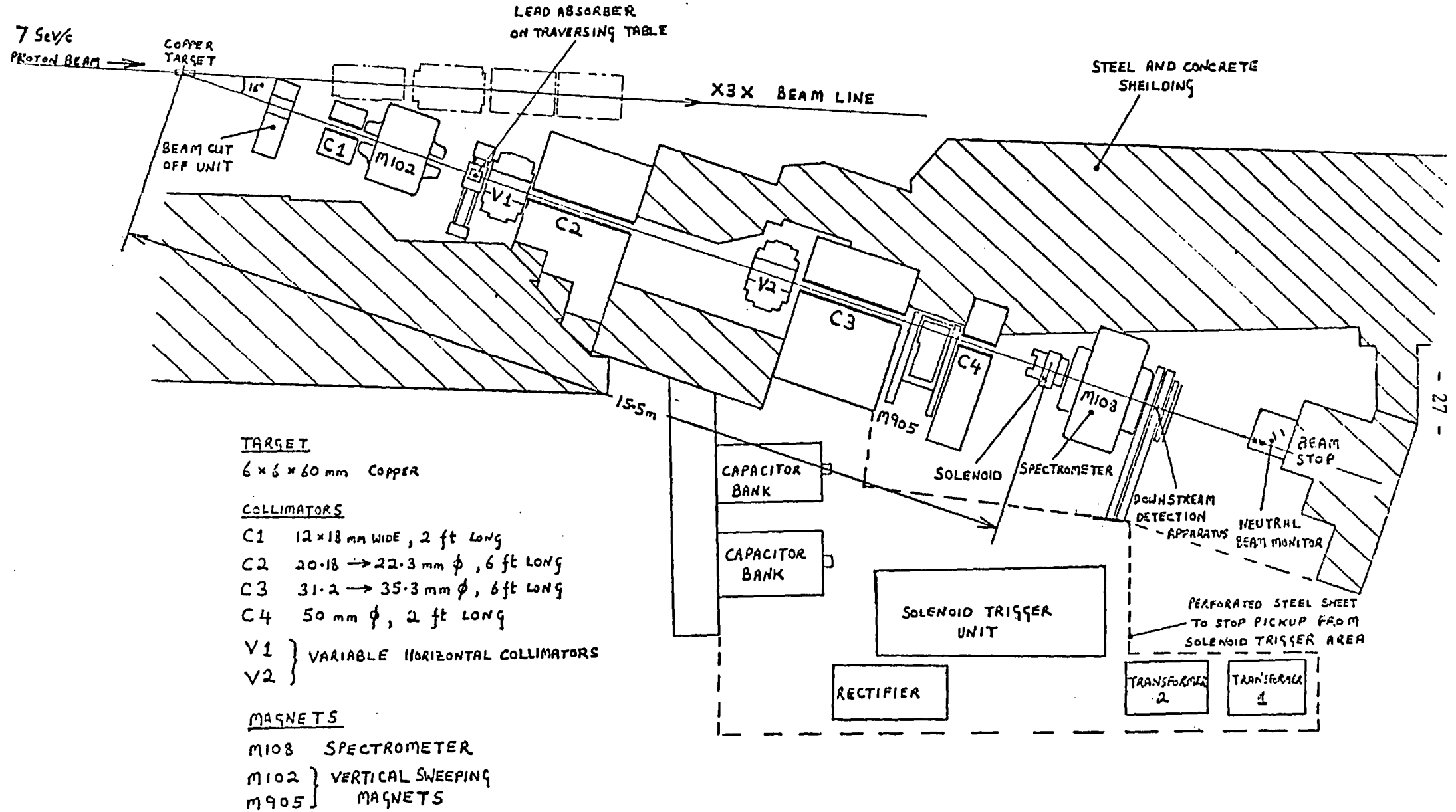

FIGURE II.2 : N5 BEAM LINE

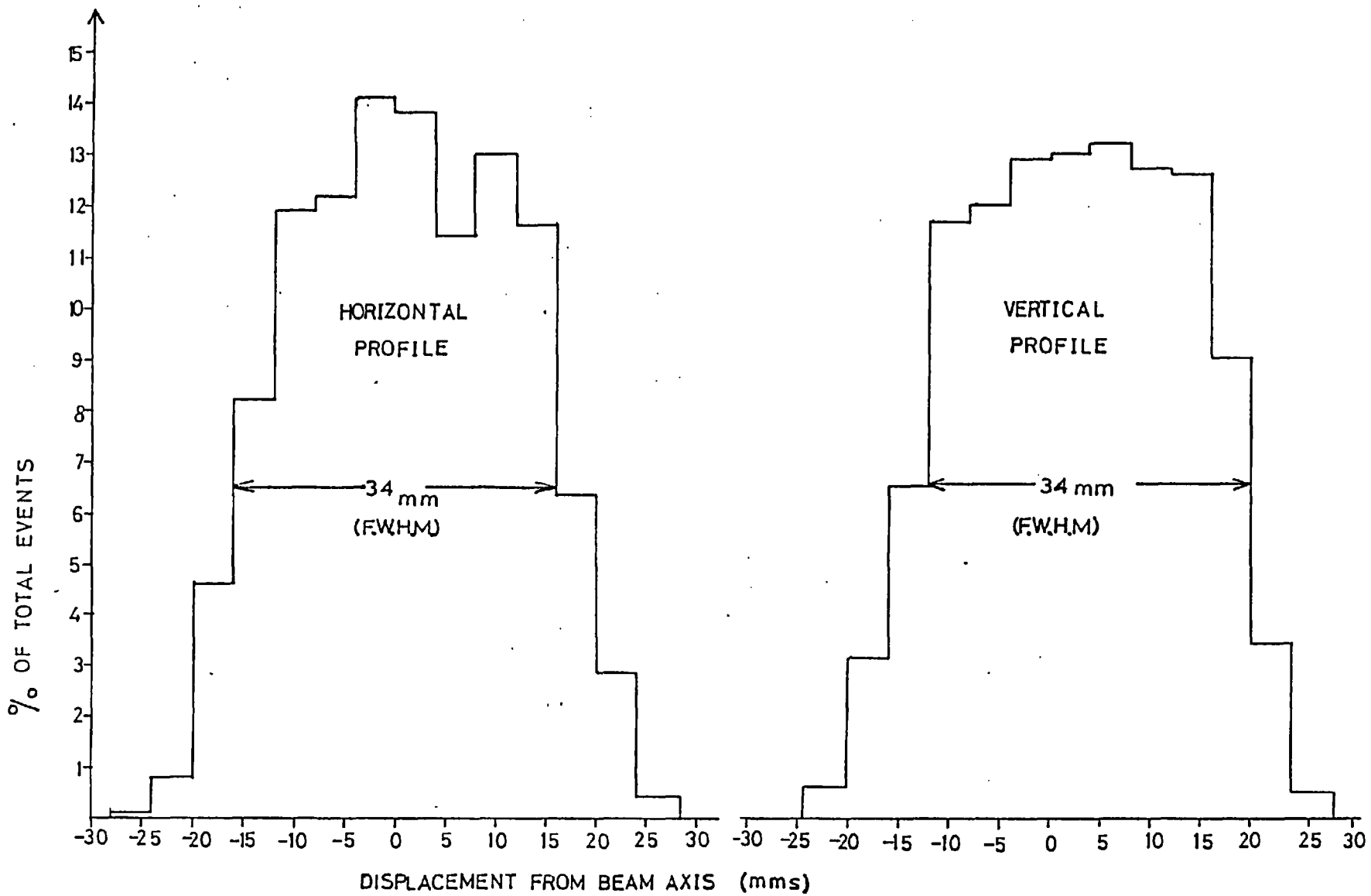
RECONSTRUCTED EVENTS FROM SLOW SPILL, RUNS 279-281
(BEAM CUTS IN ANALYSIS AT ± 25 mms)
% OF TOTAL EVENTS
HORIZONTAL PROFILE
34 mm (F.W.H.M)
VERTICAL PROFILE
34 mm (F.W.H.M)
DISPLACEMENT FROM BEAM AXIS (mms)

FIGURE II.3

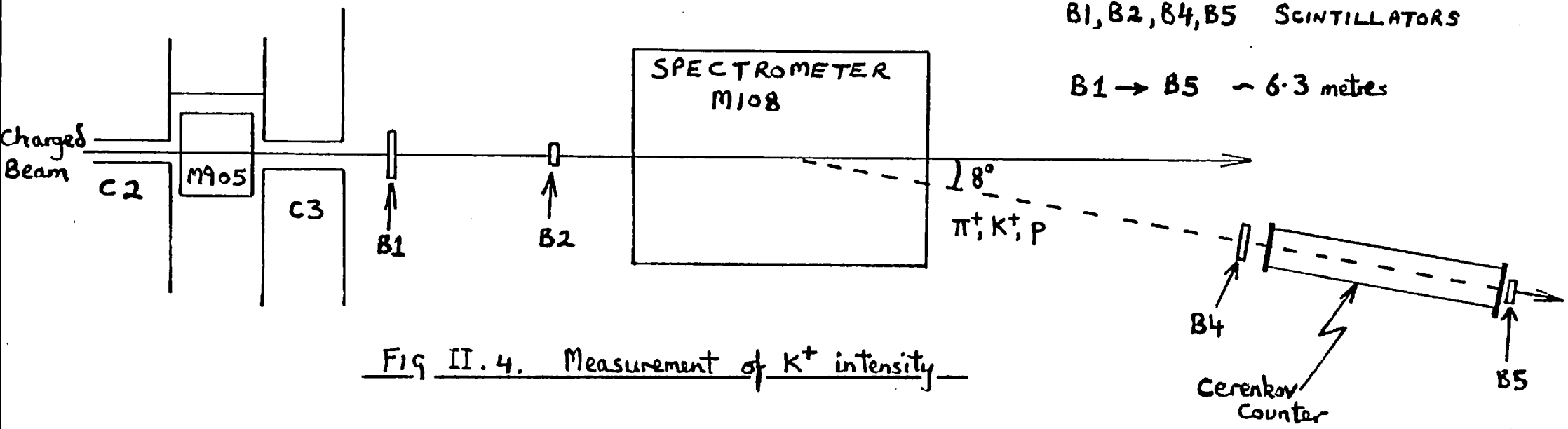

Fig II.4. Measurement of K^+ intensity

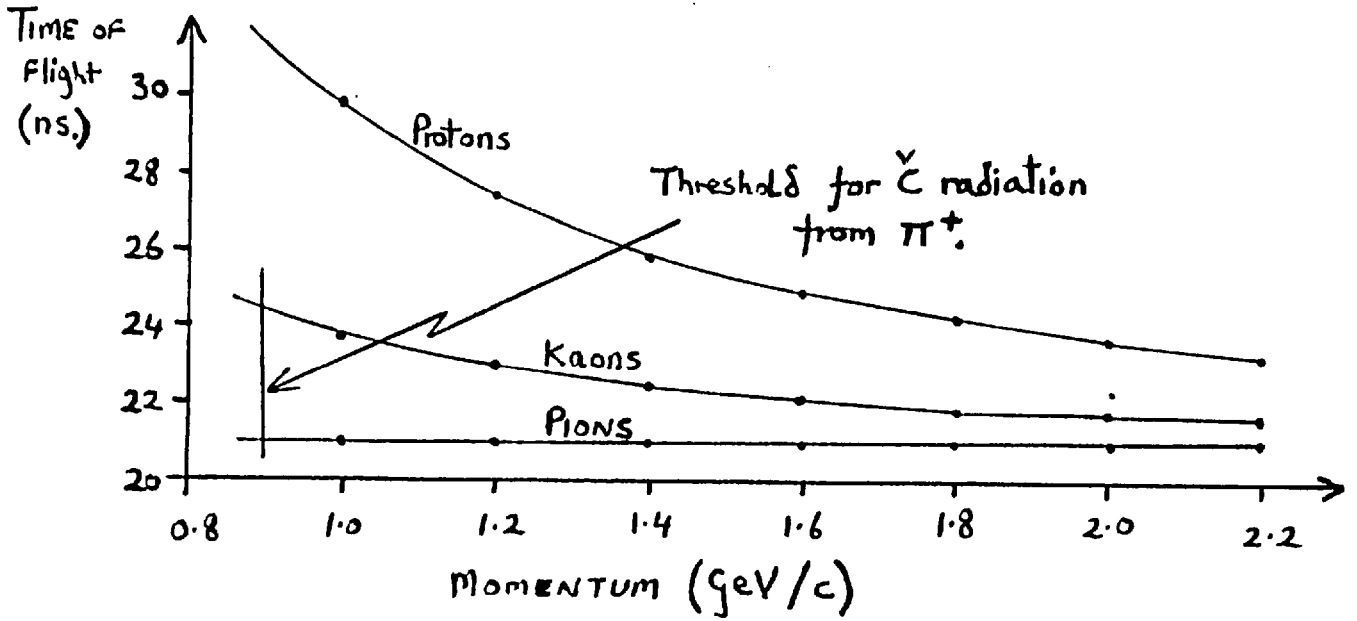

Fig II.5. Flight times for π^+, K^+, P over 6·3 m

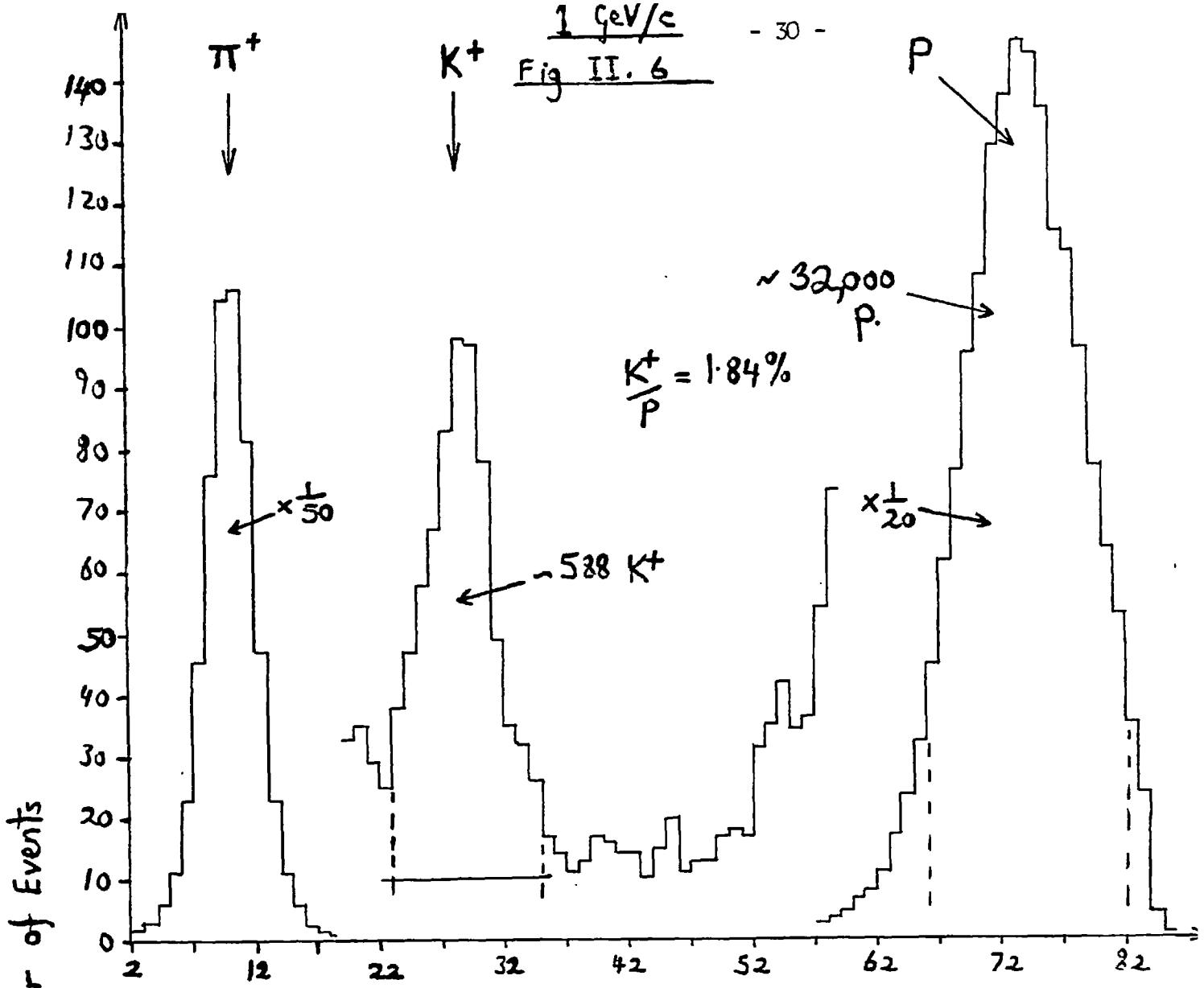

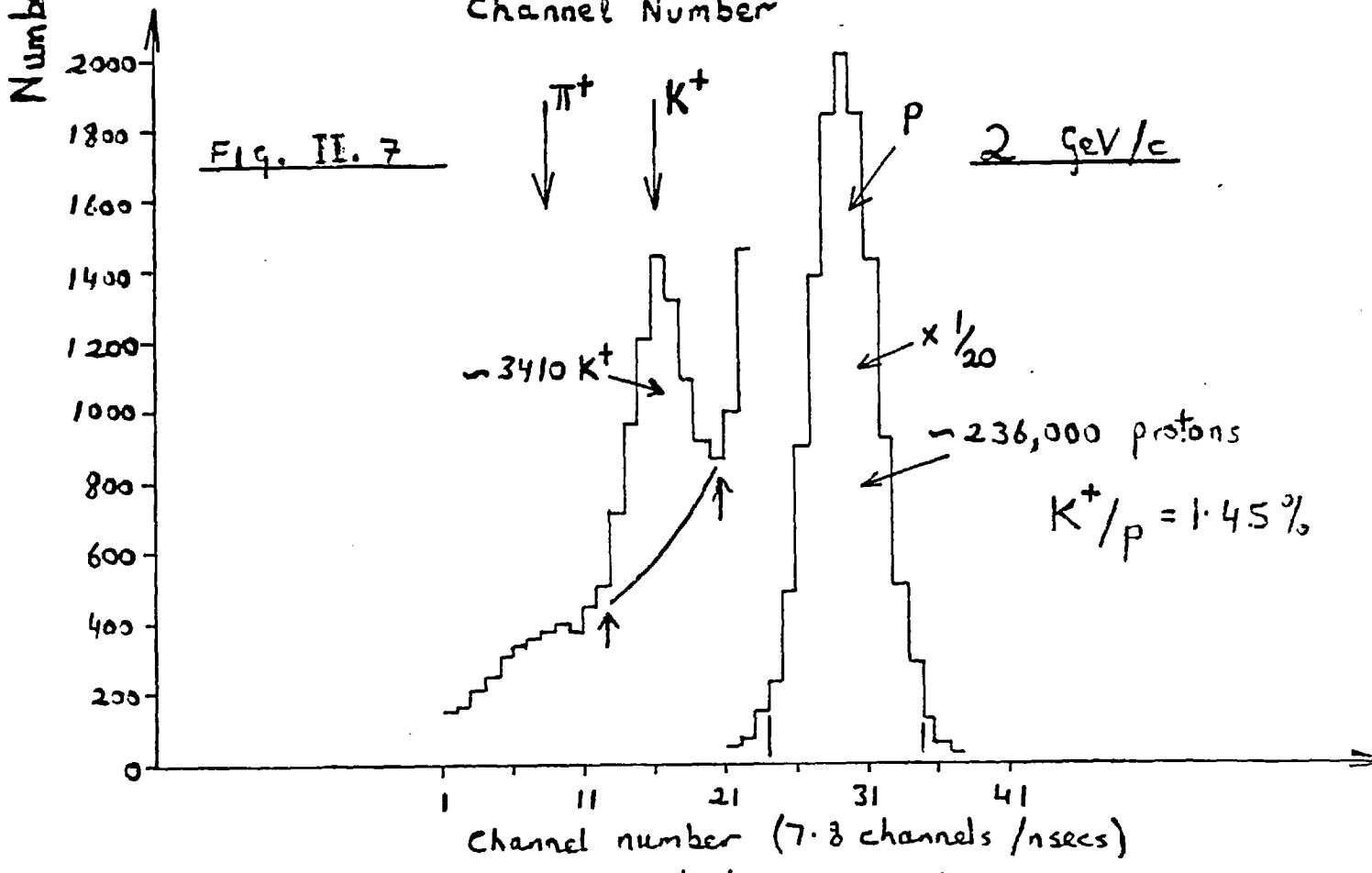

FIGURES II·6 AND II·7: $\pi^+ K^+ P$ SIGNALS

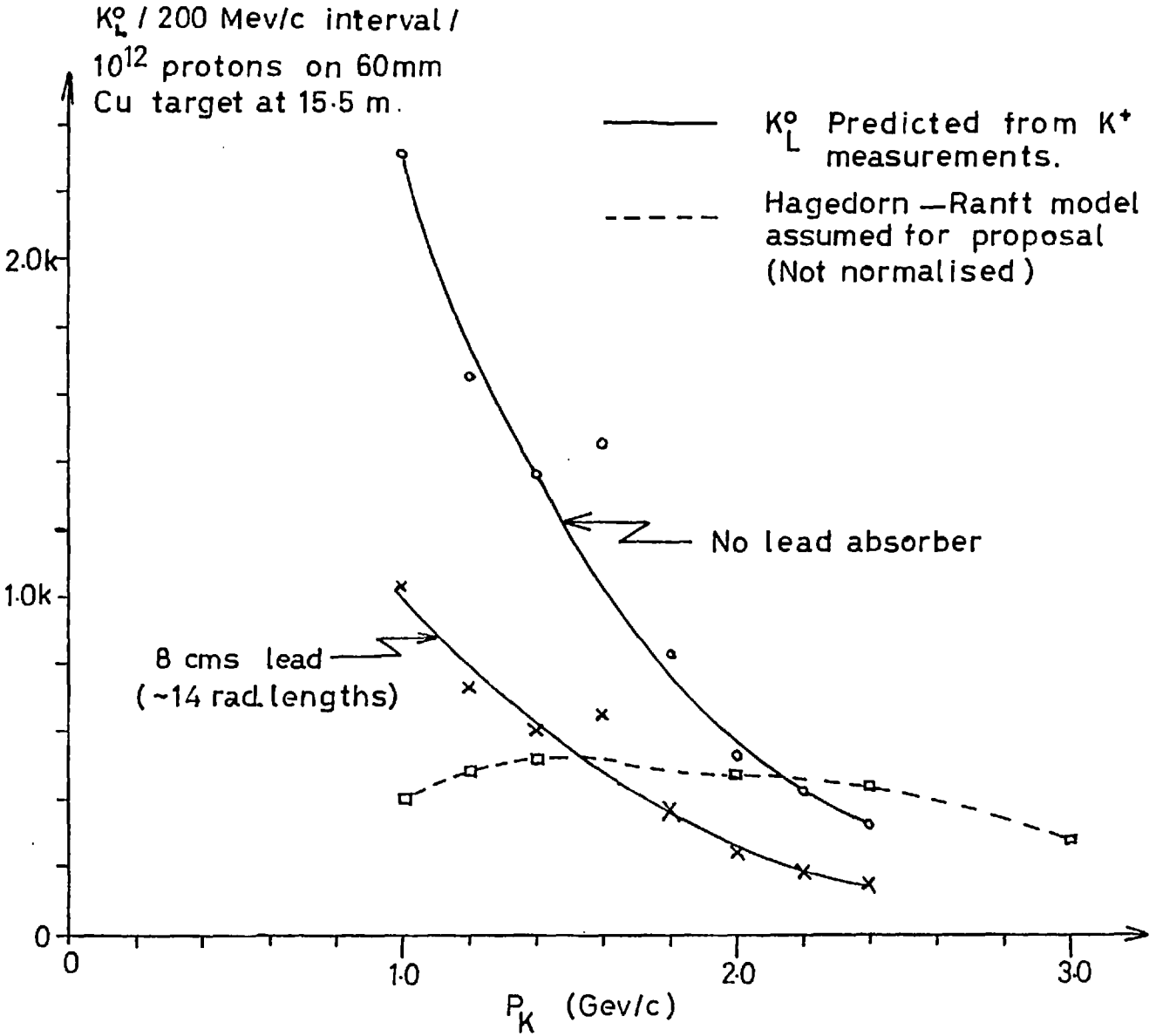

PREDICTED K^0_L SPECTRUM. : FIGURE II·8

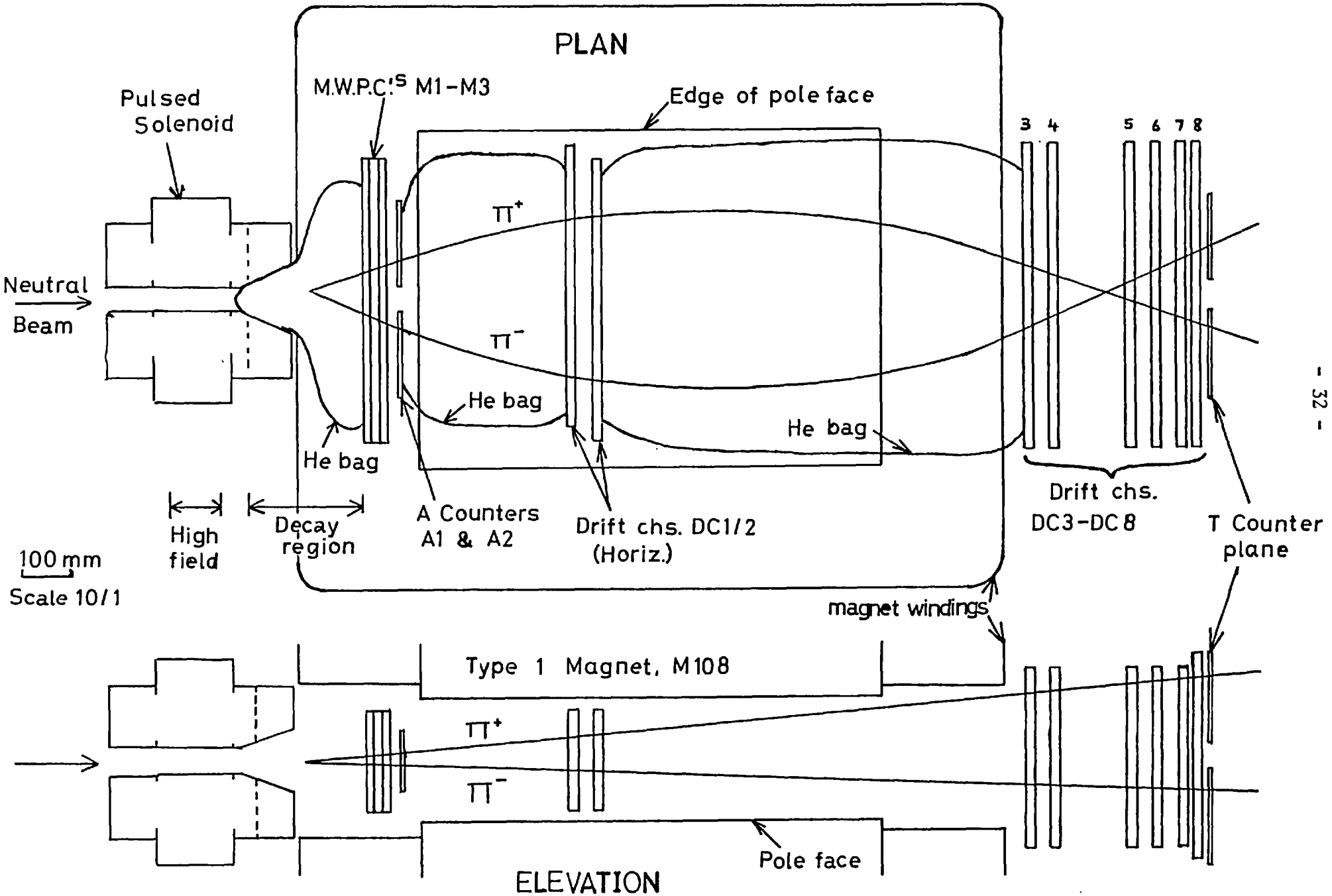

K° DETECTION SYSTEM : FIGURE II.9

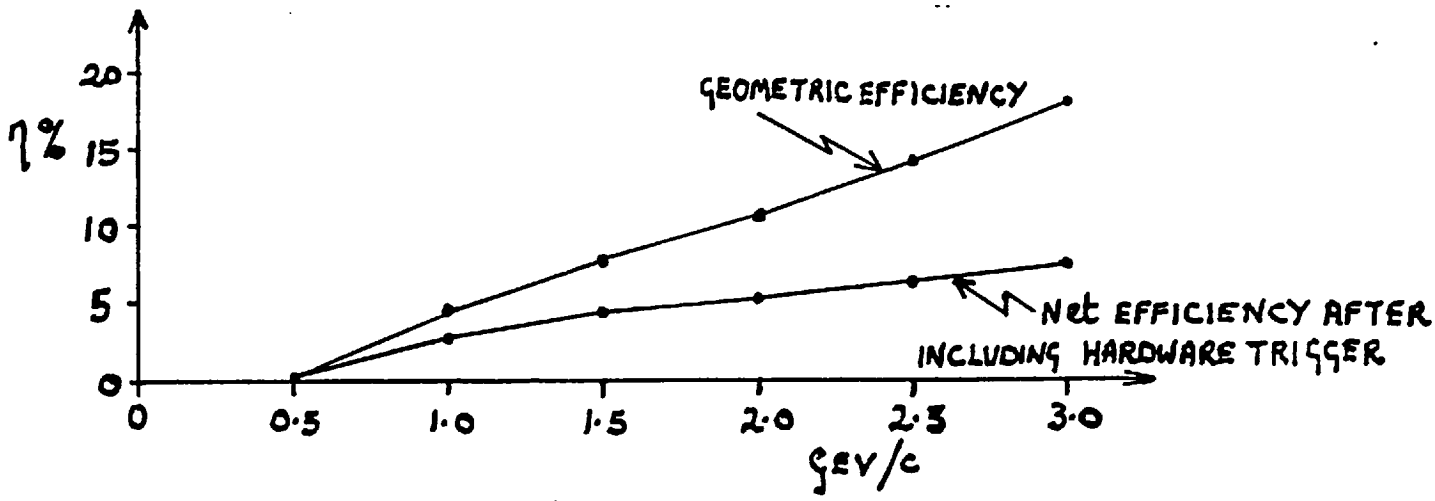

FIG II.10 $K^0 \rightarrow \pi^+ \pi^-$ DETECTION EFFICIENCY

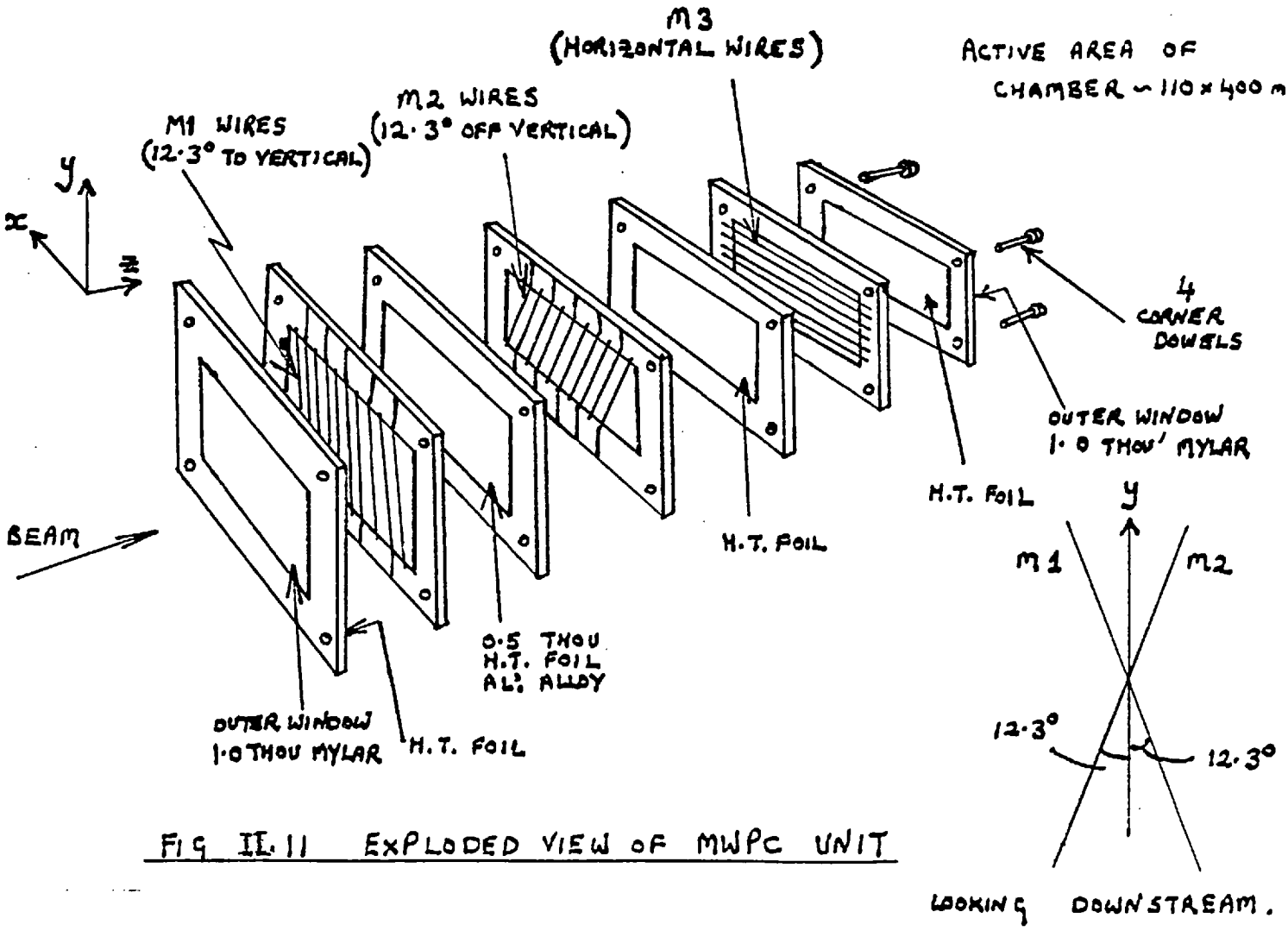

FIG II.11 EXPLODED VIEW OF MWPC UNIT

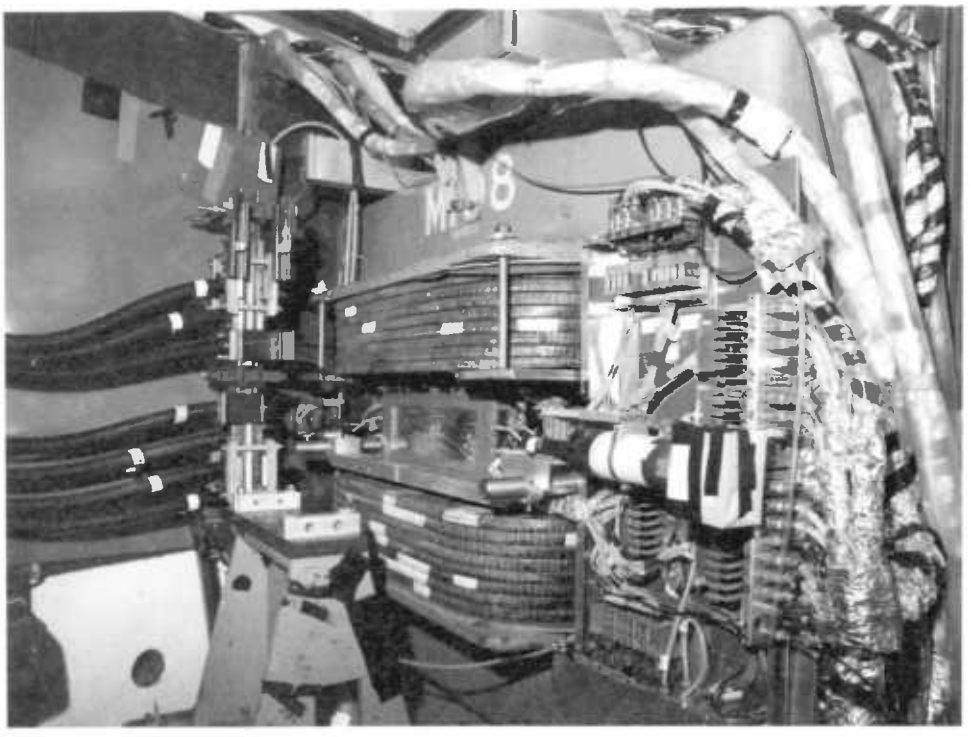

Plate 2.1 MWPC unit in position.

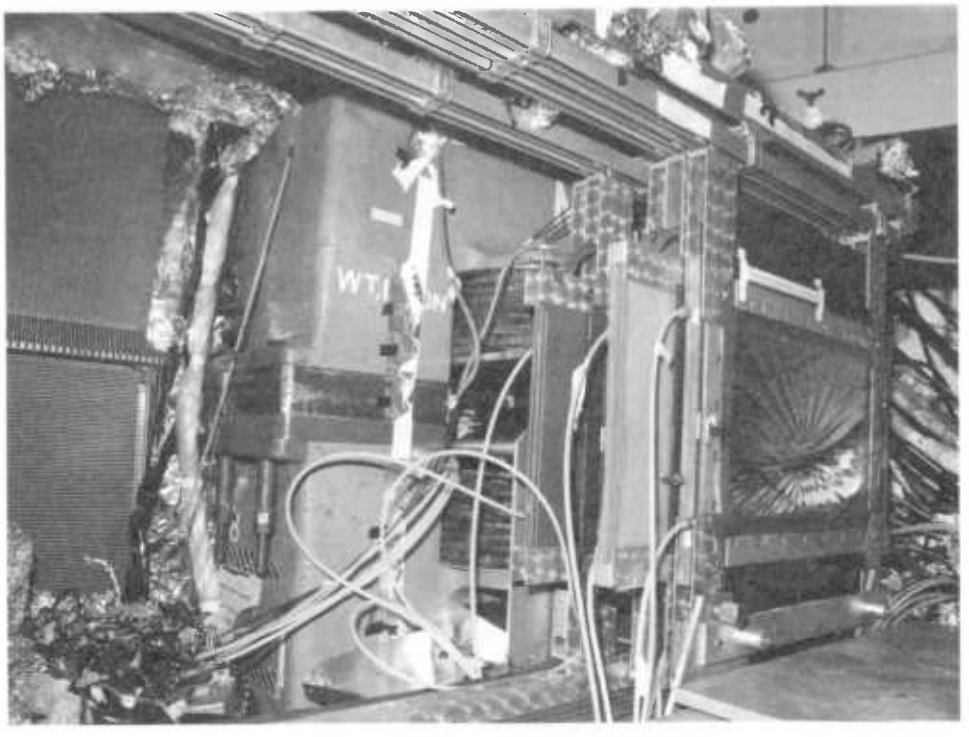

Plate 2.2 Drift chambers DC3 - DC7 behind the spectrometer.

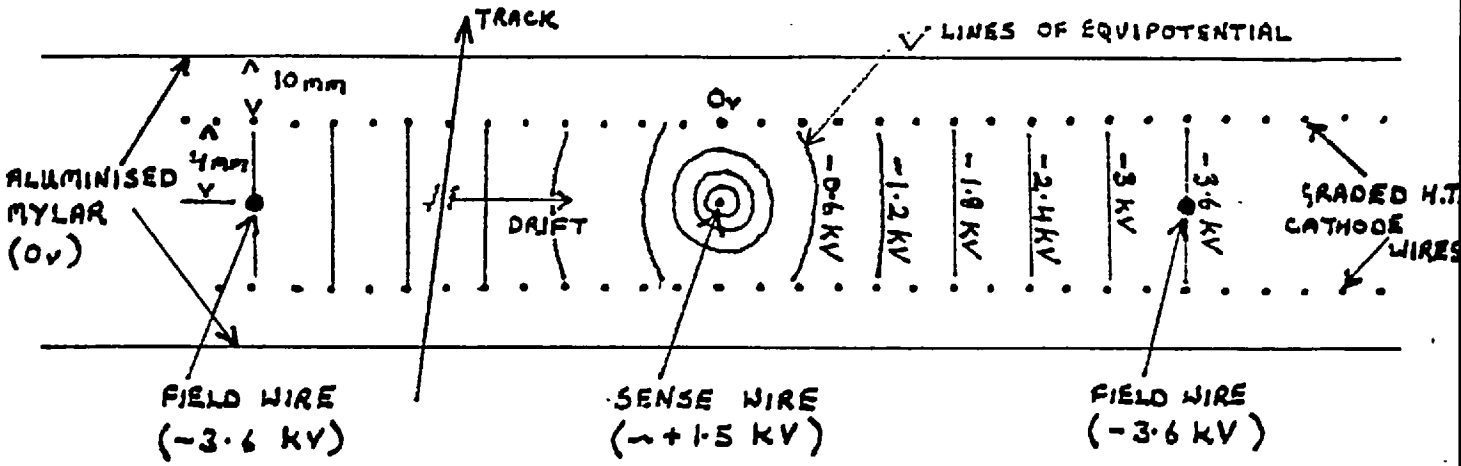

FIG II.12(a) TYPICAL DRIFT CHAMBER CELL

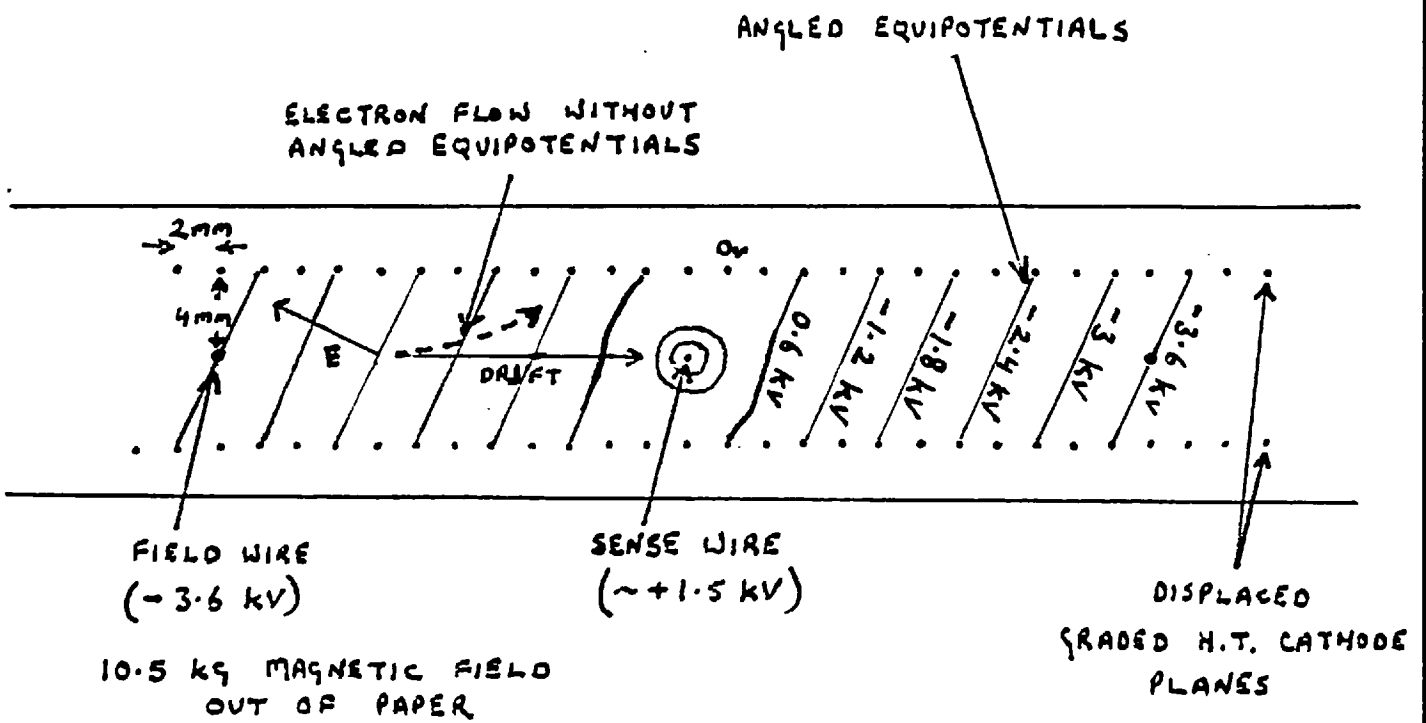

FIG II.12(b) MODIFIED DRIFT CELL FOR DC1 AND DC2 TO COMPENSATE FOR THE MAGNETIC FIELD OF M108.

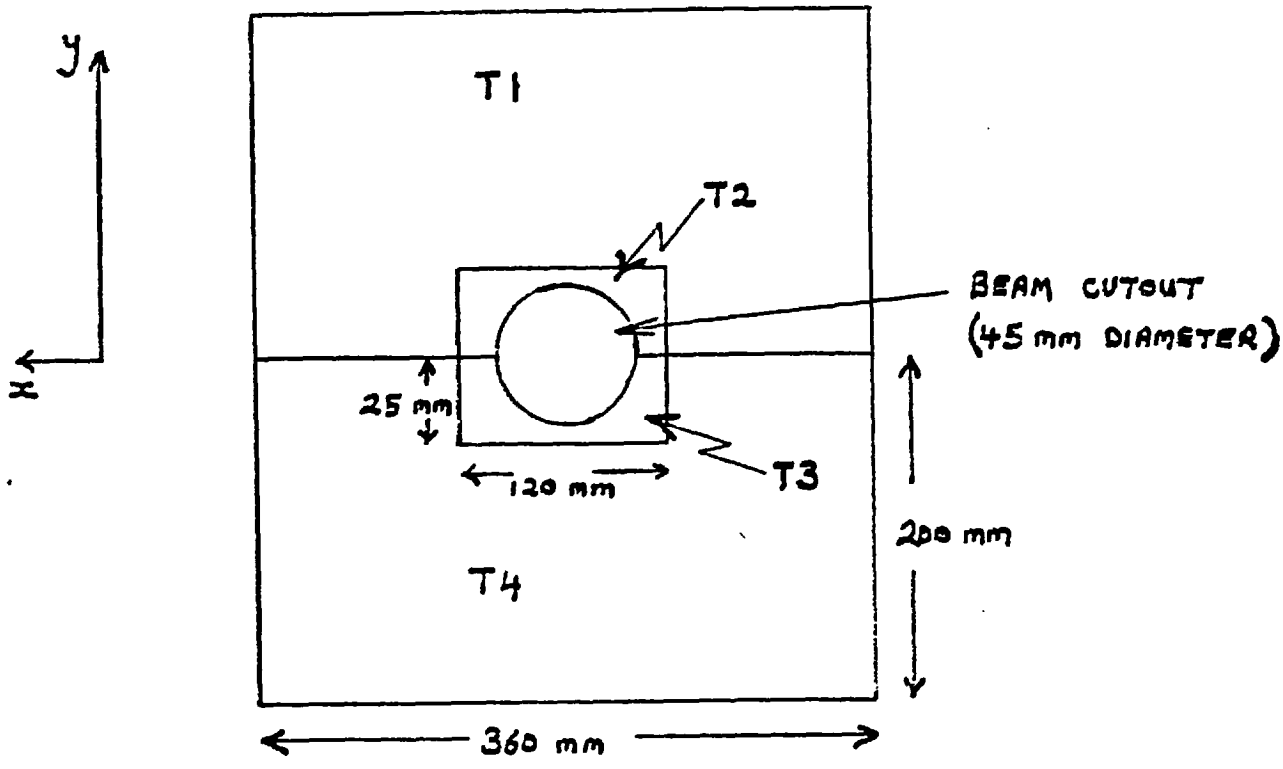

FIG II.13 T COUNTER PLANE (LOOKING DOWNSTREAM)

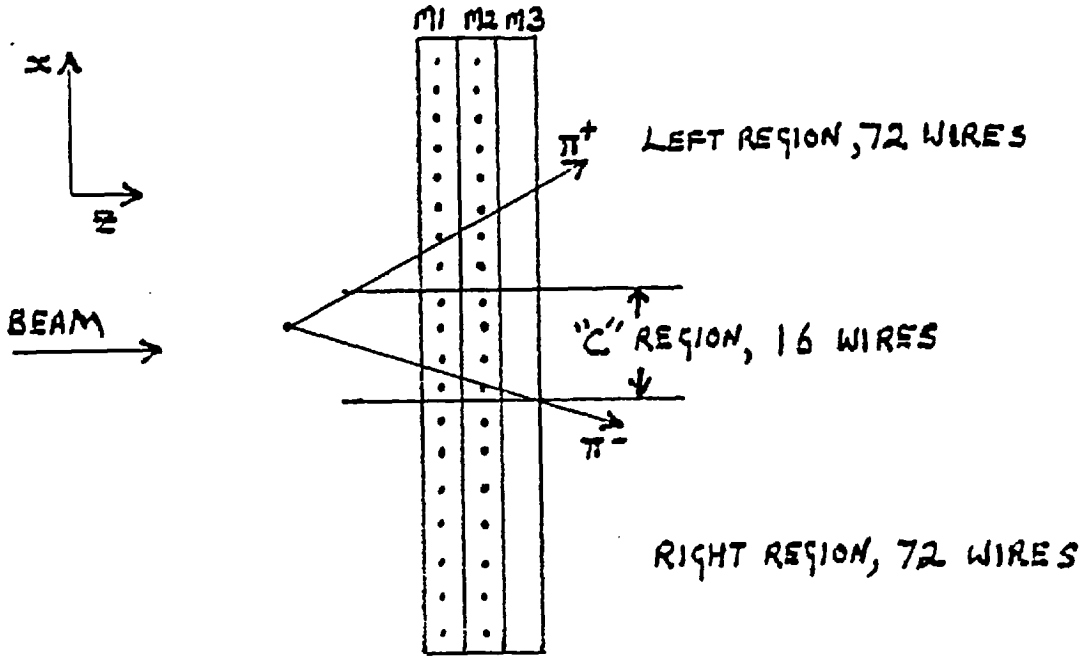

FIG II.14 PROMPT OR'S FROM M1 AND M2 FOR THE HARDWARE TRIGGER

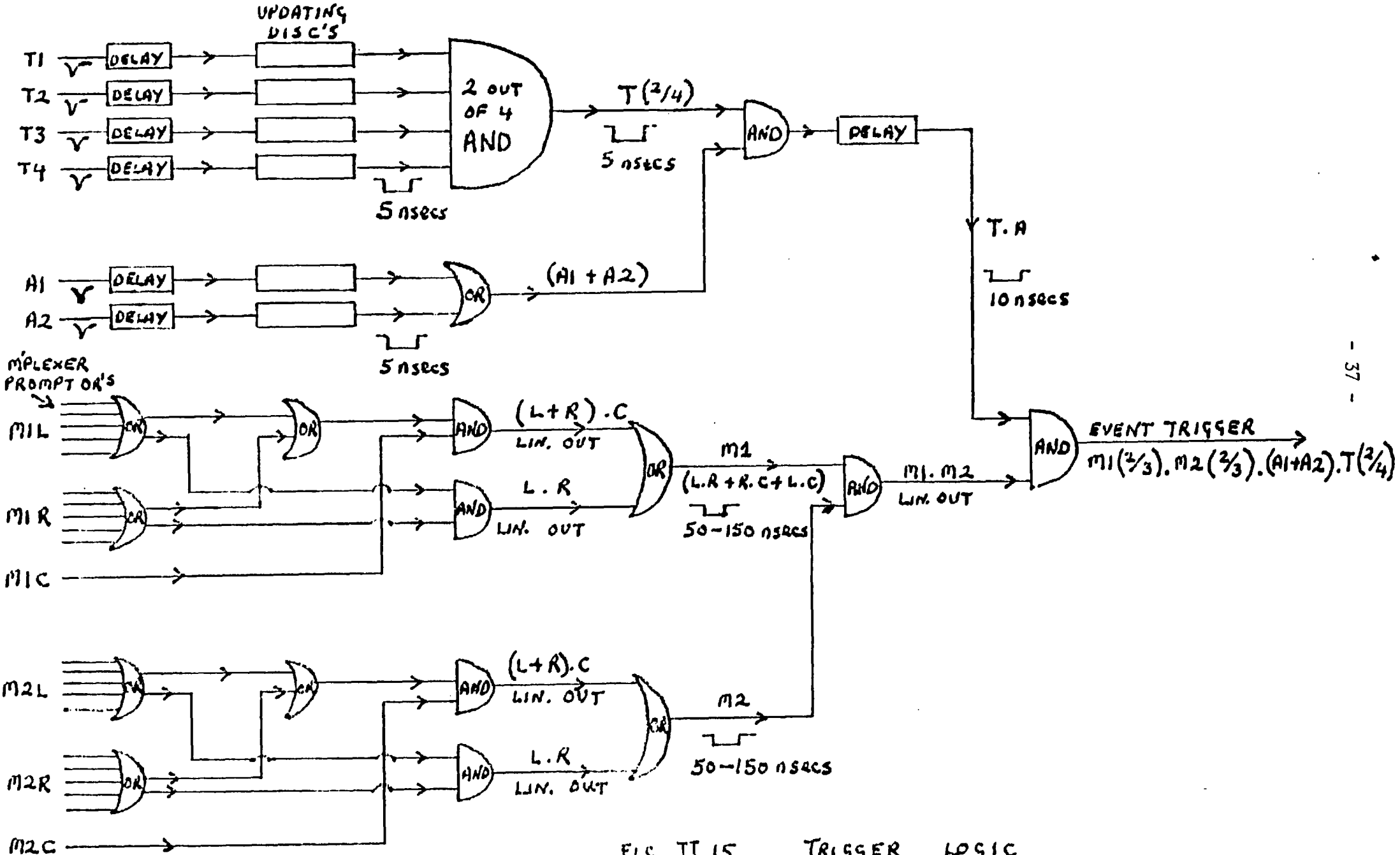

FIG II.15 TRIGGER LOGIC

CHAPTER III

THE PULSED SOLENOID

III.1 Construction

The construction of the solenoid is shown in Fig. III.1. Current through the solenoid was carried by a 30 turn flat helical coil 150mm. long with an internal bore of 50mm. and an overall diameter of 120mm. The coil was machined from a single beryllium-copper billet and then furnished with a glass fibre/resin composite as interturn insulation. It was water cooled and held inside a stainless steel jacket which supplied considerable prestressing both axially and radially. This helped to reduce damage to the conductor and insulation caused by the high forces generated during pulsing [12]. In order to reduce the fringe field beyond the solenoid, an end plate of Be/Copper with a conically-profiled central aperture was mounted on the assembly (see section III.3). The downstream end of the solenoid, with the conical end plate, is shown in Plate 3.1, the coil in Plate 3.2 and its position in the beam line in Plate 3.3.

The length of the coil was determined by the requirement that the K^o's should spend about two K^o_s lifetimes in the high field region so that there should be a significant drop in the $K^o \to \pi^+\pi^-$ rate beyond the solenoid. The main restriction on coil volume was from the number of capacitors available to the experiment. These provided enough power to ensure fields of up to 400 kgauss (the original design estimate) over a coil volume of 0.3 litres. Taken together with the requirement for a 150mm. length this therefore restricted the bore to be 50mm.

Five coils were made during the experiment and their performance is listed in Table III.1. Tests of the first two coils showed that they were unable to survive for long periods under the severe cyclic stresses set up above 300 kgauss. In order to pulse the coil once every 5 seconds for up to 200,000 shots, the maximum field was therefore limited to 250 kgauss. The third coil, Mark III, was used during data taking in summer 1977 while Marks IV and V were used during the last data taking run in November and December 1977. Mark IV was made from a Nickel Silicon/Copper billet in the hope that it would be more forgiving under the cyclic loading. Unfortunately this was not so in practice. The system parameters for pulsing the coil are shown in Table III.2.

III.2 Current Discharge Sequence

The general electrical layout for the solenoid is shown in Fig. III.2 and the LCR circuit involved is shown in Fig. III.3. The 0.015 farad capacitor bank was charged up from the thyratron rectifier which was fed via two transformers with a three phase power supply from the national grid. The charging sequence took about 3 seconds, continuing until the capacitor bank reached a preset 'aiming' voltage. This was 5 kV during data taking.

The discharge sequence was then initiated by a 'fire' pulse sent from the beam electronics (see section IV.1). This caused the current to be switched by four 'fire' ignitrons to the coil via large section coaxial cables. The risetime to maximum field was about 0.8msecs. with the field within 10% of B_{max} for about 0.4msecs. (see Fig. III.4). The maximum current was around 10^5 amps. Using four

'clamp' ignitrons a crowbar or 'clamp' resistor was introduced 1.3msecs. after the fire pulse in order to damp the current pulse. This prevented large current reversals in the solenoid thereby limiting temperature rise. It also prevented excessive voltage overswing which helped to extend the lifetime of the capacitor bank. 0.8 seconds after the coil was pulsed, the charging sequence to the capacitor bank was repeated.

The thyratrons, which were used to fire the 'fire' and 'clamp' ignitrons and which were also used in the rectifier, were found to cause pickup in the MWPC's and drift chambers. Data taking was therefore vetoed during any period of thyratron activity using a 'Fire Veto' pulse from the solenoid electronics. This caused minimal loss of beam since the 'fire' pulse came before the fast spill gate and the 'clamp' signal came well after most of the fast spill. Loss of beam from the rectifier thyratrons was also small. The whole trigger area for the solenoid was enclosed using perforated steel sheet (see Fig. II.2). This formed a virtually complete faraday cage (except for the floor) with which to stop r.f. pickup. Apart from thyratron pickup, the pickup in the counters and chambers was found to be low.

The magnetic field in the solenoid was measured before data taking using search coils. At least three different search coils were made, each of quite different n.A (number of turns times cross-sectional area), and all were found to give good agreement in the measurement of flux. An identical pair of search coils were then made and used as a standard. The accuracy achieved with these was to within 2%. They were used to calibrate the 1:1000 voltage probe on the capacitor bank and the single turn toroid used to measure the discharge current.

The voltage probe was used to monitor the maximum field generated in the solenoid during data taking. This is proportional to the bank voltage just before discharge and the linear relationship between the two is shown in Fig. III.5. The maximum bank voltage and maximum field recorded by the search coil were measured using sample and hold D.V.M.'s. With an operating voltage of 5 kV, the maximum field in the solenoid was 250 kgauss. Once every three hours the solenoid was powered down for checks. The aiming voltage for the capacitor bank was reset each time to within 1.0% of 5 kV.

The single turn toroid was used to measure the discharge current at various times during the solenoid pulse and hence the magnetic field in the solenoid. It was mounted around the copper busbar which carried the current from the ignitrons to the coaxial cables supplying the solenoid. The current induced in the windings around the toroid was measured from the voltage signal across a small 0.1 Ω series resistor. This gave a 4000:1 stepdown, in volts of the main discharge current. Figures III.6 and III.7 show plots of the peak I toroid current against B_{max} and initial bank voltage respectively. Both plots show a drop in the toroid readings from linearity by 5-10% at higher currents due to saturation in the toroid. However the magnetic field was found by taking the ratio of sampled current to peak current (see section IV.1). Since the region of interest for the experiment was for fields within 20% of B_{max}, then errors in the ratios due to the slight non-linearity observed above were negligible.

Apart from the I toroid and voltage probe,diagnostics, there were also diagnostics to monitor the mechanical behaviour of the solenoid. The most important of these was a microphone which measured the acoustic wave generated by the solenoid. It was thought

that work hardening and the appearance of any cracks in the coil would produce significant changes to the acoustic wave and that this would serve as a warning that the coil was close to a breakdown. Consequently the ADC outputs from the microphone, voltage and current pulses were closely monitored by the DDP 516 computer, and coil pulsing was automatically inhibited for significant changes in waveform (see section IV.1).

The threat of a coil breakdown was a source of much concern throughout the whole experiment due to the proximity of the MWPC's and drift chambers. A breakdown would cause a flash and a sizeable shock wave (not only to the apparatus!). Plate 3.4 shows the catastrophic results of the Mark III coil breakdown during data taking in summer 1977. The MWPC's and DC1/2 were destroyed and had to be completely rewired, delaying the experiment by 3 months. Fortunately the lessons learned during this episode prevented a similar occurence with Marks IV and V.

III.3 Effect of the Fringe Field

As mentioned earlier a Beryllium-Copper end plate conductor was mounted on the solenoid in order to reduce the fringe field in the decay region. During the solenoid pulse the magnetic field acting on the end plate changes its strength. The flux change in the end plate gives rise to an induction e.m.f. and therefore to eddy currents in the conductor. These currents then give rise to a magnetic field that, according to Lenz's law, tends to counteract the effect of the variation of the external field. The result of this is to cause a net reduction in the field strength beyond the solenoid.

Figure III.8 shows the field distribution along the axis of the solenoid found using one of the standard search coils. The field at the start of the decay region was about 3.7% of B_{max} dropping off approximately exponentially over the first 50mm. with a decay length of 8mm. and rather less steeply after that due to the increasing aperture of the conical conductor. This is in reasonable agreement with the attenuation length expected from a wave guide theory analysis of the action of the cone which gives ∿10mm. for a frequency of 500 Hz.

The effect of the field on the pions from K^o decay can be calculated approximately using Figure III.9. This shows a decay with the two pions initially in the y = 0 horizontal plane at the start of the decay region. The contributions to P_Y due to the fringe field come from B_Z with P_X and from B_X with P_Z. For the positive pion

$$\Delta P_Y = 0.3 \left(\int B_X \, dZ - \int B_Z \, dX\right) \qquad \text{(III.1)}$$

$$= 0.3 \frac{X_o}{2} B_{Z_o} - 0.3 \tan\alpha \int B_Z \, dZ \qquad \text{(III.2)}$$

where the first integral has been evaluated using div B = 0 as shown in the diagram and assuming the pion to be parallel to the axis (neglecting α).

This gives $$\Delta P_Y = 1.4 \, X_o - \frac{500}{P_\pi} \text{ MeV/c} \qquad \text{(III.3)}$$

where P_π is the pion momentum in MeV/c and X_o is the off axis decay position in cm. (max ∿2.0cm.). Tanα was evaluated assuming the pions have the maximum transverse momentum allowed in K^o decay which gives $\tan\alpha \approx \frac{200}{P_\pi}$. $\int B_Z \, dZ$ was evaluated assuming an 8mm. decay length for the field with B_{Z_o} = 3.7% of 250 KG.

With most of the decays within 2cm. of the beam axis and with pion momenta going from ∿500 to 1000 MeV/c, the contributions to P_Y for the π^+ should then be less than +2 MeV/c even for the worst case (i.e. at the start of the decay region and 2.5cms. off axis).

For the π^-, the contribution to P_Y from $\int B_Z\, dX$ is the same as for the π^+, assuming both have maximum P_T. The $\int B_X\, dZ$ is more complicated if the π^- crosses the beam axis with a reversal in the sign of B_X. However the maximum contribution to P_Y comes if it does not cross the axis giving

$$\Delta P_Y = -1.4\ X_o\ -\frac{500}{P_\pi}\ \text{MeV/c} \qquad \text{(III.4)}$$

so that contributions to P_Y for the π^- are at most -4 MeV/c.

The vertical acceptance of the spectrometer was about ±50 MeV/c for decays at the start of the decay region so loss of pion tracks due to P_Y contributions was probably well below the 3-4% level. Combining equations III.3 and III.4 gives the net contribution to P_Y for both π^+ and π^- and thus the broadening that might be expected in reconstructing the K^o vertical transverse momentum. This is $\sim -\frac{1000}{P_\pi}$ MeV/c giving a broadening of 1-2 MeV/c. This broadening was observed and is discussed in Section IV.4.

The effect of the fringe field on P_X can be found as above except that tanα is limited by the vertical acceptance. Previously tanα varied from 0.4 to 0.2 for pions between 500 and 1000 MeV/c. The vertical acceptance limits tanα in the YZ plane to < 0.1 thus the second term in equations (III.3) and (III.4) will be small. Therefore little if any broadening of the K^o horizontal transverse momentum was expected.

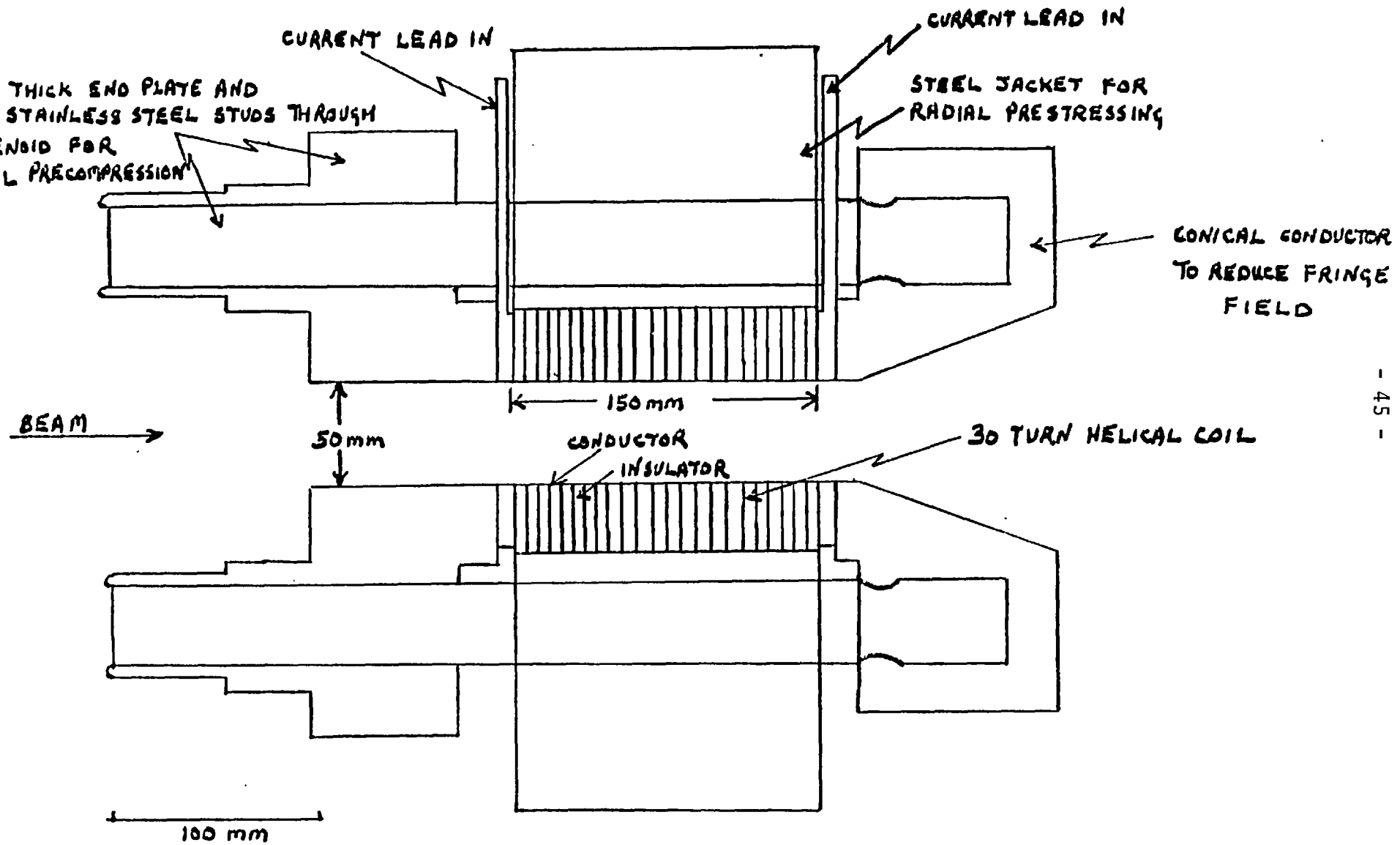

FIG III.1 SECTION OF SOLENOID THROUGH BEAM AXIS

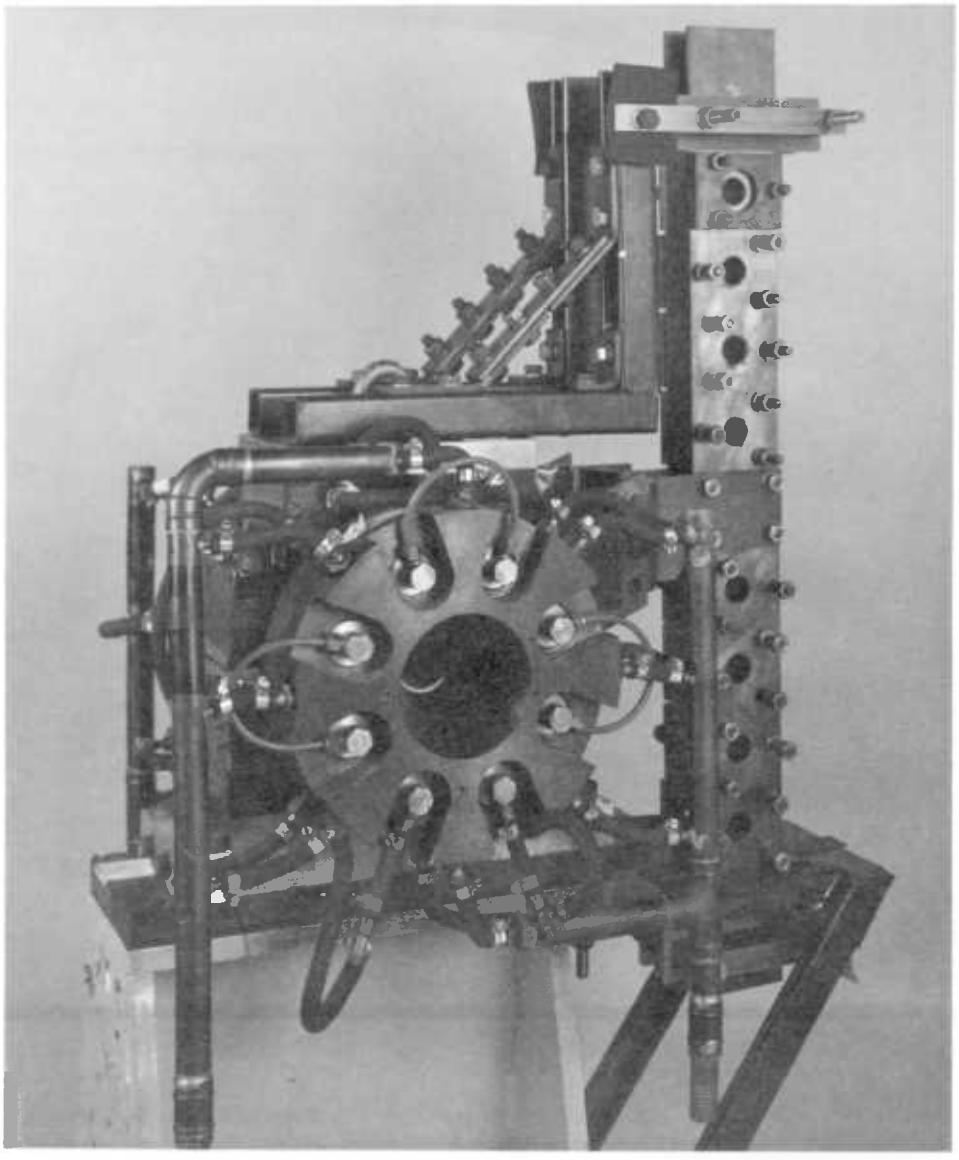

Plate 3.1 Downstream magnet assembly showing the conically apertured end plate.

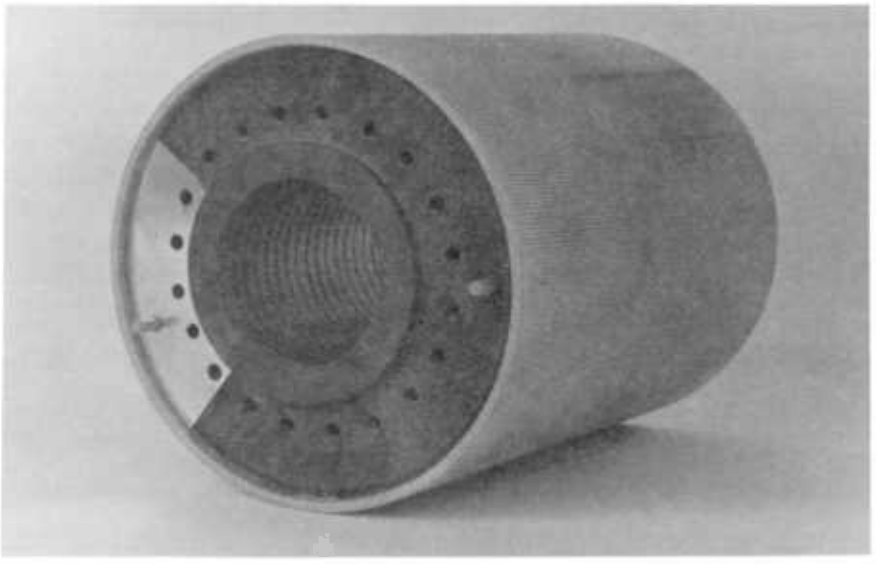

Plate 3.2 30 turn coil in insulating sleeve.

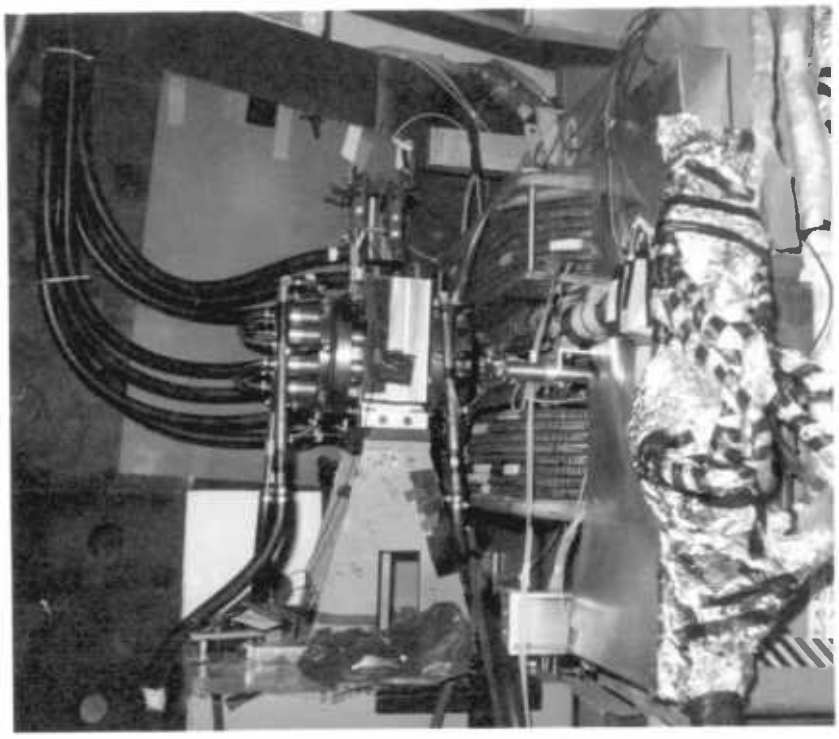

Plate 3.3 Solenoid in position in beam line.

Plate 3.4 Catastrophic results of the mark III flashdown.

TYPE	CONDUCTOR	INSULATION	TURNS	LENGTH, mms	SHOTS AT FIELD, B	COMMENTS
I	3.5 mm Cr Cu	1.5 mm GLASS ROVING/ EPOXY RESIN	30	154	13,000 22-30T 4 35-36T	INSULATION BROKE, WATER LEAKS, SEVERE CRACKING
II	4 mm 0.2% Be Cu	1.2 mm GLASS MAT/ POLYIMIDE RESIN	29	159	2,000 29-34T 1,000 28-34T	FLASHDOWN/CRACKS
III	4 mm 0.2% Be Cu	1 mm GLASS MAT/ POLYIMIDE RESIN	30	154	150,000-200,000 25T 8,000 30T	LONG DATA TAKING PERIOD FLASHDOWN
IV	4 mm Ni/Si Cu	1 mm GLASS MAT/ POLYIMIDE RESIN	30	150	80,000 25T	FLASHDOWN
V	4 mm 0.2% Be Cu	1 mm GLASS MAT/ POLYIMIDE RESIN	30	150	160,000 25T	CRACKS OBSERVED AT END OF LAST DATA TAKING PERIOD

TABLE III.1 COIL VARIABLES AND PERFORMANCE

BORE DIAMETER	50 mm	RISETIME TO B_{MAX}	0.8 msec
COIL OUTSIDE DIAMETER	120 mm	PULSE LENGTH	3.0 msec
BORE LENGTH	150 mm	PULSE INTERVAL	5.2 sec
COIL INDUCTANCE (MEAN)	16μH	BANK CAPACITY	0.015 F
R_{DC}	1-2 mΩ	V_{MAX}	5 KV } AT 250 KG
R_{AC} (MEAN) TO I_{MAX}	12 mΩ	I_{MAX}	100 KA } AT 250 KG
CLAMP RESISTOR	8 mΩ	CLAMP TIME	1.3 msec

TABLE III.2 SYSTEM PARAMETERS

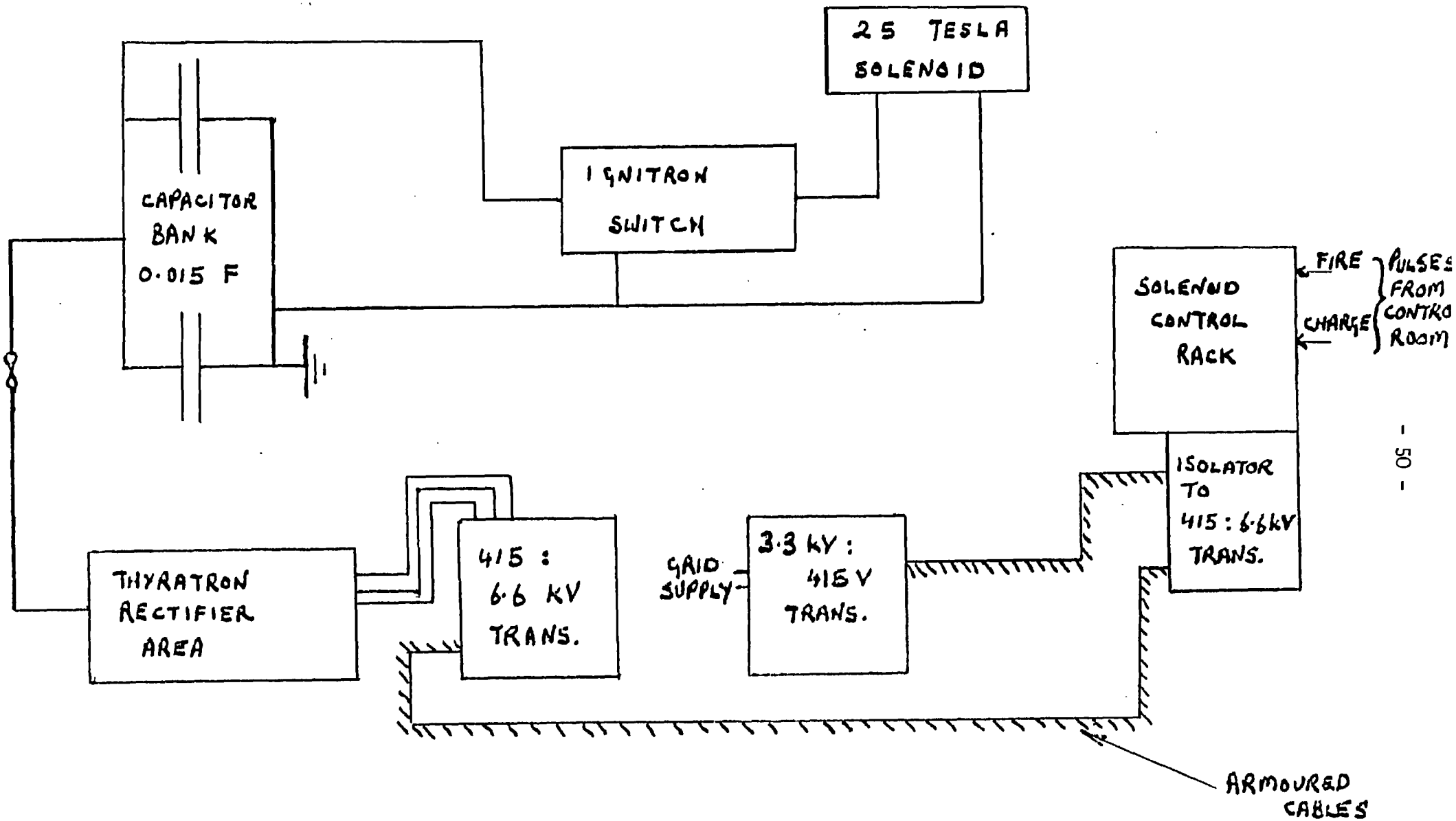

FIG III.2 GENERAL ELECTRICAL LAYOUT

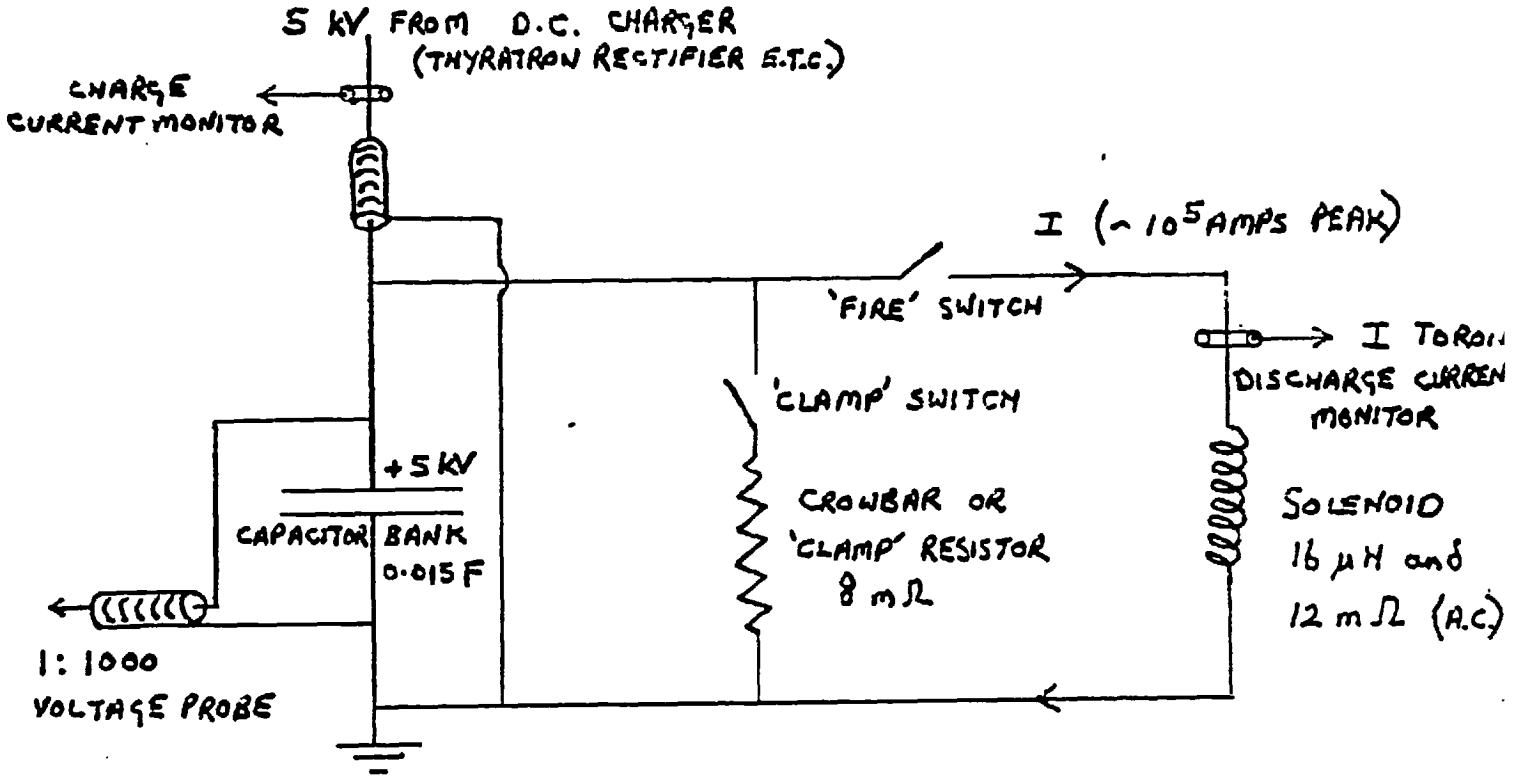

FIG III·3 L.C.R. CIRCUIT FOR PULSING SOLENOID

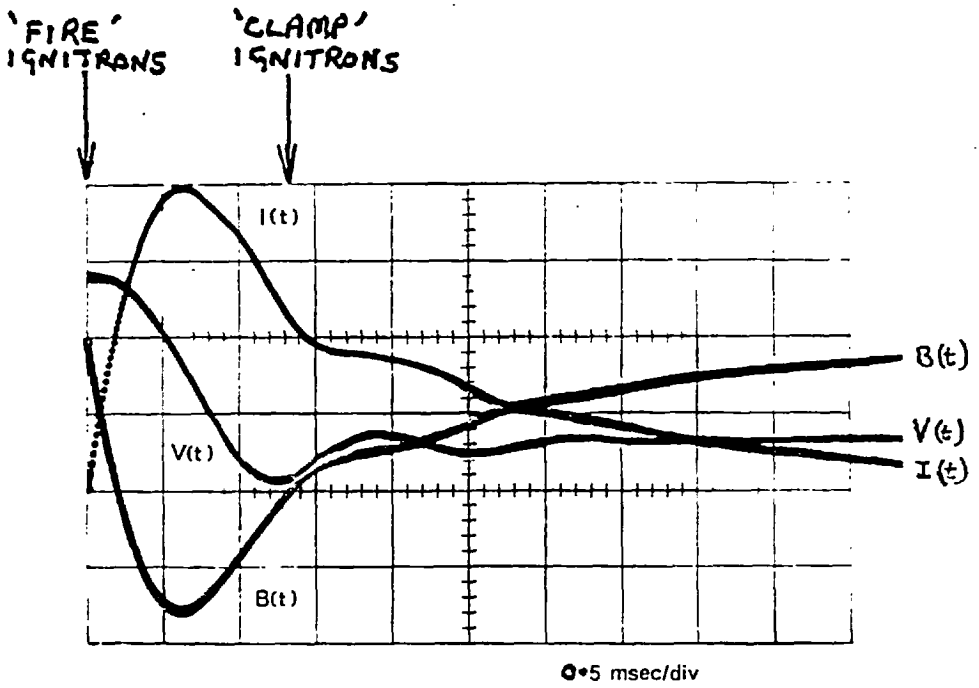

FIG III·4 OSCILLOGRAMS SHOWING CURRENT, BANK VOLTAGE AND MAGNETIC FIELD DURING THE PULSE

Fig. III·5

SOLENOID PEAK FIELD V.S. CAPACITOR BANK STARTING VOLTAGE

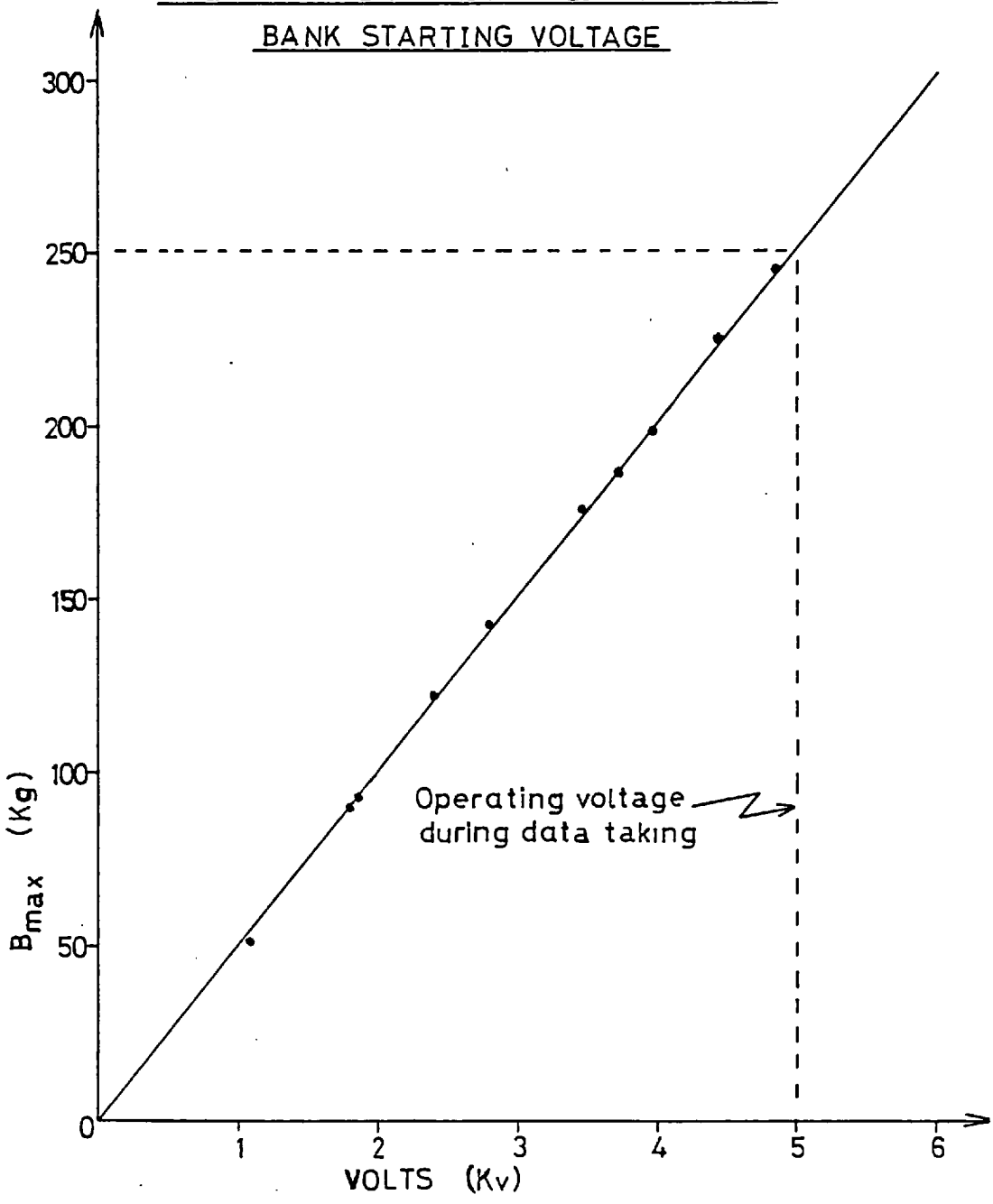

FIG III.6

PEAK CURRENT (USING I TOROID) V.S. PEAK FIELD

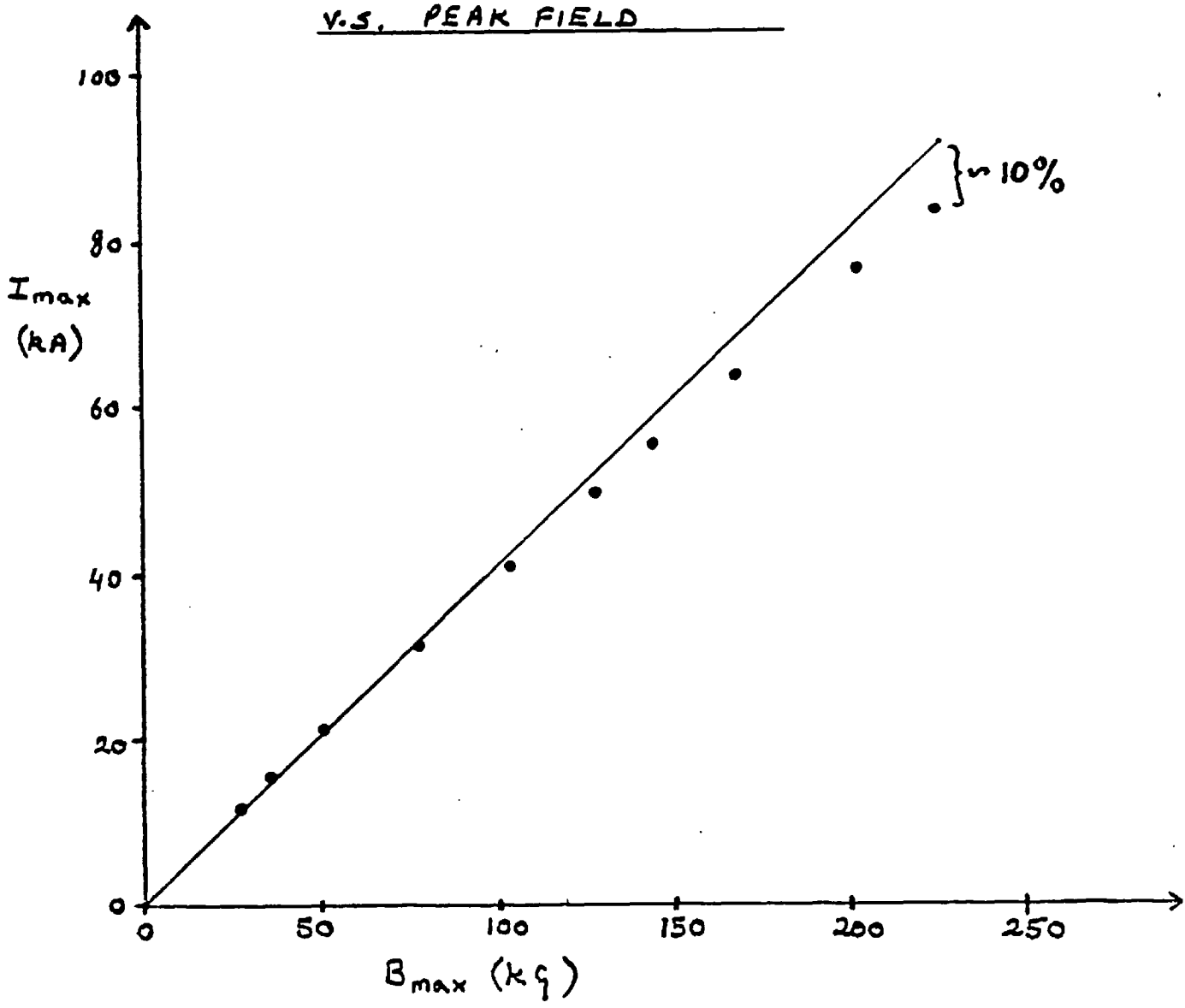

Fig. III.7

PEAK CURRENT (Using I Toroid) V.S.
CAPACITOR BANK STARTING VOLTAGE

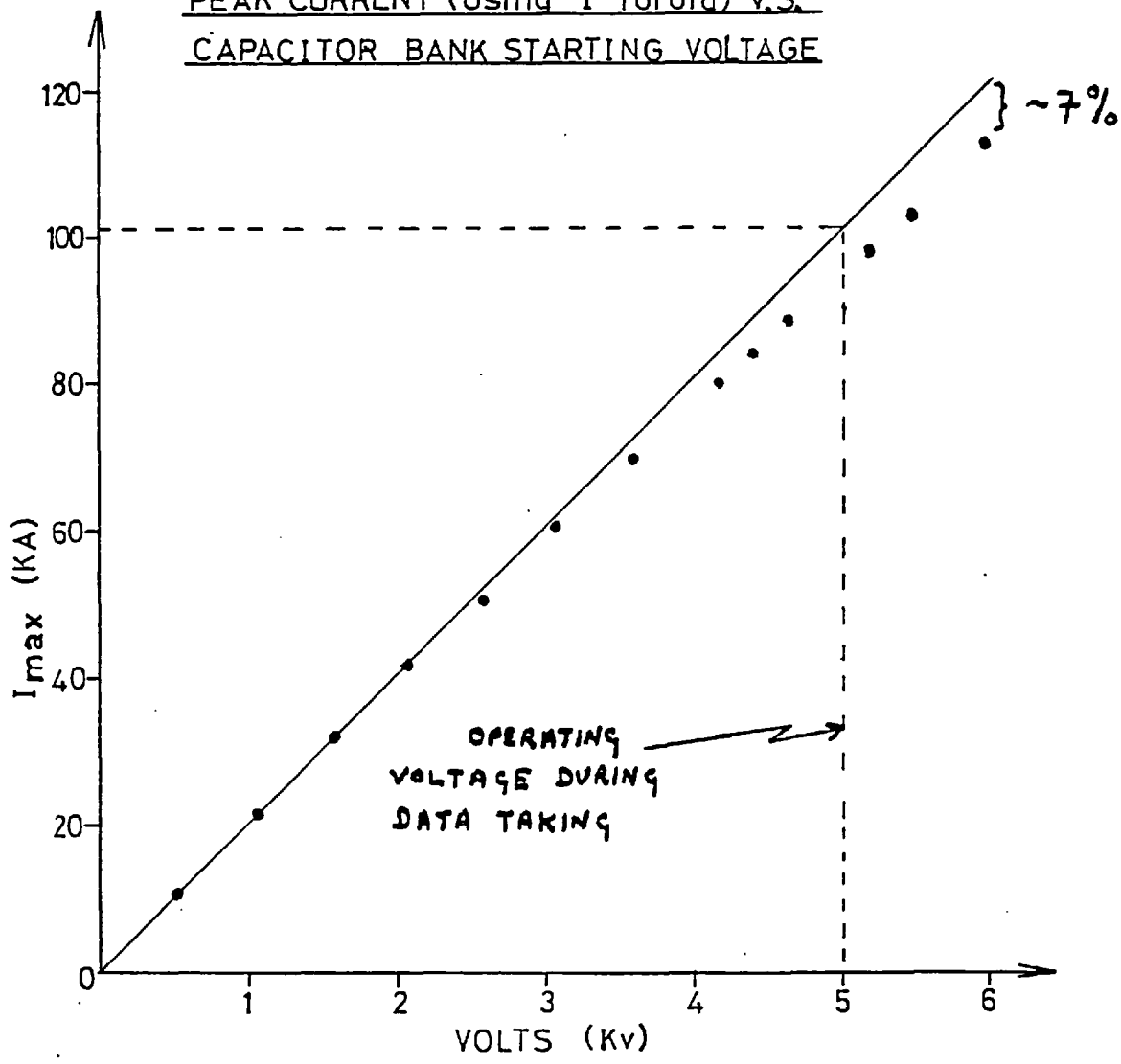

FIELD VARIATION ALONG THE AXIS OF THE SOLENOID : FIG III·8

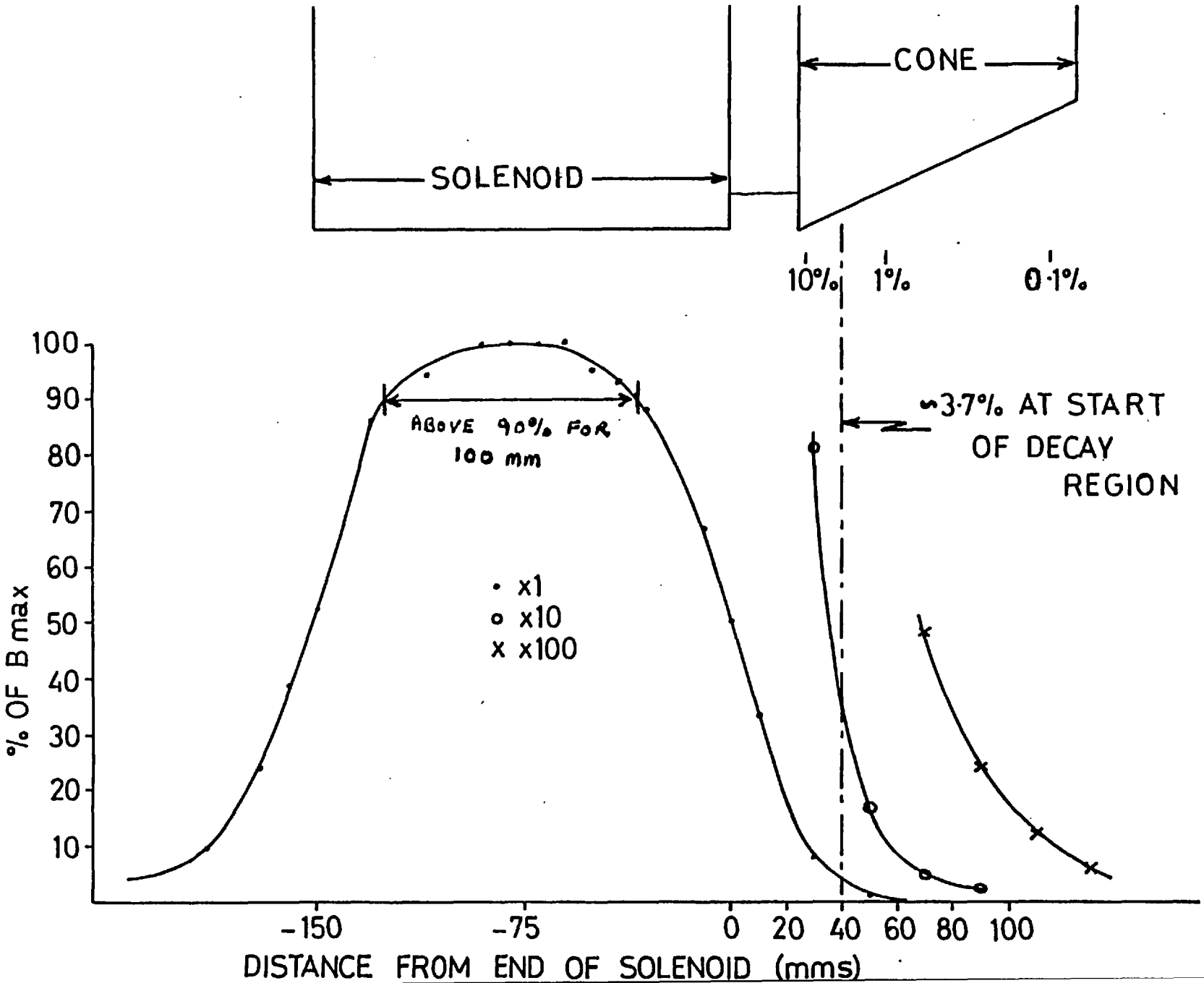

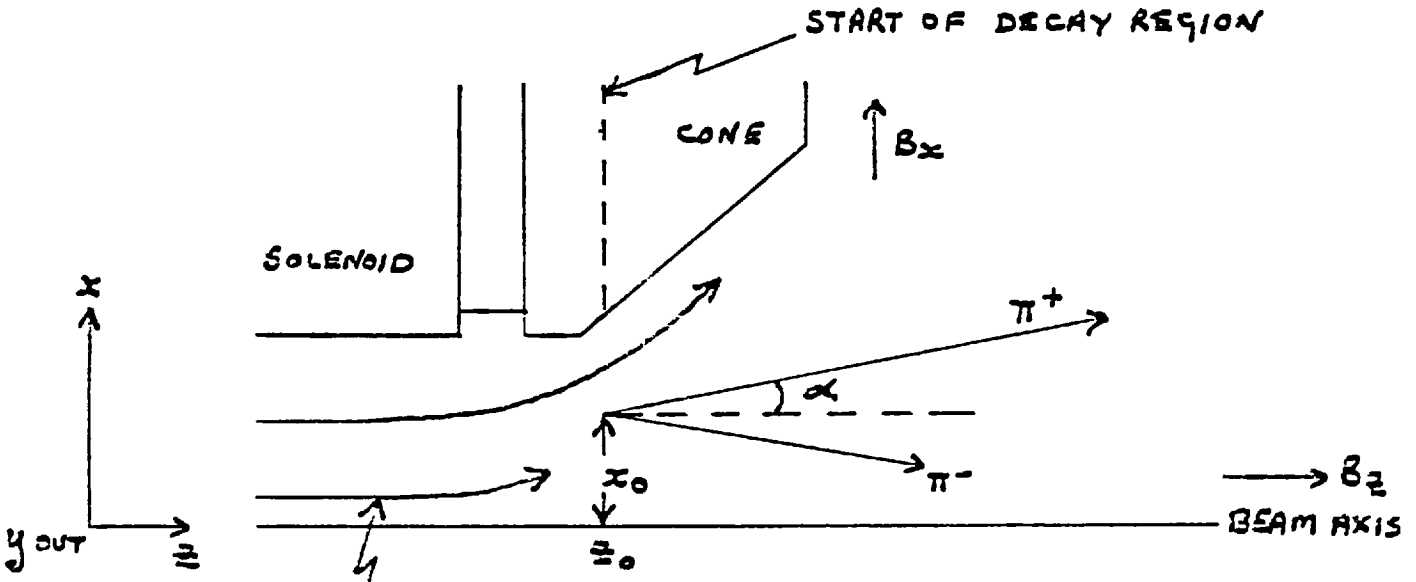

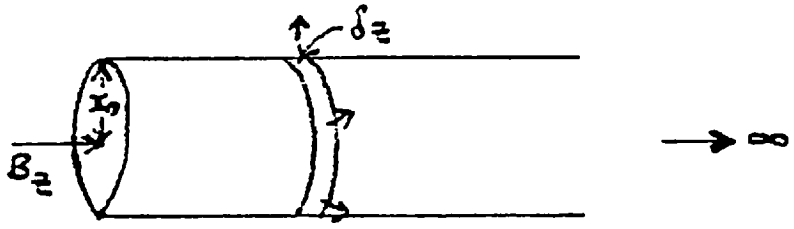

USING DIV B = 0, TOTAL FLUX OUT OF CYLINDER $= \int_{z_0}^{\infty} 2\pi x_0 \, \delta z \, B_x - \pi x_0^2 B_{z_0} = 0$

$$\Rightarrow \int_{z_0}^{\infty} \delta z \, B_x = \frac{x_0}{2} B_{z_0}$$

Fig III.9 EFFECT OF FRINGE FIELD ON π TRAJECTORIES

CHAPTER IV

DATA TAKING AND ANALYSIS

IV.1 Data Taking

The data taking sequence is shown in Fig. IV.1. The solenoid was pulsed once every five seconds to coincide with alternate bursts of fast spill from Nimrod. The data from the intermediate bursts was then used to compare $K_L^o \to \pi^+\pi^-$ rates with and without the magnetic field. The 0.4msec. fast spill was immediately followed by slow spill ($\sim$0.5 sec.). Data from this was used in analysis to set up cuts and to monitor the fast spill event reconstruction. The data taking gate, which spanned both the fast and slow spill, was used to indicate the start and end of burst for the DDP 516 computer.

Before the extraction of fast spill, a trigger pulse was sent from Nimrod as shown in Fig. IV.2. This was used to trigger the solenoid and also to open the fast spill gate which enabled a 10^5 Hz event clock to start scaling. The beam and solenoid sampling procedure was then started, 13 μsecs. later, using a device known as the beam 'bacon slicer'. This generated a train of 10 gates, each 70 μsecs wide. Each gate was used to enable a pair of CAMAC scalars which then recorded the beam counting rates and solenoid ADC levels for that 'slice'. The ADC's were sampled using a 10nsec. gate generated from the leading edge of each bacon slice and their thresholds taken from the intervening bursts without the solenoid.

The values obtained for the field, as a percentage of B_{max}, using the I toroid ADC data are shown in Table IV.1 together with

a plot of the field in Fig. IV.3. The results show that the magnetic field was very reproducible from run to run with changes of less than 2% at each bacon slice. Therefore in the analysis program the magnetic field was not worked out explicitly for each event but rather the events were required to come within a certain range of clock counts. The event clock counts corresponding to the start of each slice are shown in the Figure, together with the counts required for the field to be > 200 kg and > 225 kg. During data taking checks were made to ensure that the peak field was aligned with maximum spill and typical beam monitor counts from each slice are shown in the Figure. The alignment was not done to the event trigger distribution due to accidental events which distort the true event distribution, particularly in the high spill region.

In conjunction with the beam bacon slicer there was a second sampler known as the solenoid bacon slicer which was used by the 516 to monitor the I toroid, voltage and microphone diagnostics across the whole of the solenoid pulse. This sampled the ADC's at 600 μsec intervals using 8 gates (Fig. IV.2). The first gate was opened before the solenoid pulse to give information on the starting bank voltage. The computer gave warnings if ADC levels changed by more than 5%, and inhibited the charging and fire sequences for changes above 10%.

During each burst from Nimrod, events were stored in a fast memory buffer to reduce the loss of spill from event read in time. The memory was enabled by the event trigger as shown in Fig. IV.4 and the status of the bit pattern register and event clock recorded. The register was used to record the trigger counters involved in the event and to indicate whether the event took place in fast or

slow spill. Drift chamber time digitizings were recorded for up to 500nsecs. after the receipt of the event trigger. The event trigger was also used to gate in the wire hits from the MWPC multiplexers. The average event read in time was 25-30μsecs. during which further data taking by the experiment was vetoed. Scalars recording counting rates were inhibited during such vetoes to ensure correct normalisation. Separate sets of CAMAC scalars were used for the fast and slow spill.

At the end of burst, the CAMAC scalars, bacon slicers and the fast memory were read out to the DDP 516 disk and from there onto 7-track magnetic tape. A flag was set for the burst if the solenoid had been fired. The data on tape was stored in blocks, with the first block containing the solenoid flag together with the CAMAC and bacon slicer data. This 'End of Burst' block was used to indicate the number of data blocks following containing the event data from the fast memory. Events were written out in reverse order, with the event header appearing last, so that in the analysis event decoding was done by working through the data blocks backwards.

Between bursts the 516 was used to update histograms and scalar tables and to undertake a cursory event analysis for the 516 display. The tables were used to compare field on and field off counting rates from the CAMAC scalars. Typically these rates were within 5% of each other, with the excess usually on the solenoid side. Fluctuations greater than this usually indicated pickup, and such runs were halted to allow the solenoid rig to be checked.

Each run was about 3 hours long and contained about 700 events from both types of fast spill (field on and field off), and about 1200 events from the slow spill. At the end of each run, the

accumulation of CAMAC data was printed out for checks on the relative timing of the beam intensity distribution and the solenoid magnetic field together with checks on multiplicity and wire distributions for the MWPC's and drift chambers. About three runs were stored on each 7-track tape. These were later condensed onto 9-track tape for analysis with each tape containing about 10 runs.

IV.2 General Summary of Analysis

The data presented in this thesis concerns runs 182-297 from the last data taking period, that of Nov/Dec 1977. Earlier runs have not been included since they were at high beam rates and were without M3. The solenoid was pulsed to a maximum field of 250 kg throughout with data taken from about $2.2 \cdot 10^5$ pulses.

The runs were analysed on the I.B.M. 360 computer at the Rutherford Laboratory using a program called CP168. Events from the three types of data - field on fast spill, field off fast spill and slow spill - were analysed separately using the solenoid flag from the End of Burst data and the fast and slow spill flags from the bit pattern register. Apart from this initial sorting procedure the analysis was identical for all events. Low transverse momentum events were written out to disk and categorized according to spill. These events were then used to obtain the $K^0 \to \pi^+\pi^-$ decay distributions.

IV.3 Event Reconstruction

The main features of event reconstruction are shown in Fig. IV.5 together with flow diagrams describing the geometric reconstruction and momentum fitting in Figures IV.6 and IV.7. Only 'cowboy' vee events were detected and analysed by the spectrometer system with the positive and negative tracks passing through the left and right sides of the spectrometer respectively before being brought back together downstream. Tracks were first found through DC1 and DC2 where pions from K^o decays are usually well away from the beam region and the products of neutron interactions. Horizontal and vertical positions were then found at the median plane of M1/2 by combining the wire information from M1 and M2 and assuming the chambers to be coplanar. Errors in the vertical reconstruction from tracks in the horizontal plane crossing M1/2 at large angles were corrected for using the slope of line AB. This is shown in Fig. IV.5 which shows the wires which should have fired (dashed lines) if the tracks had passed normally through M1 and M2.

As a consequence of the near circular trajectory of a pion through the spectrometer, AB was required to intersect with ED (from the straight line fitting in DC3, 5, 7) at C within narrow bounds along Z (70mm.). This was a powerful cut in reducing background from accidental tracks and for eliminating events which were accidental coincidences between the upstream and downstream ends of the apparatus. In the vertical plane, DC8 was used to solve the ambiguity which arises when different vertical positions in M3, associated with positive and negative tracks in the horizontal, can be fitted with the same points at DC4 and DC6.

Momentum fitting was done using a quintic spline model for each track [13]. Resolutions of 0.8mm. for the MWPC's and 0.5mm. for the drift chambers were used to find the best track fit and to calculate chisquared. To find the vertex position and to account for the magnetic field where no detectors were present, the spline model was fitted to the magnetic field at twenty reference planes along Z. The vertex was found from the crossover point of the two tracks in the horizontal plane using the four reference planes from the start of the decay region to M1. Events upstream from Z=0 were found by extrapolating tracks from the first reference plane. To check the vertex reconstruction a glass sheet 1.5mm. thick was placed in the beam line near the start of the decay region. Neutron interactions in the glass were detected by the spectrometer using the full event trigger to ensure two charged particles from the interaction. The reconstructed events are shown in Fig. IV.8. The peak has a f.w.h.m. of 6mm. suggesting that decays are reconstructed to within ±3mm. This agrees well with the Monte Carlo results in section II.3.

From Monte Carlo studies the pions from K^o decays were found to crossover downstream within the beam region and within certain bounds along Z. Therefore analysis was biased towards this type of event by requiring tracks to crossover within 50mm. of the beam axis. This is shown by point F in Figure IV.5. Finally the track combination with lowest P_T was chosen for the event. In calculating P_T, the values of P_X and P_Y were corrected to account for a systematic shift in the distributions from zero and this is discussed further in the next section. Events with low P_T were then written onto disk.

Two examples of reconstructed $K^o \to \pi^+\pi^-$ decays from slow spill and fast spill (field on) are shown in Figures IV.9 and IV.10 respectively. NV(1) and NV(2) give the total number of positive and negative tracks found in each event. The multiplicity of tracks is nearly always due to drift chamber ambiguities for tracks passing near sense wires and therefore such trajectories tend to be very closely related. The raw wire data from M1, M2 and M3 is shown in the box.

IV.4 Leptonic and $K^o \to \pi^+\pi^-$ Distributions

The $K^o \to \pi^+\pi^-$ signal was extracted from the events on disk by making cuts on P_X, P_Y and effective mass. These distributions are shown in Figures IV.11, IV.12 and IV.13 respectively for events in the decay region (Z>0) with the field above 225 KG. The histograms contain about 80% of the $K^o \to \pi^+\pi^-$ events found in the analysis. Data from slow spill is also shown to aid comparisons between the field on and field off data and to show that the systematic shifts in the P_X and P_Y distributions were not a consequence of fast spill but inherent in the apparatus.

The P_X distributions, in Figure IV.11, are shown after making cuts on P_Y and effective mass. The distribution for field on shows little if any broadening due to fringe field effects from the solenoid. However all the P_X distributions show a systematic shift from zero by about - 2.5 MeV/c. The reason for this is not known but may be due to slight asymmetry in the magnetic field about the beam axis since the grid of points of the magnetic field map used in the spline fitting was taken from only one quadrant of the magnet. Contributions to P_X from errors in chamber position (particularly

the MWPC's) are unlikely since the corresponding shift in P_X for each track tends to compensate. Cuts of ±6 MeV/c were therefore made about - 2.5 MeV/c to extract the $K^o \rightarrow \pi^+\pi^-$ signal.

The P_Y distributions are shown in Fig. IV.12 after making cuts on P_X and effective mass. The field on distribution shows some broadening with respect to the field off and slow spill distributions as was expected from the calculations on the effect of the fringe field in Chapter III. The f.w.h.m. for slow spill and field off is about 6 MeV/c whereas for the field on it is about 8 MeV/c. Assuming the curves to be gaussian then the loss of events due to the broadening is less than 3% for cuts on P_Y at ±8 MeV/c about the centre of the distribution. A direct examination of the histogram agrees with this and suggests that broadening losses can be neglected. All the histograms show a systematic shift of - 1 MeV/c so the cuts were made about this to extract the two pi signal.

The effective mass was found by assuming that both tracks were pions. The mass plots for the three different data samples (field on, field off and slow spill) are shown in Figure IV.13 using the P_X and P_Y cuts mentioned above. They all show a good $K^o \rightarrow \pi^+\pi^-$ peak at 496 ± 8 MeV/c^2. The slow spill data has been normalized to the number of $K^o \rightarrow \pi^+\pi^-$ events found in the fast spill (115 slow spill events against 116 for field on and 114 for field off). By comparing the slow spill distribution to the field on and field off, one can gauge the amount of broadening at the base of the peak from $K^o \rightarrow \pi^+\pi^-$ decays which have been fitted with incorrect tracks in fast spill. This appears to be

slightly worse for field on, below the cuts for $K^o \to \pi^+\pi^-$, though the extra events in this region may be K^o decays from the high field region with incorrect vertices in the decay region and this is discussed later. The field off data, on the other hand, shows extra events on the high mass side which suggests that the losses in both distributions are probably equal and any differences likely to be negligible.

The momentum spectra for $K^o \to \pi^+\pi^-$ are shown in Figure IV.14 for all events in the decay region (no cuts on field). The spectra peak at around 1.3 GeV/c and follow the same fall off to 3 GeV/c as was found with the K^+ spectrum in Section II.2. Below 1 GeV/c the spectra fall off sharply due to the low geometrical efficiency between 0.5 and 1.0 GeV/c. The Monte Carlo calculation described in Section II.3 predicted a leptonic background of about 12% for $K^o \to \pi^+\pi^-$ at 1.5 GeV/c. This is consistent with the background seen in the tail of the slow spill mass distribution in Figure IV.13. The background was subtracted from the $K^o \to \pi^+\pi^-$ data used in the statistical analysis in Chapter V, together with the background from K^o regeneration which is calculated in the next section.

Total event rates for the experiment are shown in Table IV.2 and represent data from about $2.25 \cdot 10^5$ bursts from Nimrod for both field on and field off. The beam monitor counts for field on and field off were within 0.5% of each other so no renormalisation to beam spill was required. The slow spill data was normalised to the beam received in fast spill and used to compare event rates. From the table one can see that the total number of triggers in fast spill for field on and field off are almost identical and are about twice the number formed in slow spill. This indicates an accidental trigger rate in fast spill of about 50%.

The total number of 'vee' events reconstructed by the analysis program is given in the next column, for those from the decay region (Z>0) and for those upstream coming from the solenoid region (Z<0). Event reconstruction in fast spill was about 10-15% lower than in slow spill, probably as a result of drift chamber inefficiency in fast spill. Apart from about 2.5% which were designated as $K^o \to \pi^+\pi^-$ decays, all the 'vees' were attributed to K^o leptonic decays. These provide a useful check on the performance of the experiment since the leptonic decay rate over the decay region should remain constant whether or not CP symmetry is restored. After subtracting the $K^o \to \pi^+\pi^-$ events, one obtains about 5260 leptonic events with the field on against about 4860 with the field off. This gives a statistically significant ($\sim$5 std. dev.) 8% excess of leptonic events in the decay region with the field on.

The situation persists for leptonics written to disk with low transverse momenta as given by the penultimate column in Table IV.2, though the excess is much less significant ($\sim$1-2 std. dev.). The decay point distributions for these events are compared in Figure IV.15(a) after making cuts for B > 225 KG. The distributions contain about 90% of the leptonics written to disk. The number of events occurring with Z>0 and Z<0 are shown in Table IV.3. The outline of the solenoid and the cone to reduce the field are shown on the figure, with a dashed line drawn on the cone to indicate the start of the decay region. Figures IV.15(b) and (c) show comparisons of the decay point distributions of slow spill events to those of the fast spill, for field on and field off respectively. In both cases the slow spill data was normalised to the same number of events in the decay region.

With the field on one would expect few events from the solenoid region because distortions to track trajectories, particularly in the vertical projection, should throw events outside the acceptance range of the spectrometer. However, in Figure IV.15(a), there appears to be no diminution of events over the high field region and indeed a general excess from Z = -40mm. to Z = 80mm. This is also the case in Figure IV.15(b) especially for Z = -60mm. to Z = 20mm. although a comparison of the 'control' data, field off with slow spill in Figure IV.15(c), shows an excess for field off over Z = -60mm. to Z = -20mm. so the discrepancies between the histograms may be partly due to the limited statistics. However the general tendency shows that the field has some effect on the leptonic decay point distribution, that it appears to allow more tracks to reach the spectrometer and that these tracks are then fitted with an incorrect vertex to give the impression of extra events in the decay region.

The tendency for extra events to be reconstructed further downstream could be serious since this could hide any depletion in the $K^0 \to \pi^+\pi^-$ rate if the magnetic field restored CP symmetry. However there are strong arguments that for $K^0 \to \pi^+\pi^-$, this effect should be small and that if it exists it should be much less than the 8% excess seen for the leptonics. From Chapter III the fringe field was shown to cause broadening to P_Y for events at the start of the decay region. The broadening on P_Y for $K^0 \to \pi^+\pi^-$ events in the solenoid would be much greater than the 1-2 MeV/c seen for 2π events in the decay region and such events should be largelyeliminated using the P_Y cuts for $K^0 \to \pi^+\pi^-$ which do not apply to the leptonic decay point distributions.

Furthermore, event reconstruction, which takes place in the horizontal plane, is sensitive to contributions to P_X. The P_X contribution for $K^o \to \pi^+\pi^-$ shows little if any broadening for B > 225 KG. Indeed even for a 2 MeV/c contribution to each track for pions with P_X of 100-200 MeV/c, the vertex error in Z would be under 5mm. for 1 GeV/c K^o decays near the start of the decay region. Thus for a K^o decay in the solenoid to be reconstructed in the decay region would surely require such contributions to P_X that the event would fail the cuts in P_X.

The total number of $K^o \to \pi^+\pi^-$ decays found by the experiment are shown in Table IV.2. The results show that $K^o \to \pi^+\pi^-$ reconstruction was only 57% efficient with respect to slow spill with 148 events found for both field on and field off in comparison to 259 for slow spill. The reconstruction efficiency was worse than that for the 'vee' events (mostly leptonics) since the leptonic events are not subject to the stringent cuts applied for $K^o \to \pi^+\pi^-$ events. The missing two pi decays are probably due to incorrect track fitting, caused largely through the ambiguities resulting from chamber inefficiency, which quickly throws two pi events outside the P_X, P_Y and effective mass cuts used to select $K^o \to \pi^+\pi^-$. The number of two pi events found in slow spill agrees well with the number expected from the K^+ measurements in Section II.2. About 3000 K^o_L were expected per burst so assuming K's at 1.5 GeV/c then the number of events expected, with a 5% detection efficiency over a decay region of 250mm., was about 300 for $2.2 \cdot 10^5$ bursts. In fact, 259 were found.

The timing for the $K^o \to \pi^+\pi^-$ events in fast spill is shown in Figure IV.16 together with the cuts used to extract events with B > 200 KG and B > 225 KG. The results are listed in Table IV.3. Roughly the same number of $K^o \to \pi^+\pi^-$ decays were found in the decay region for field on and field off at both levels of the magnetic field (to within 3%) which gives the first indication that the field was not sufficient to restore CP symmetry. 90% of the two pi events occured with B > 200 KG and about 80% with B > 225 KG.

The $K^o \to \pi^+\pi^-$ decay point distributions are shown in Fig. IV.17 for B > 225 KG with the field on and field off data compared in IV.17(a). Taking into account the limited statistics, the distributions look very similar and the $K^o \to \pi^+\pi^-$ event rate drops off as one would expect towards the high field region in the solenoid. From Z = 0 to Z = 20 there are more field on events (16 compared to 5) but this is probably a statistical fluctuation as there are 11 events on either side of this bin for the field off. The field on data is compared with slow spill data (normalised to 115 events in the decay region) in Figure IV.17(b), and the field off compared with slow spill in Figure IV.17(c). Similar histograms are shown for B > 200 KG in Figure IV.18. The field on data agrees fairly well with the slow spill decay point distribution for both B > 225 KG and B > 200 KG though a slight excess of events tends to persist from 0 to 20mm. but this is of marginal statistical significance.

IV.5 K^o Regeneration

For the experiment to be valid, K_S^o regeneration in the ½ thou' mylar window at the start of the decay region must be small in comparison to the $K_L^o \to \pi^+\pi^-$ decay rate over the first few centimetres of the decay region. The two most important types of regeneration are transmission regeneration and diffraction regeneration [14,15]. Transmission regeneration occurs through the interaction of the kaons with all the nuclei of the medium acting coherently in the forward direction. The amplitude for transmission regeneration is given by

$$\rho = -\frac{K}{2}\left(1 - e^{-m\Delta M\, D/p}\right) \quad ; \quad K = \frac{2\pi N \Delta f}{m\Delta M}$$

Where N = number of nuclei/$cm^3 \approx 10^{23}$ for mylar

$\Delta f = |f(o) - \bar{f}(o)|$, the difference between the K^o and $\bar{K}^o$ elastic forward scattering amplitudes. $\Delta f \approx 3.10^{-13}$cm. for kaons on carbon at 1.5 GeV/c [16]

m = mass of the kaon

ΔM = complex mass difference = $m_L - m_s - \frac{i}{2}\Gamma_1$, neglecting Γ_2 with respect to Γ_1

p = kaon momentum taken as 1.5 GeV/c

D = thickness of mylar = $\frac{1}{800}$ cm.

The K_S^o regenerated intensity is $\rho^2 N_{K_L}$ where N_{K_L} is the number of K_L^o entering the mylar window. This gives an estimated K_S^o intensity of $3.10^{-9}\, N_{K_L}$.

Diffraction regeneration is usually less than the transmission regeneration. The K_S^o diffracted intensity per unit solid angle is given by

$$\left(\frac{d\sigma}{d\Omega}\right)_o = |\Delta f|^2 N (1 - e^{-\Gamma_1 D m/p}) \approx 1.5 \cdot 10^{-6}$$

This gives a predicted K_S^o intensity of $1.5 \cdot 10^{-6} \pi(\Delta\theta_{meas})^2 N_{K_L}$ where $\Delta\theta_{meas}$ is the standard error in determining the K_S^o direction. With cuts on P_X of ± 6 MeV/c for kaons at ∿ 1 GeV/c or above, then $\Delta\theta_{meas} < 6.10^{-3}$ radians. This gives $K_S^o \approx 2.10^{-10} N_{K_L}$ thus showing that it is negligible in comparison to the transmission regeneration.

The regenerated K_S^o would decay over the first 5-10 cms. from the mylar window. The $K_L^o \to \pi^+\pi^-$ rate, assuming a branching ratio of 0.2%, is ∿ $2.10^{-6} N_{K_L}$ over the first 5 cms. Therefore regeneration contributes less than 0.15% to the observed $\pi^+\pi^-$ signal. Regeneration in the helium can be neglected since the density of the gas is low and the transmission regeneration goes as N^2.

From Section II.3 a leptonic background of about 12% was predicted from the Monte Carlo studies on $K_L^o \to \pi^+\pi^-$ at 1.5 GeV/c. Since the momentum spectrum for $K_L^o \to \pi^+\pi^-$ extends to 3 GeV/c (see Section IV.4), an overall background subtraction of 15% was made to the $K^o \to \pi^+\pi^-$ signal in Chapter V.

FIGURE IV.1

Solenoid firing sequence showing Nimrod bursts every 2·5 secs. Each burst has fast spill followed by slow spill.

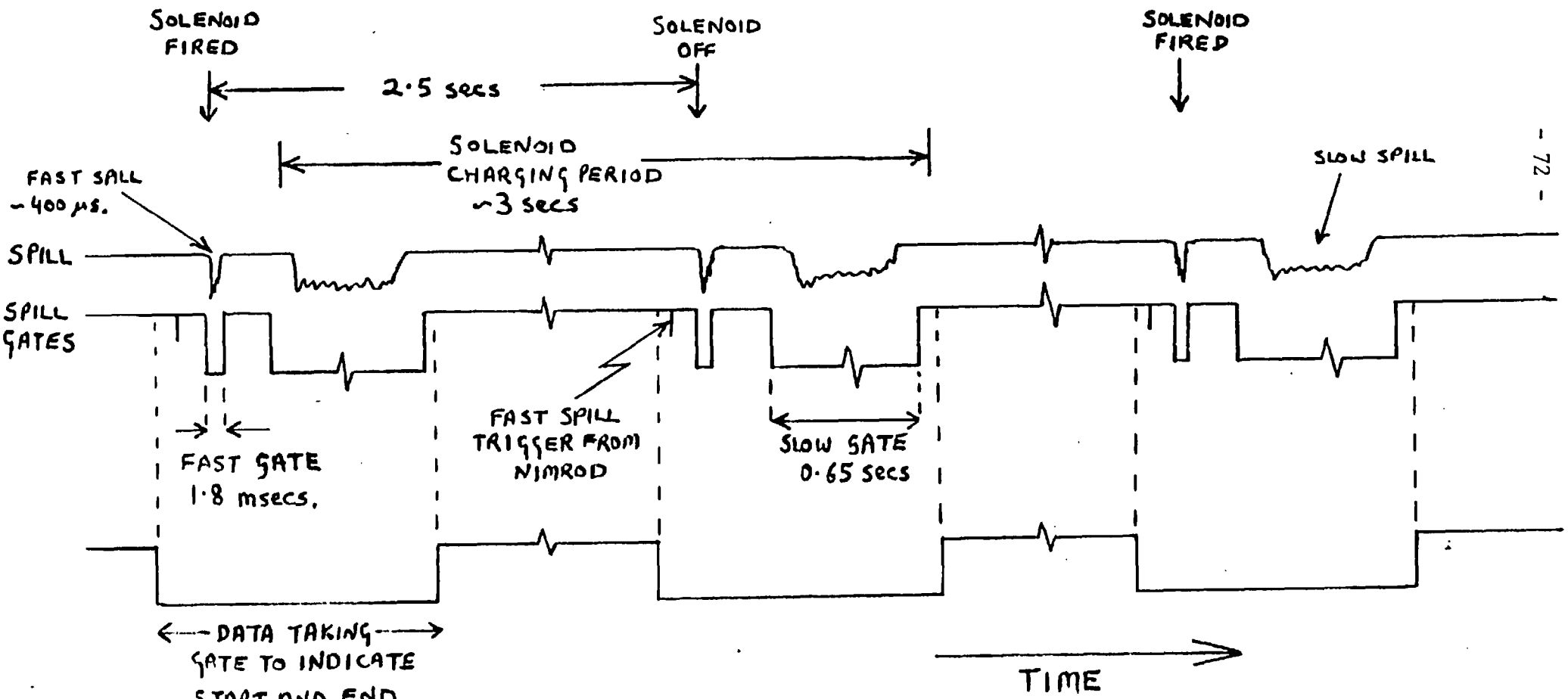

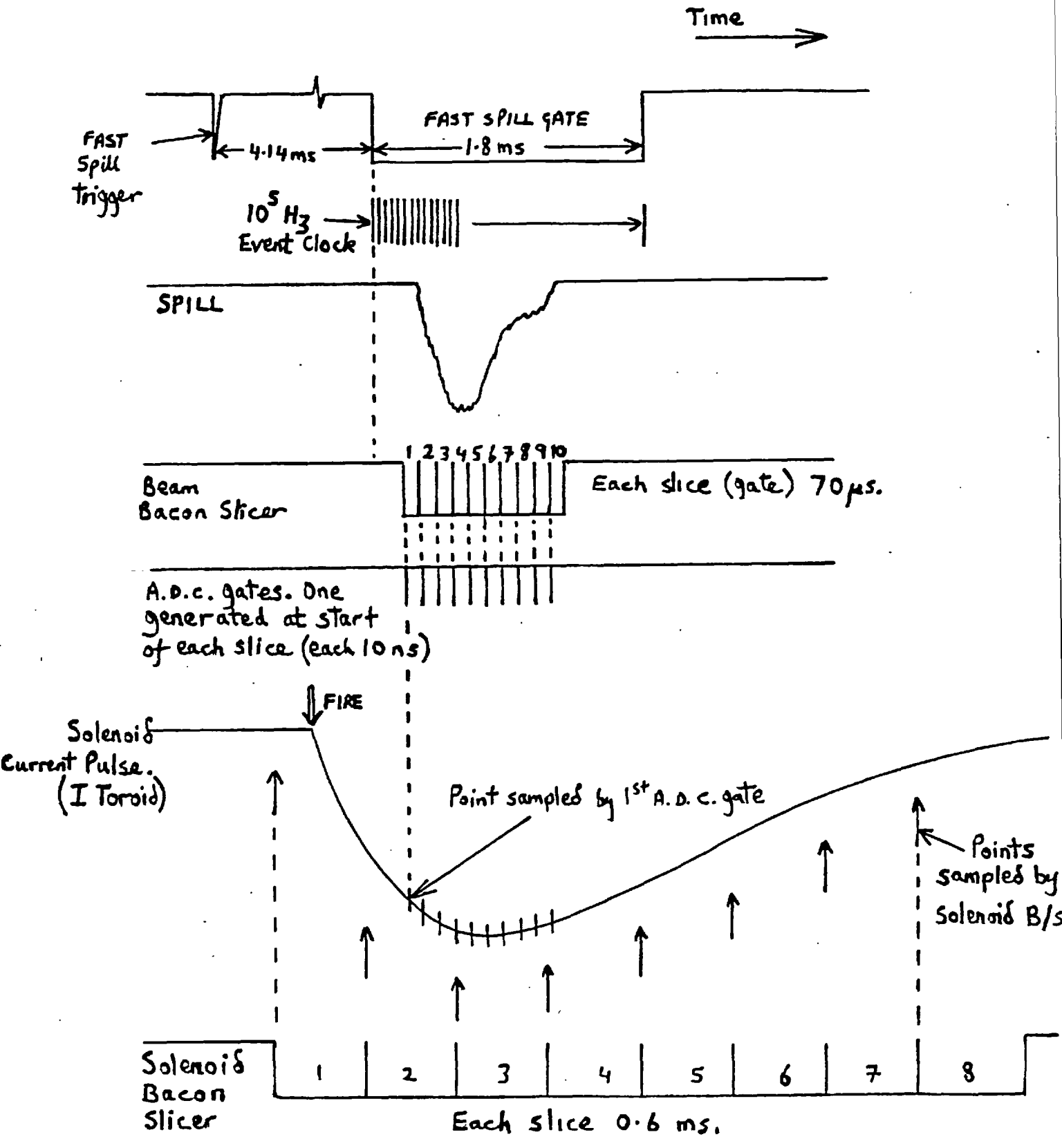

FIG IV.2 : BACON SLICER OPERATION

TABLE IV.1 FIELD VALUES FROM THE I TOROID A.D.C. DATA

$$\% \text{ OF } B_{MAX} = \frac{\text{A.D.C. LEVEL - THRESHOLD}}{\text{MAX A.D.C. LEVEL - THRESHOLD}} \times 100$$

RUN	182	189	204	231	264	280	297
SLICE 1	78%	77	77	78	77	78	78
2	86	86	86	86	85	85	86
3	92	92	92	93	92	92	92
4	97	97	97	97	97	97	97
5	99	99	99	100	99	100	100
6	100	100	100	100	100	100	100
7	99	99	99	99	98	98	98
8	96	96	96	95	95	95	95
9	91	92	91	90	90	90	90
10	87	87	88	84	83	84	84

(RUNS 182-297 COVER THE MAIN DATA TAKING PERIOD OF THE EXPERIMENT)

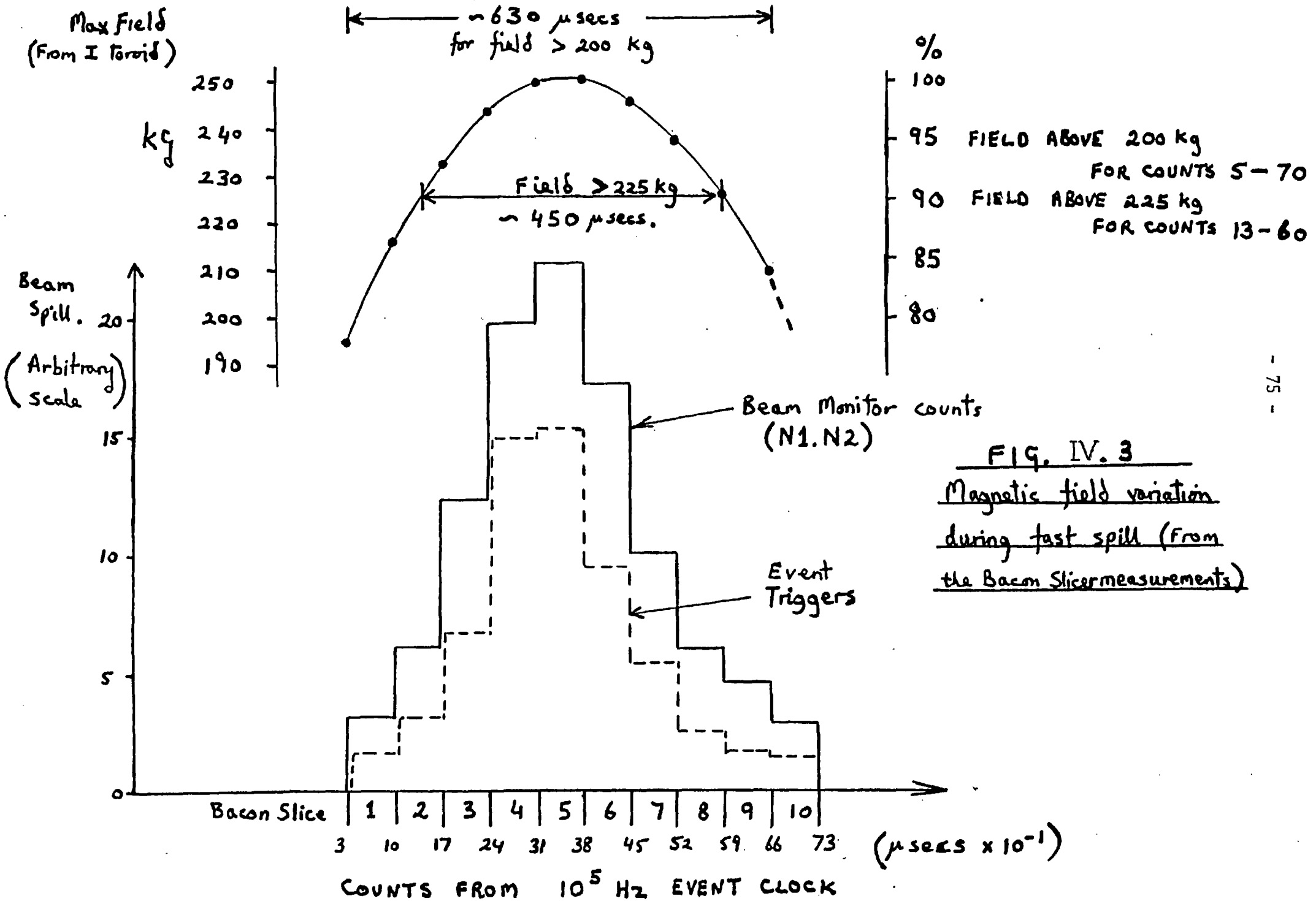

FIG. IV. 3

Magnetic field variation during fast spill (from the Bacon Slicer measurements)

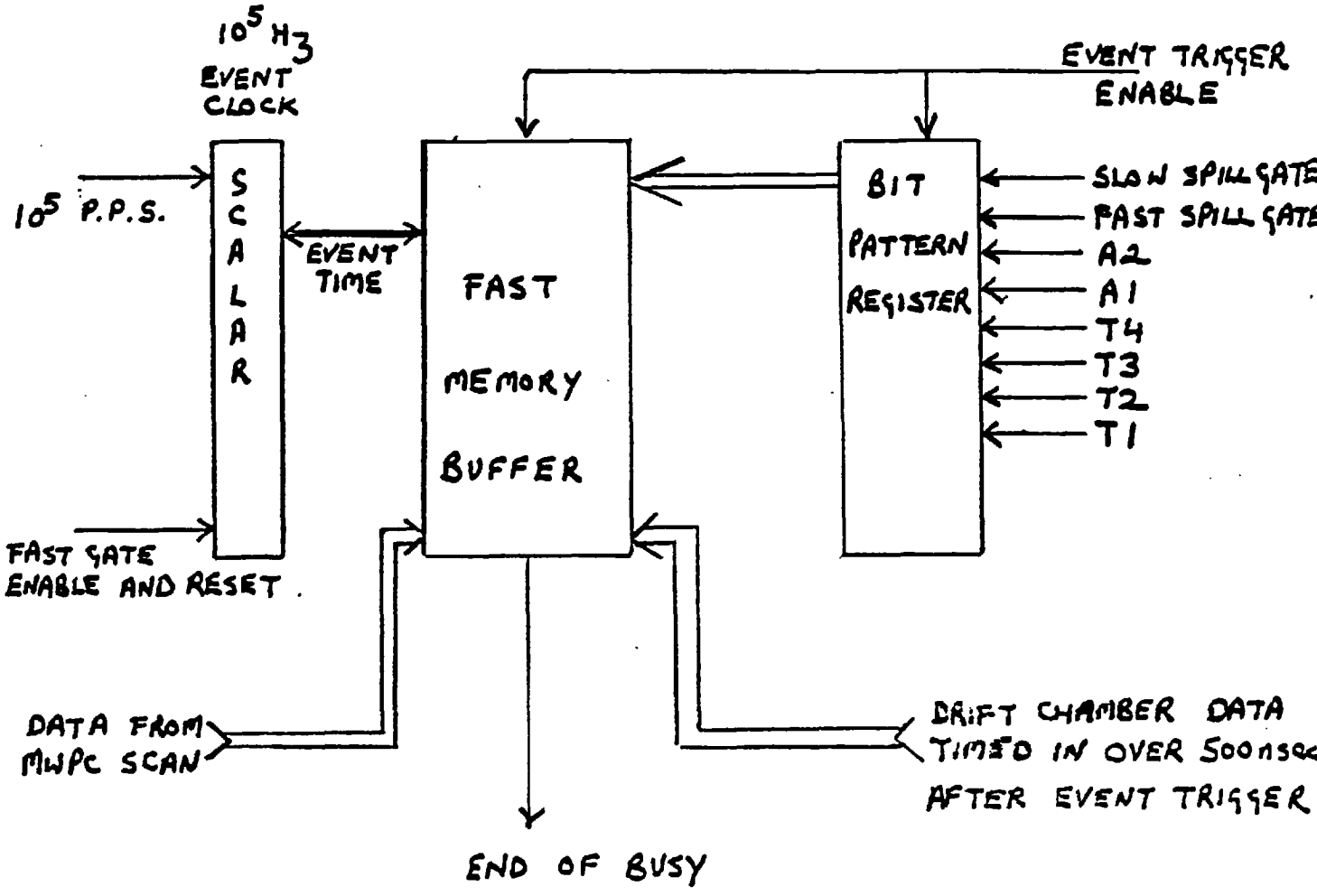

FIG. IV.4 STORAGE OF EVENT DATA DURING BURST

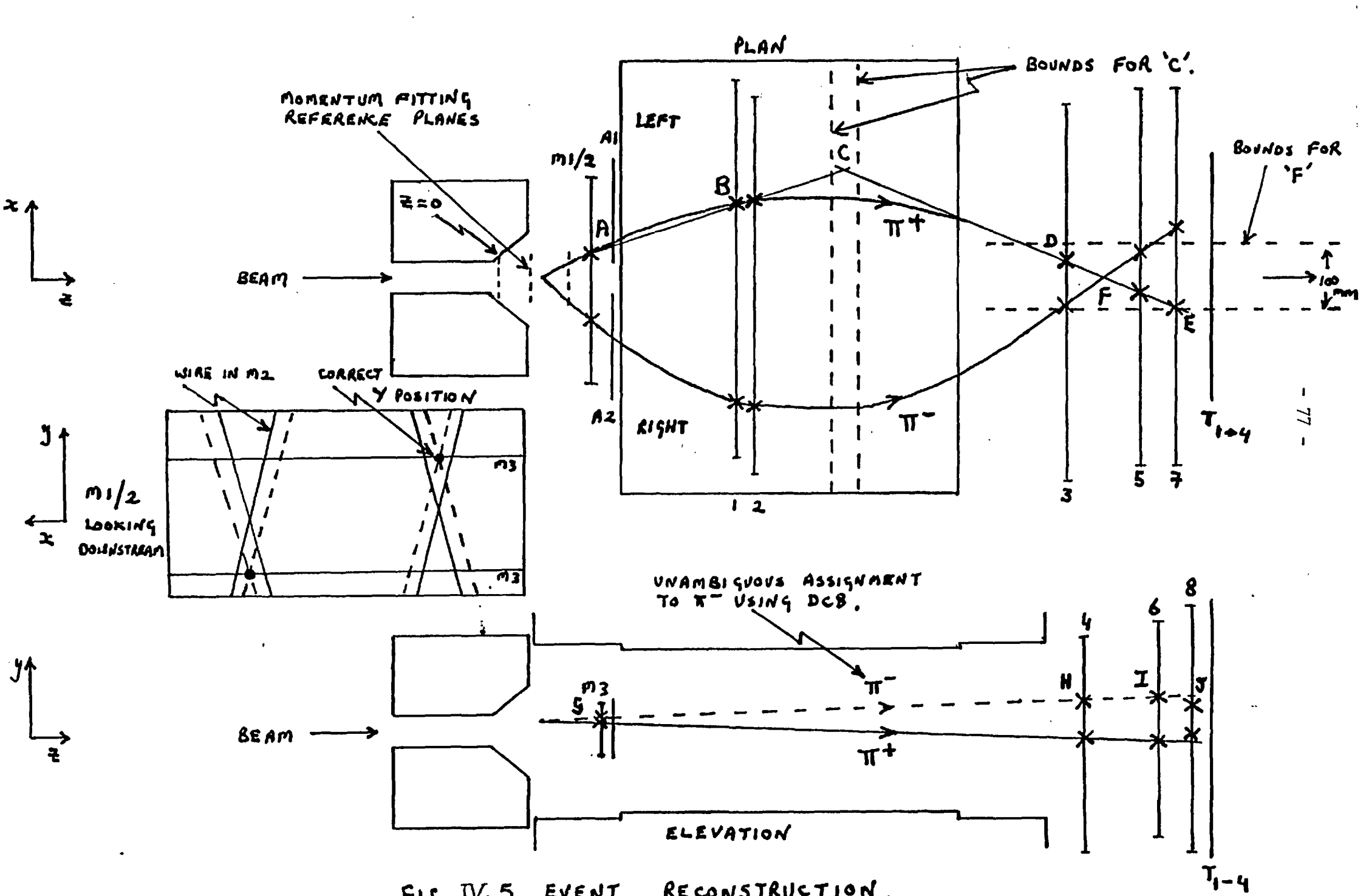

FIG IV.5 EVENT RECONSTRUCTION.

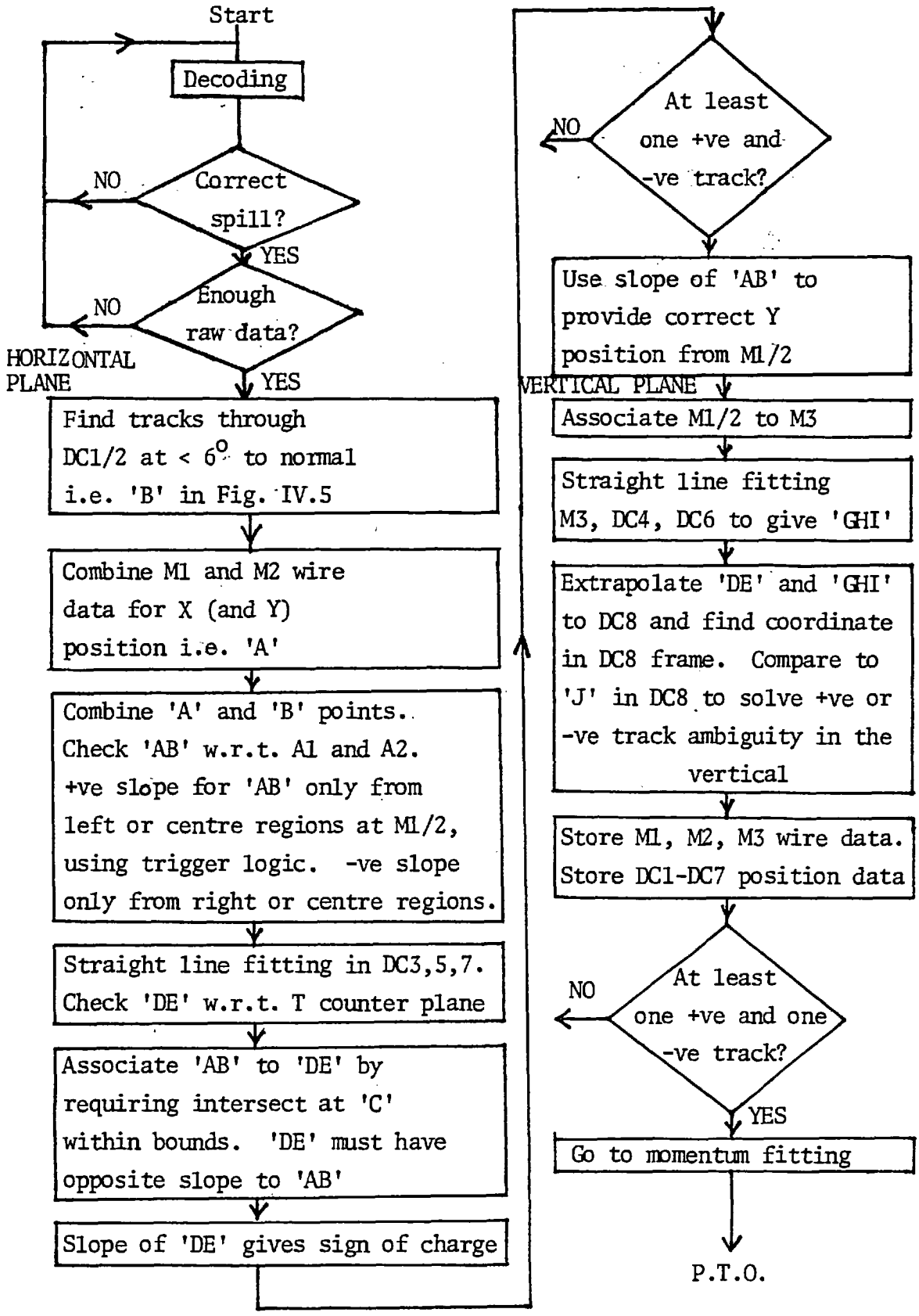

Figure IV.6 Flow Diagram for the Geometric Reconstruction

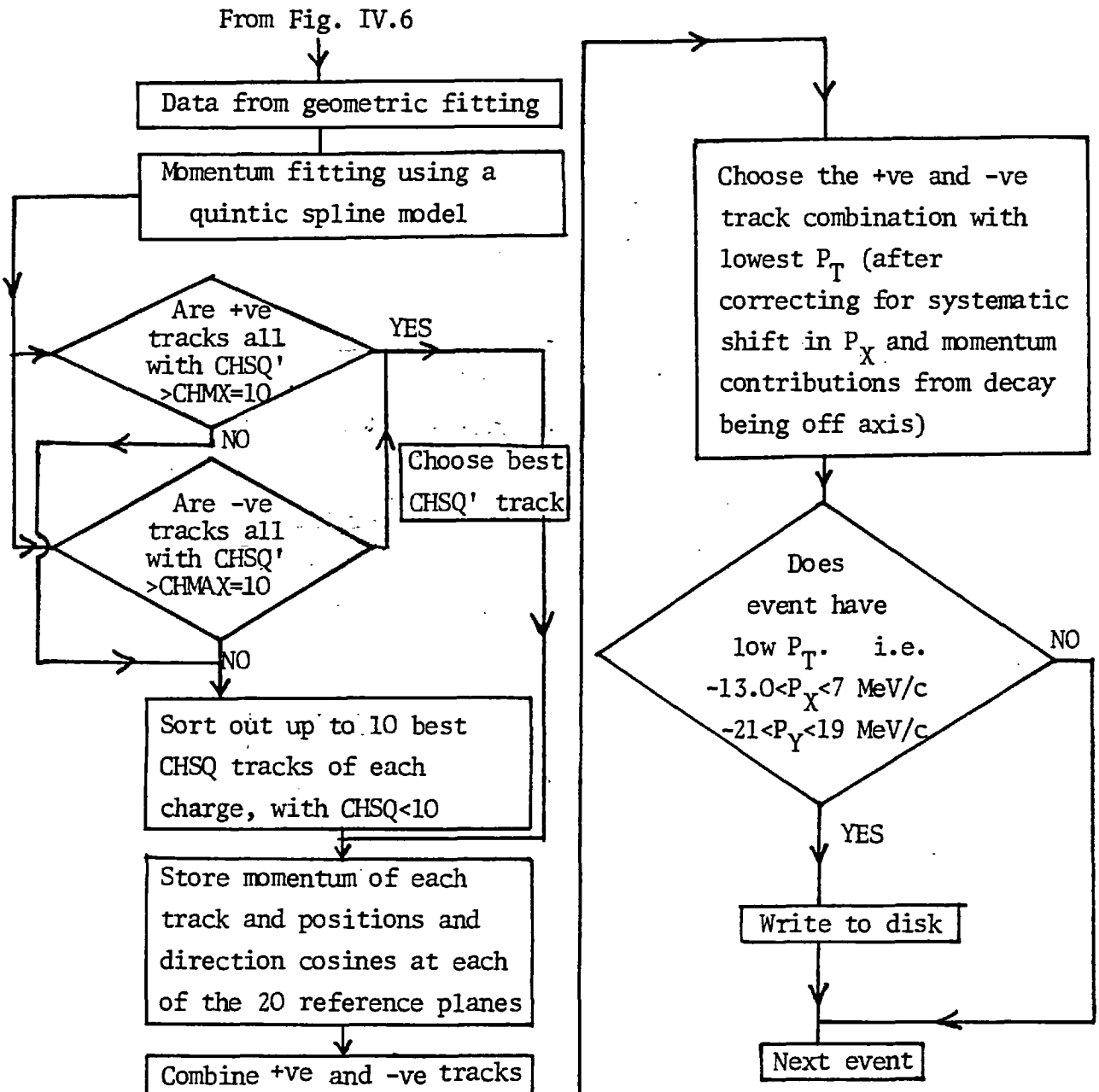

Figure IV.7 Flow Diagram for Momentum Fitting

FIG IV. 8 VERTEX RECONSTRUCTION USING 1·5 mm GLASS SHEET IN BEAM LINE (SLOW SPILL)

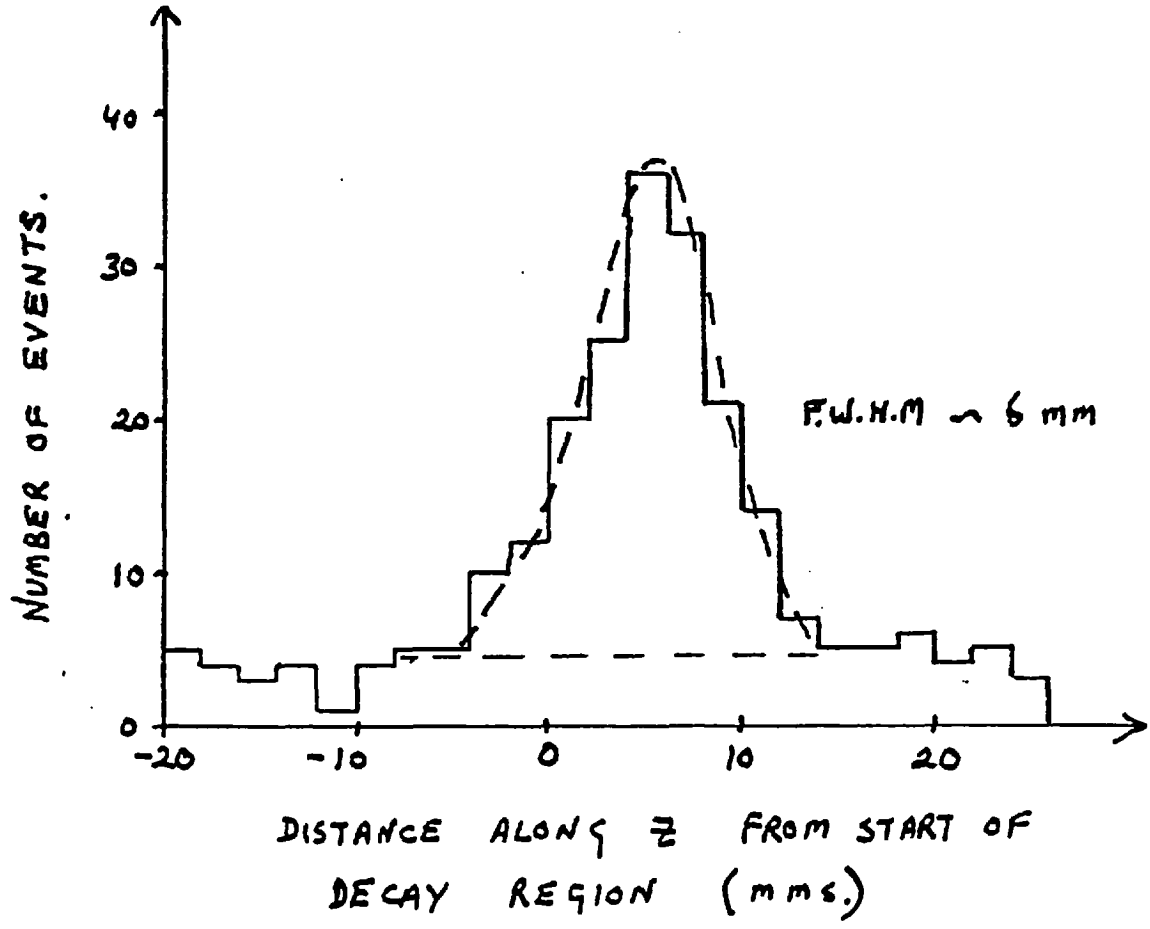

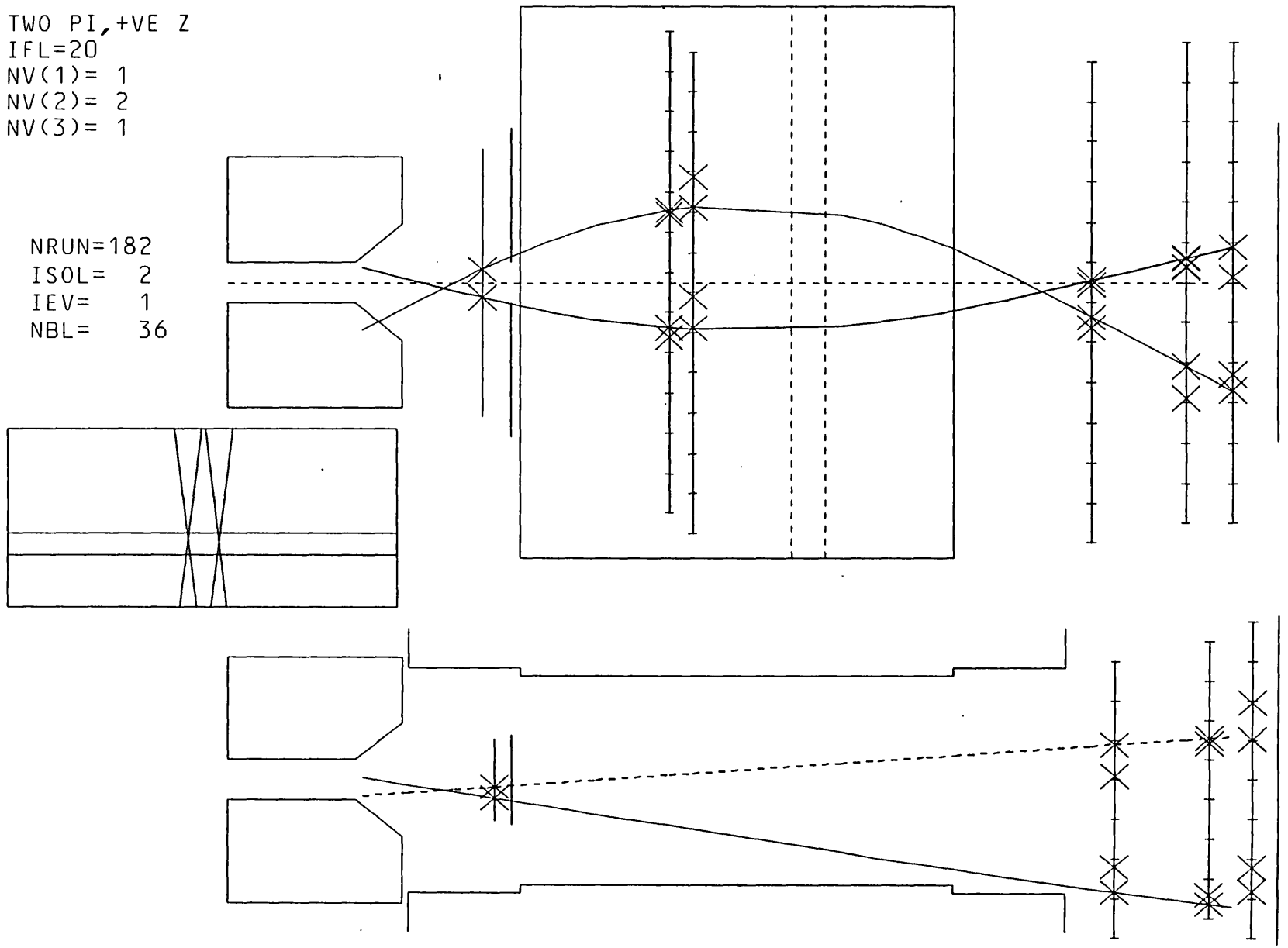

FIG. IV.9 Reconstructed $K^{o} \rightarrow \pi^{+}\pi^{-}$ event from slow spill.

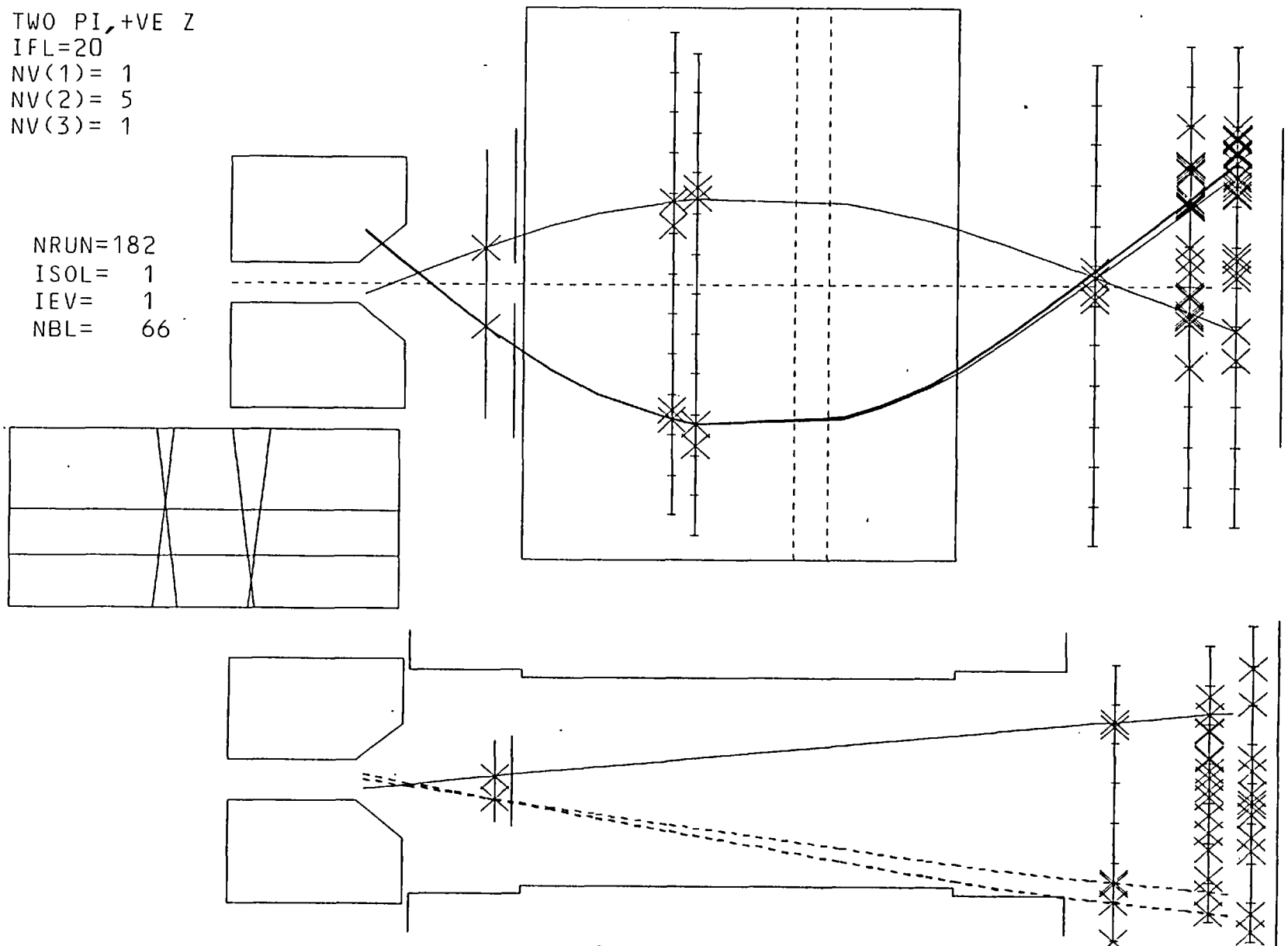

FIG. IV.10 Reconstructed $K^{\circ} \rightarrow \pi^{+}\pi^{-}$ event from fast spill, field on.

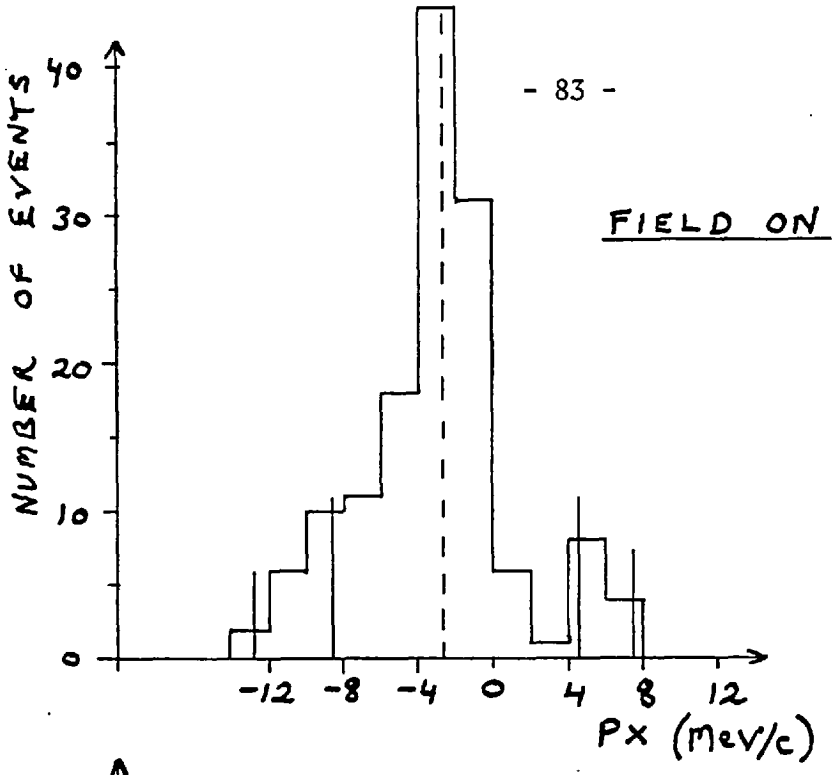

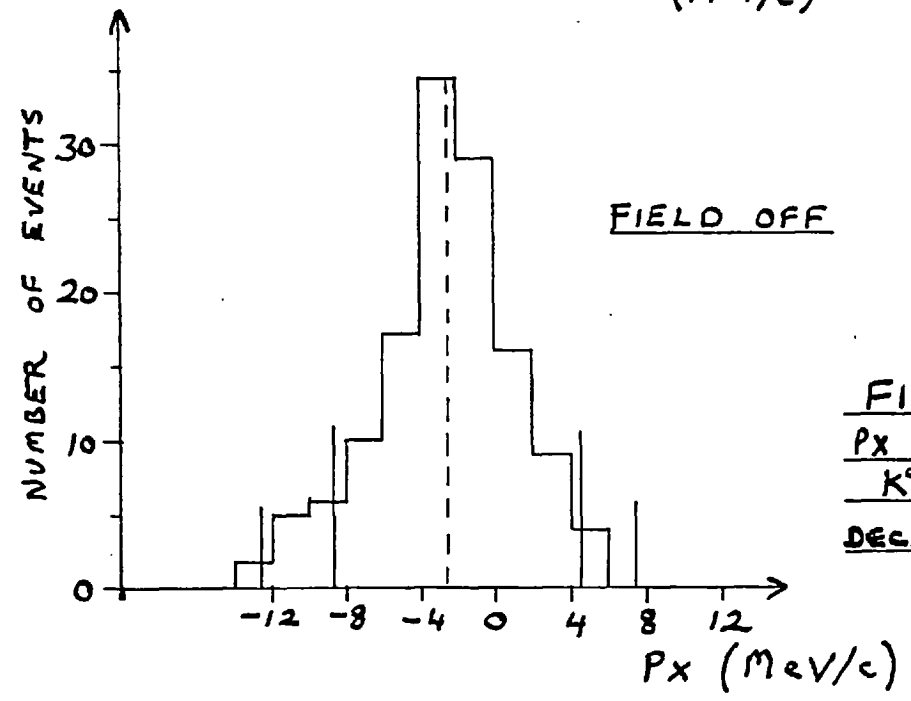

FIGURE IV. 11
Px DISTRIBUTIONS FOR $K^0 \rightarrow \pi^+\pi^-$ EVENTS IN DECAY REGION, B>225 kG

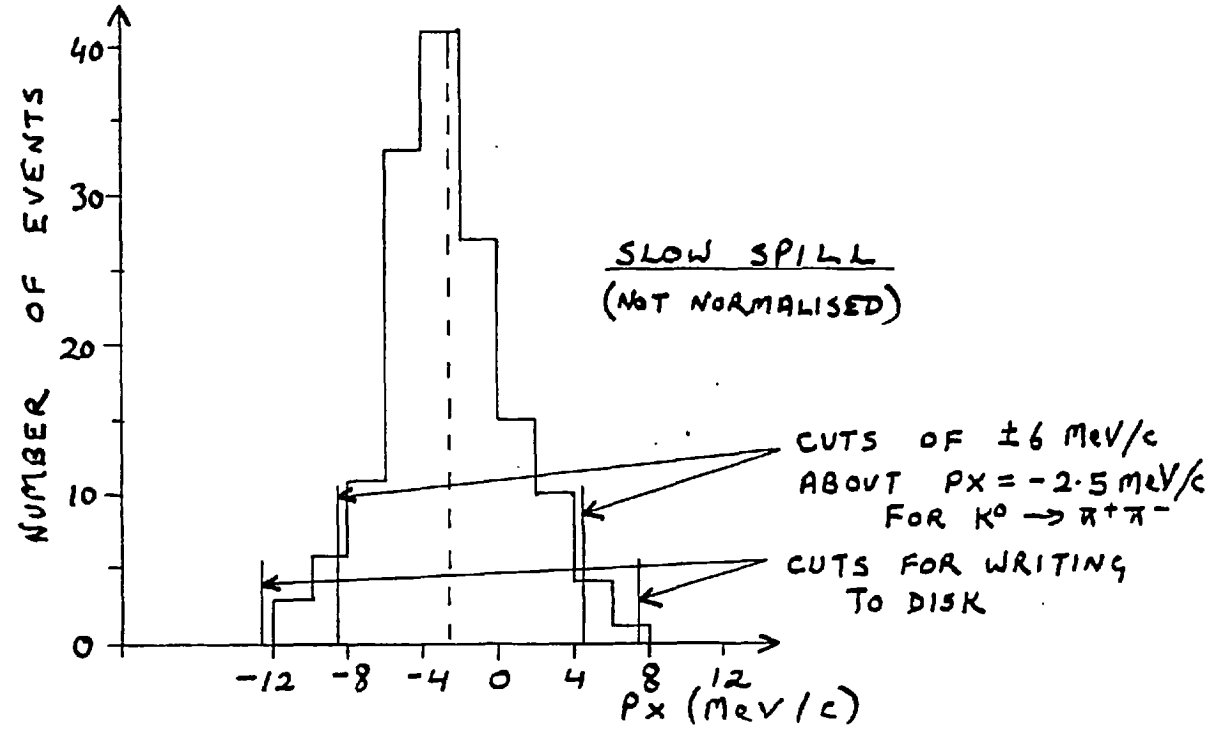

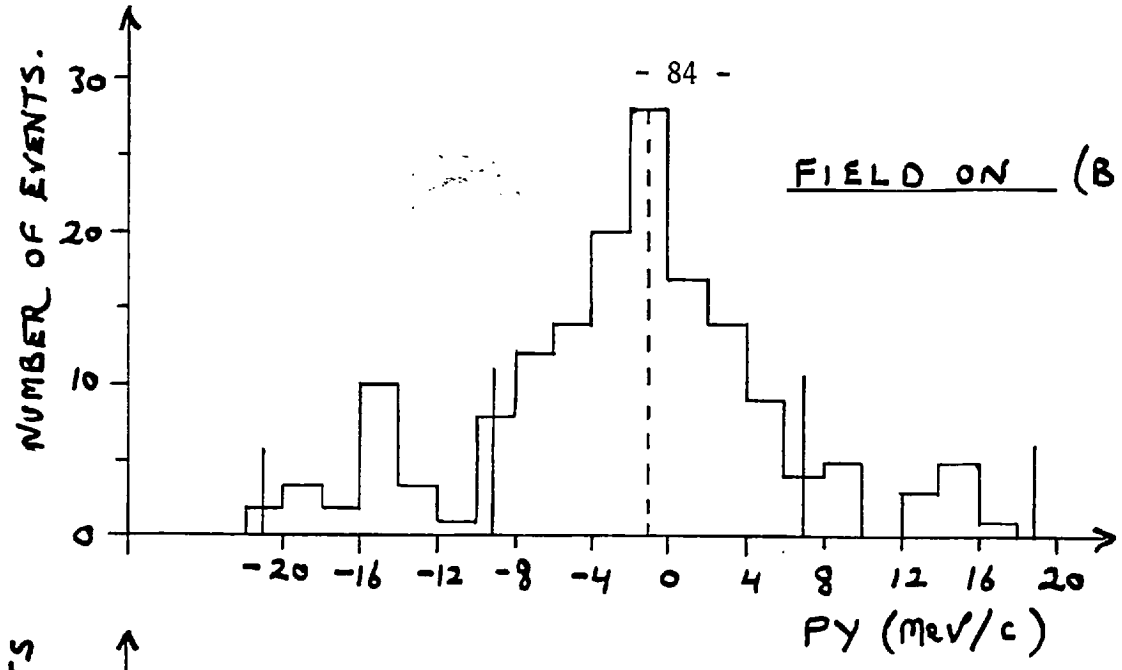

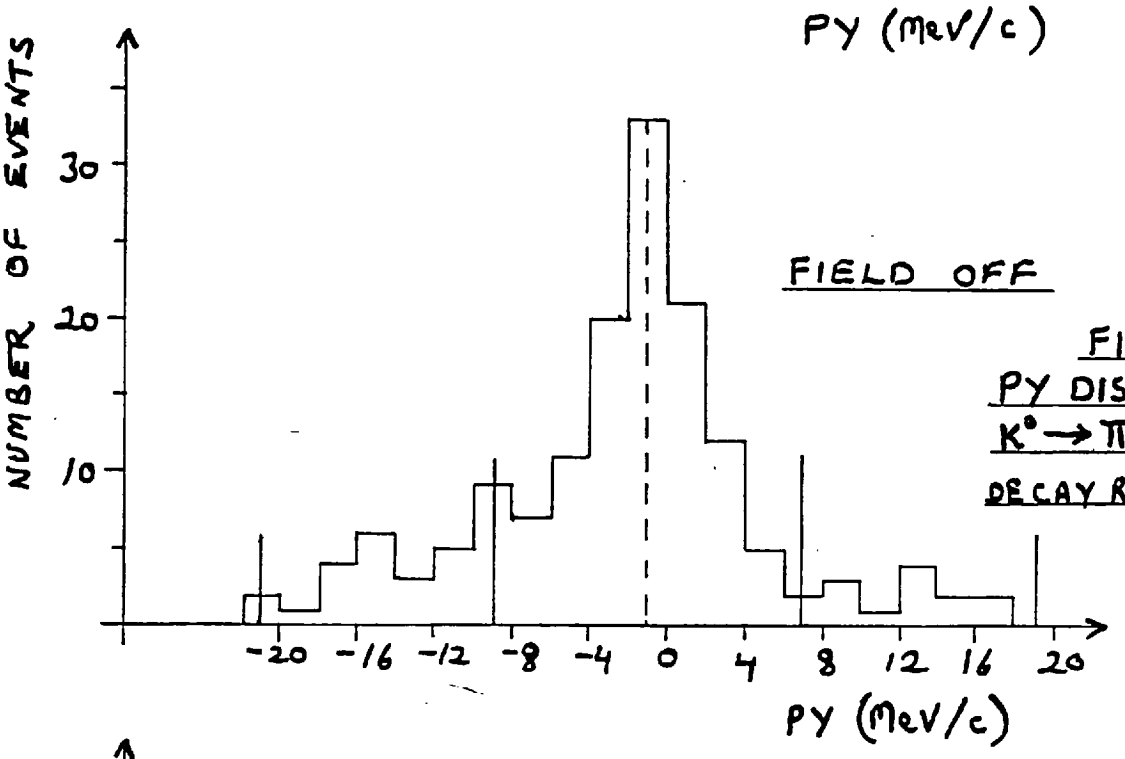

FIGURE IV.12
PY DISTRIBUTIONS FOR $K^0 \rightarrow \pi^+\pi^-$ EVENTS IN DECAY REGION, B > 225 kG

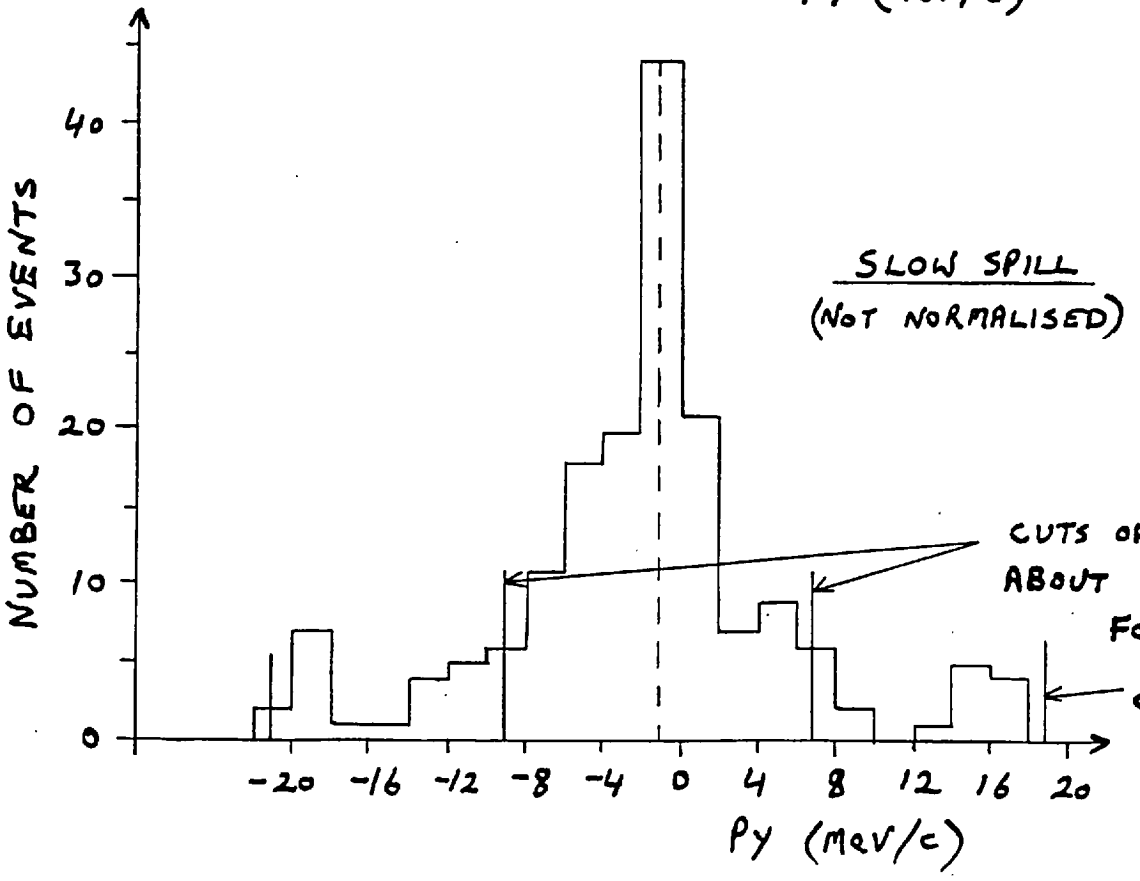

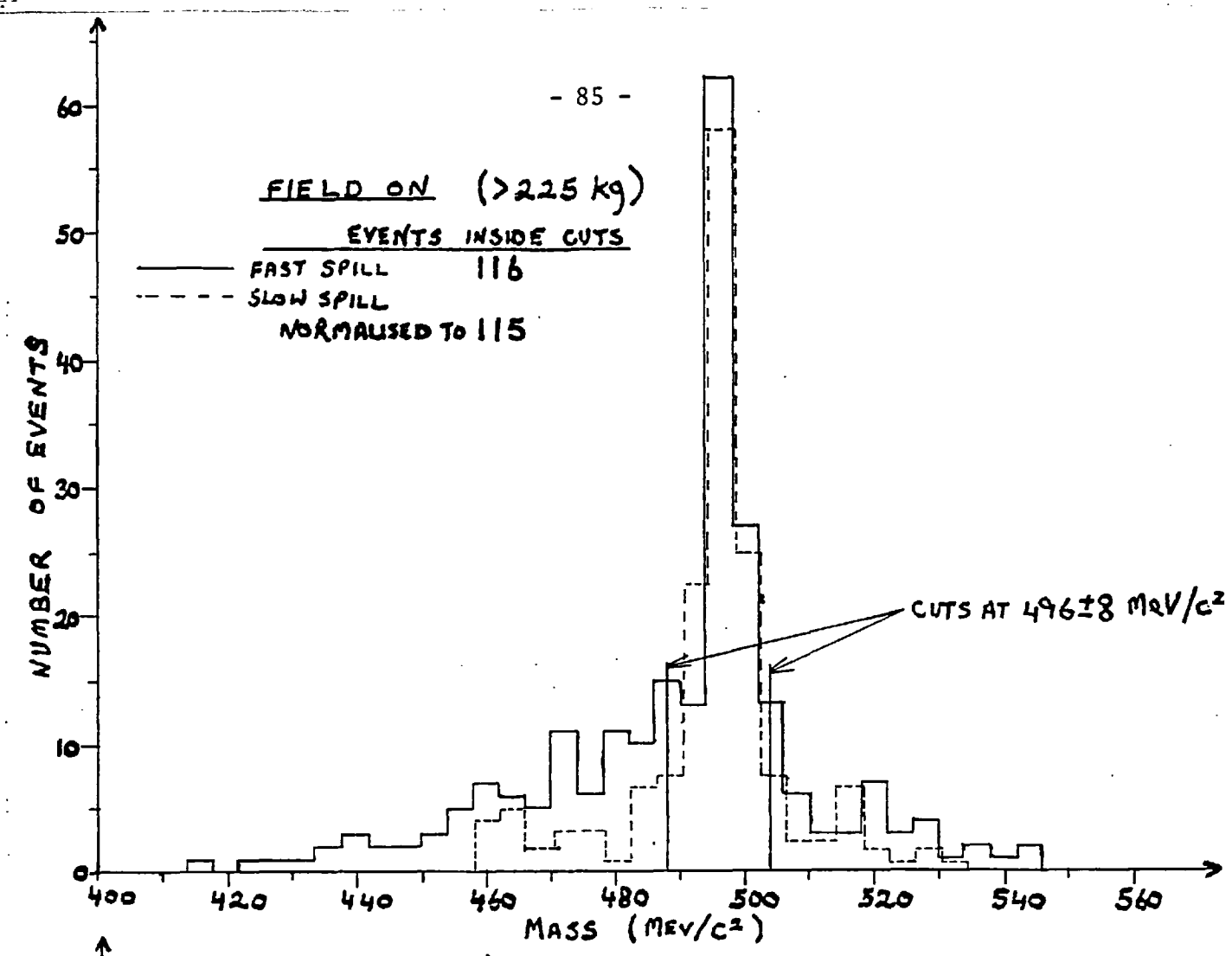

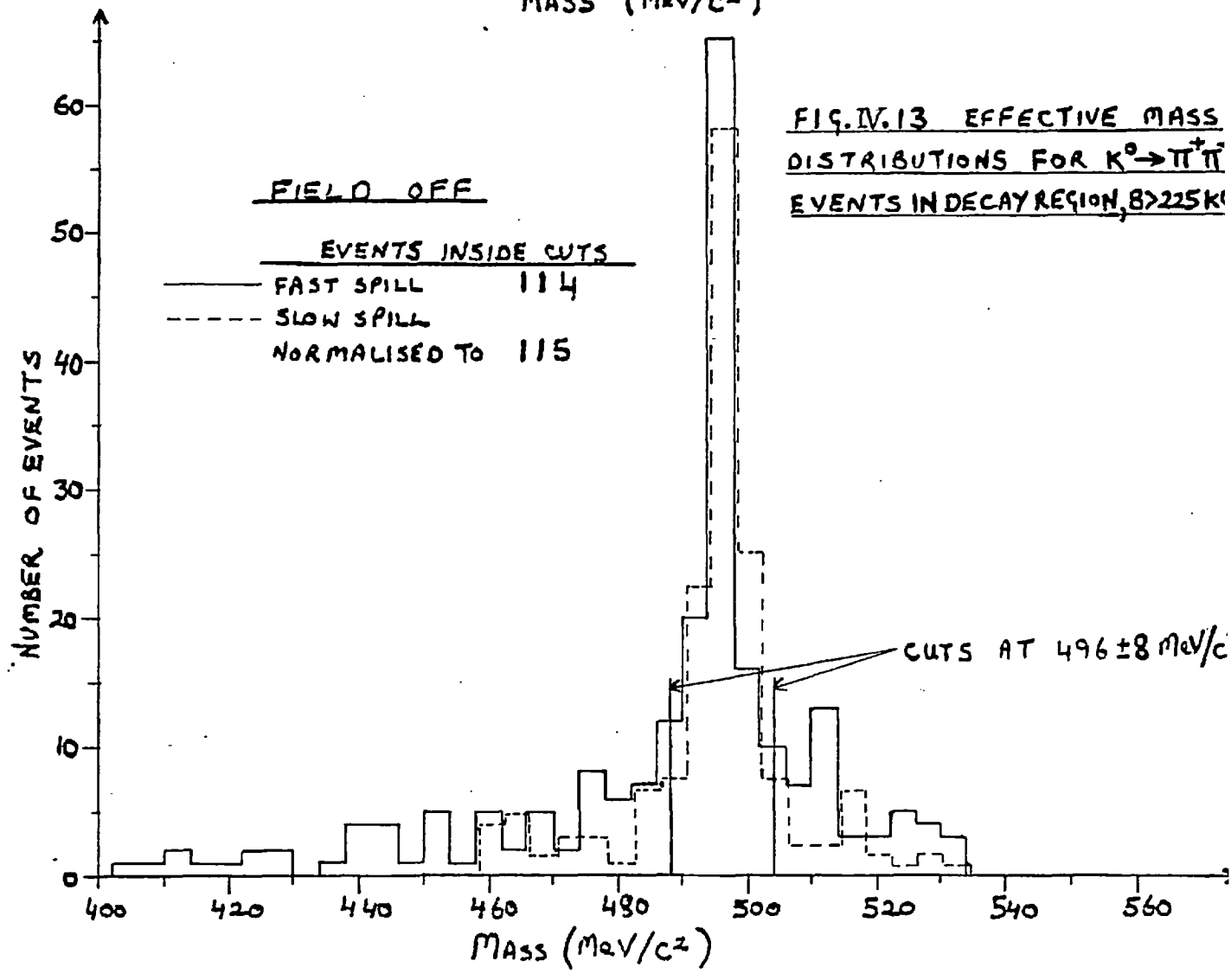

FIG. IV.13 EFFECTIVE MASS DISTRIBUTIONS FOR $K^0 \to \pi^+\pi^-$ EVENTS IN DECAY REGION, B>225 kG

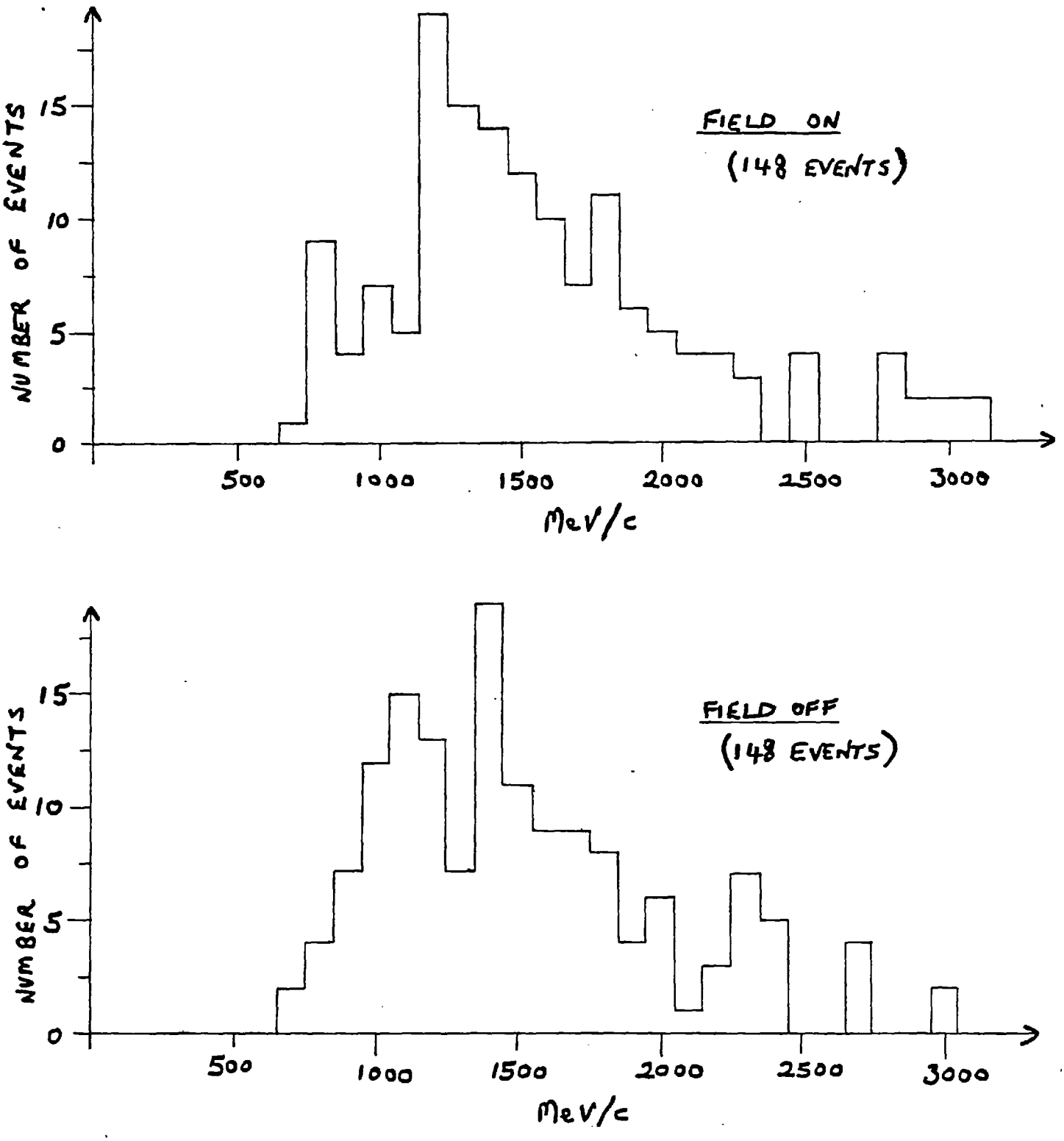

FIG. IV.14 $K^0 \rightarrow \pi^+ \pi^-$ MOMENTUM SPECTRA FOR ALL EVENTS IN THE DECAY REGION.

BEAM MONITOR

N1.N2 ∿ 40 COUNTS/FAST SPILL BURST

			EVENTS WRITTEN TO DISK WITH LOW P_T					
			'VEE' EVENTS		TOTAL 2 PI EVENTS		LEPTONICS	
	BEAM MONITOR	EVENT TRIGGERS	Z>0	Z<0	Z>0	Z<0	Z>0	Z<0
FIELD ON	$9.30 \cdot 10^6$	59.2^k	5407	2649	148	17	542	240
FIELD OFF	$9.26 \cdot 10^6$	59.2^k	5012	2973	148	46	511	225
SLOW SPILL	NORMALISED TO $9.30 \cdot 10^6$	27.8^k	6025	3526	259	61	596	254

TABLE IV.2 TOTAL EVENT RATES

	$K^o \to \pi^+\pi^-$ TOTAL EVENTS				LEPTONICS	
	B > 200kG		B > 225kG		B > 225kG	
	Z>0	Z<0	Z>0	Z<0	Z>0	Z<0
ON	135	16	116	14	473	210
OFF	131	43	114	37	438	197

TABLE IV.3 TOTAL $K^o \to \pi^+\pi^-$ RATES FOR B > 200kG AND B > 225kG

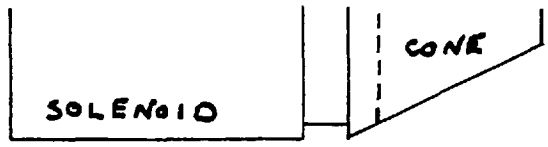

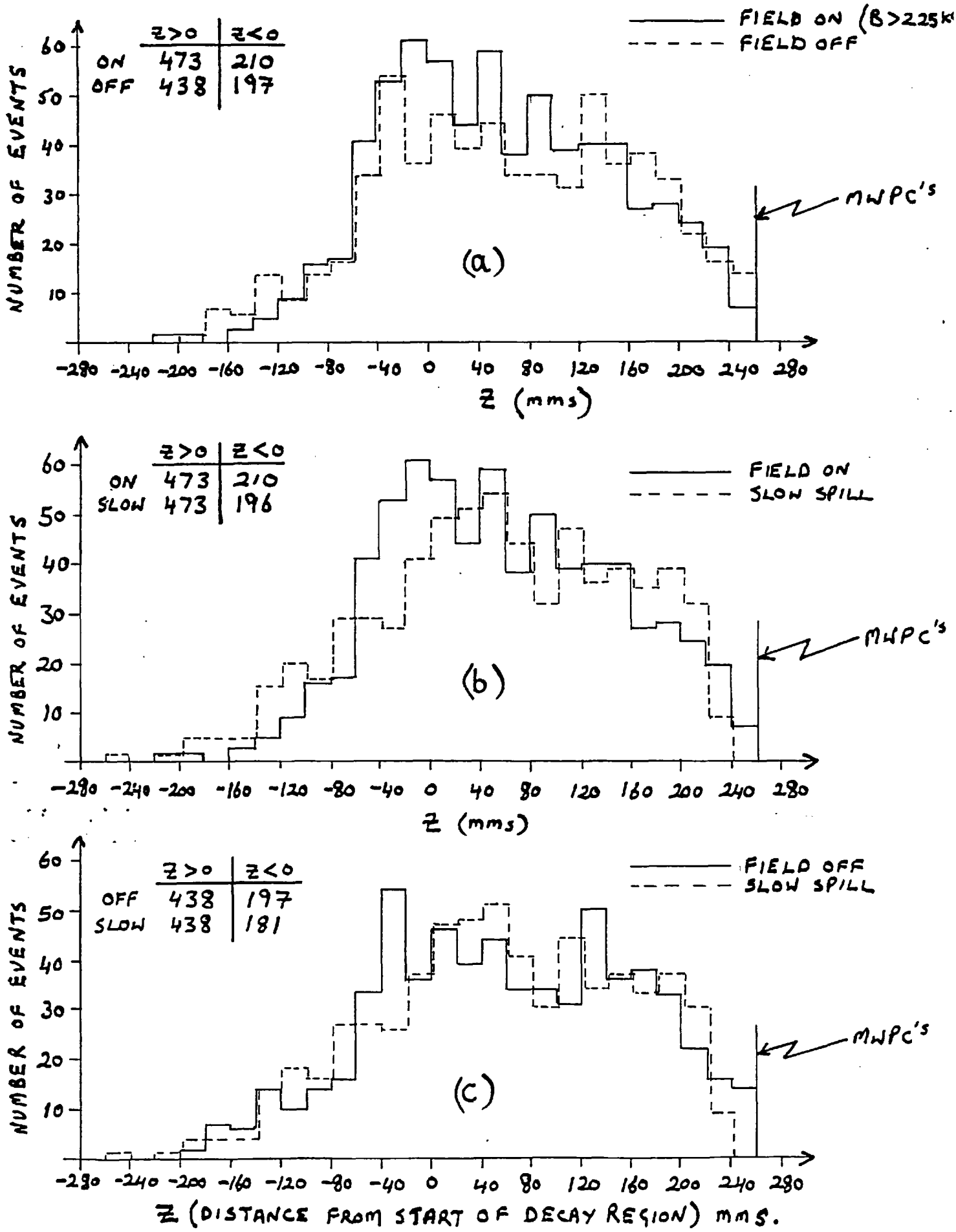

FIG. IV.15(a→c) HISTOGRAMS SHOWING LEPTONIC DECAYS ALONG Z FOR B > 225 KG

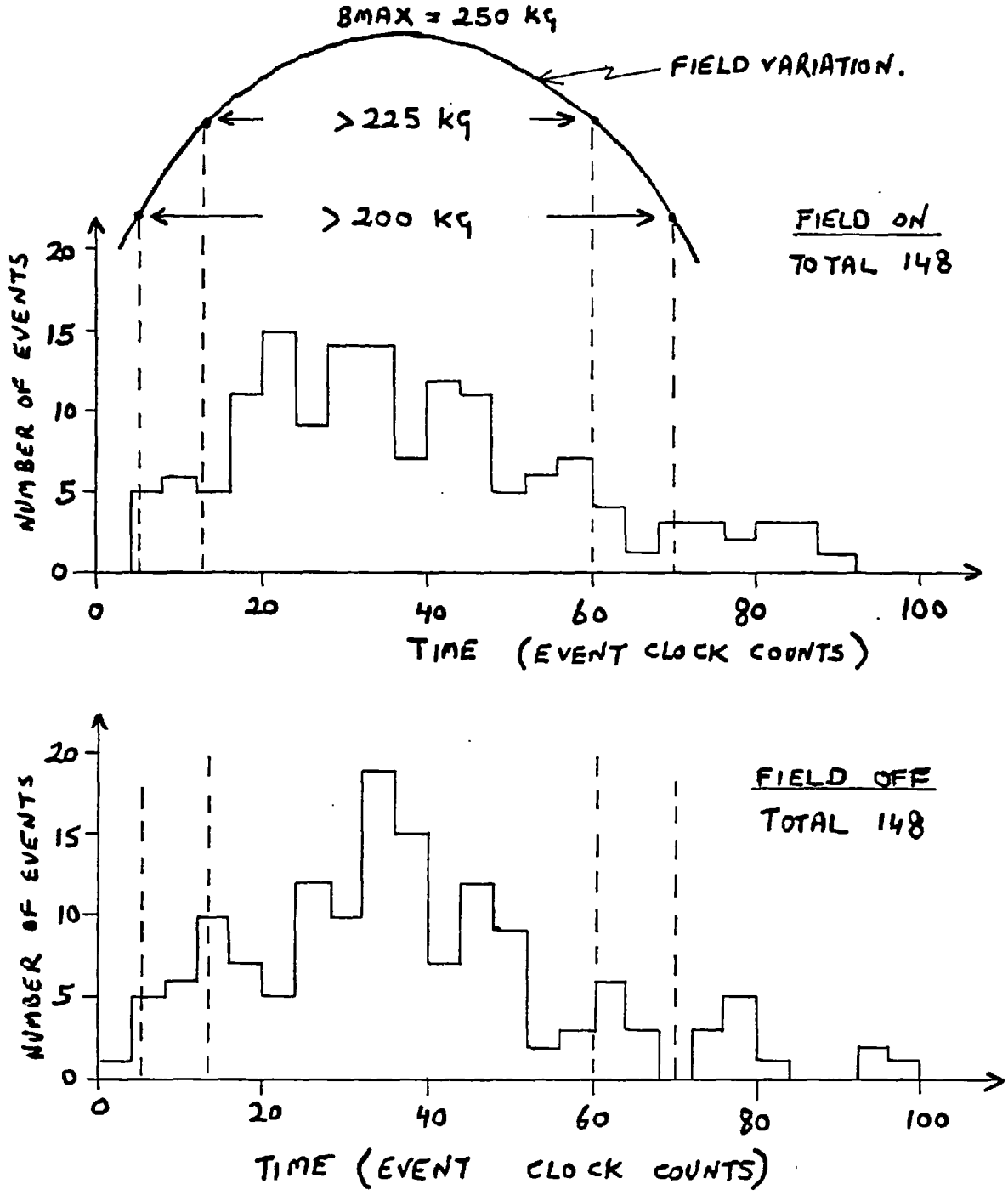

FIG. IV.16 K^0 EVENT TIMES WITH CUTS FOR FIELD.

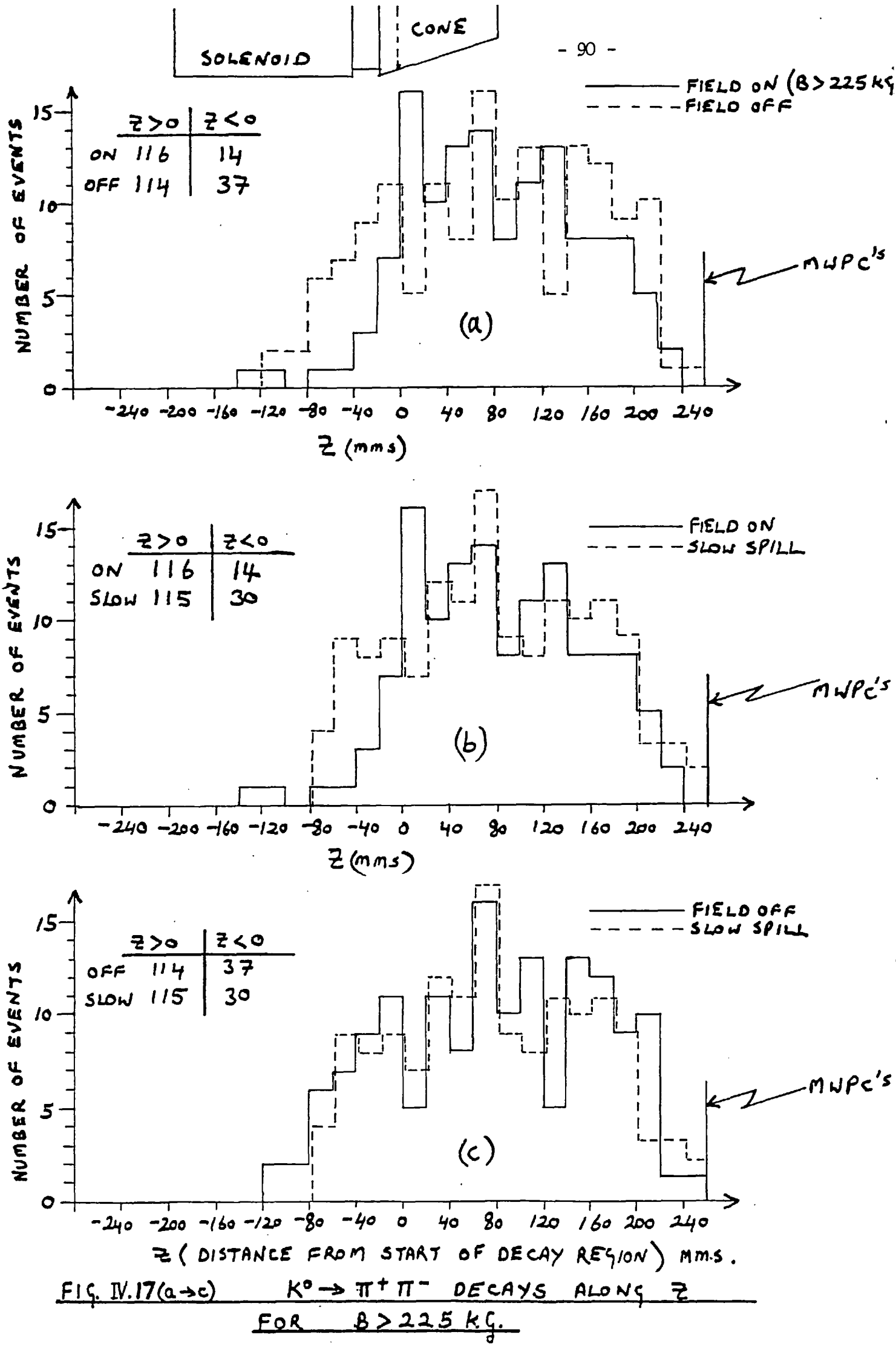

FIG. IV.17(a→c) $K^0 \rightarrow \pi^+\pi^-$ DECAYS ALONG Z FOR B > 225 kG.

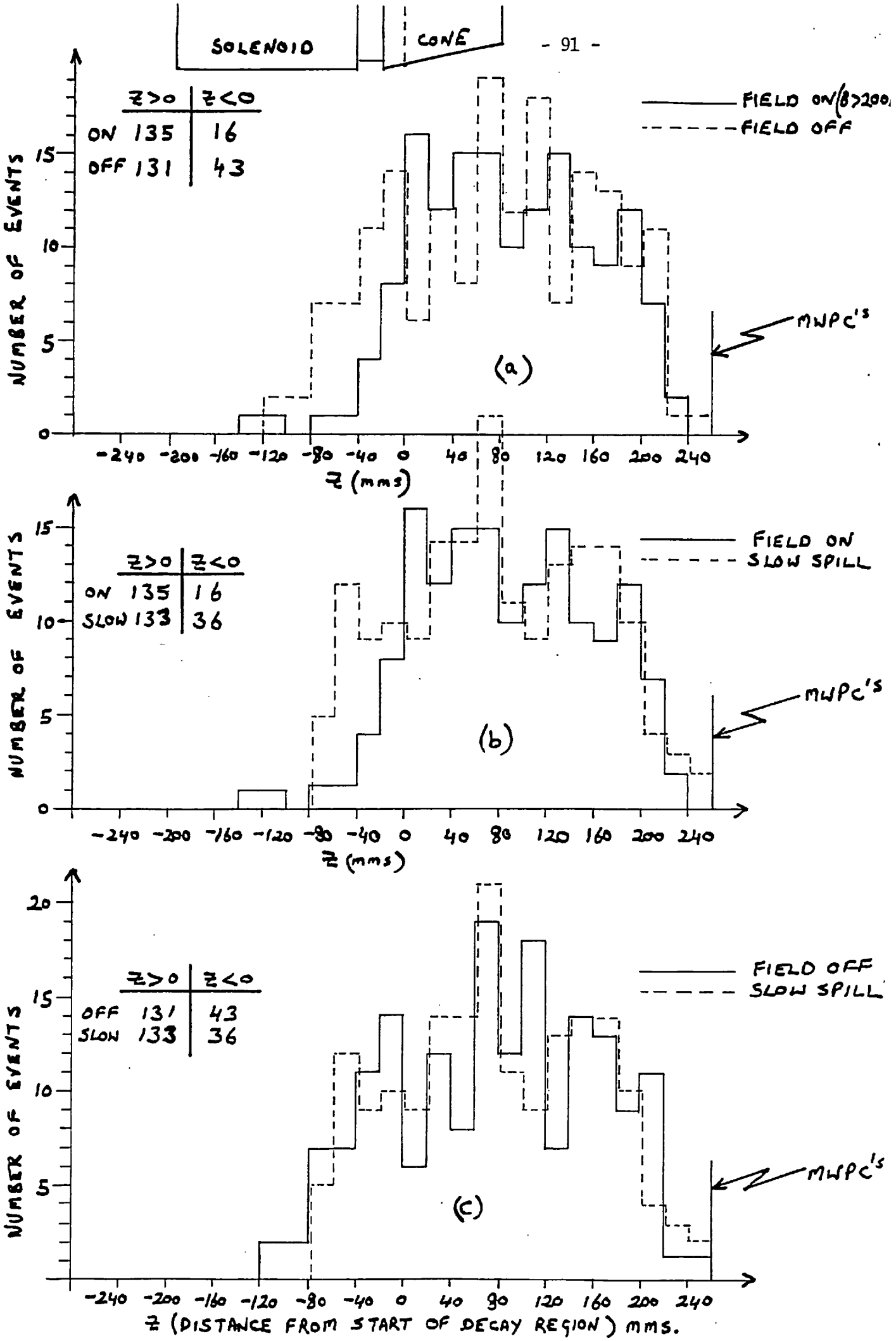

FIG IV.18 (a→c) $K^0 \to \pi^+\pi^-$ DECAYS ALONG z FOR B > 200 kG.

CHAPTER V

RESULTS

V.1 Statistical Comparisons

The $\pi^+\pi^-$ invariant mass distributions for field on (B > 225 kG) and field off events are shown in Figure V.1. Apart from the broadening at the base of the mass peaks, discussed in Section IV.4, the two spectra look very similar. There is no diminution of the K^o signal with the field on which is in contrast to the effect expected if the experiment were above the critical field.

Figure V.2(a) shows the $K^o \to \pi^+\pi^-$ decay point distributions for events with B > 225 kG. 116 events were found in the decay region with the field on compared to 114 with the field off, which further suggests that we were not above the critical field. The hypothesis that the field on and field off decay point distributions are two samples drawn from the same distribution gives a χ^2 of 15.1 for 12 degrees of freedom (from the 12 bins, each 20 mms. wide, making up the decay region). This corresponds to a confidence level of 0.25. Figure V.2(b) shows the decay point distribution for the 135 events with B > 200 kG. A comparison of this distribution to the 131 events from the field off gives a χ^2 of 14.5 for the above hypothesis, corresponding to a confidence level of 0.3.

To make statistical comparisons of the hypotheses that we were below or above the critical field the procedure was as follows. We assumed a high field region 100 mm. long, as in Section I.3,

with the interference region starting 50 mms. downstream from the centre of the solenoid. From the measured decay position and momentum for each event, we calculated the proper time, t, from the start of the interference region before decay. From this the intensity expectation, the quantity I(p,d) of equation I.7, was calculated. Events were then grouped in bins of I, with values ranging from 0.3 for low momentum decays very close to Z=0, to 1.1 for similar decays towards the end of the decay region (see Fig. I.1). A bin width of 0.1 was chosen, giving 8 values of I at which the number of events with field off could be compared to the number with field on.

The I(p,d) distribution for field on (B > 225 kG) is shown in Figure V.3(a) together with the slow spill (control) distribution normalised to 115 events. The two distributions are very similar, except for a slight excess at I = 0.35 for field on events. The field off I(p,d) distribution is shown in Figure V.3(b) and follows the slow spill well except for a drop at $\sim$ I = 0.45 which reflects the fall in the number of events from Z = 0 to Z = 20 noted in Section IV.4. Similar distributions for B > 200 kG are shown in Figure V.4.

The field on and field off I(p,d) distributions were used to test two hypotheses; one that there was no effect, the other that the effect suggested by Salam and Strathdee was present and that the resulting 2π distribution was given correctly by equation I.7 based on the superweak theory. If the latter hypothesis is correct, the number of events in each I(p,d) bin should be $I_i N_i$ where I_i is the intensity expectation for bin i and N_i is the number of events found from the field off data. Thus the chisquared for no effect is given by

$$\chi^2 = \sum_{i=1,8} \frac{(M_i - N_i)^2}{M_i + N_i}$$

where M_i is the number of field on events in bin i, and the chisquared for the hypothesis that there is an effect, is given by

$$\chi^2 = \sum_{i=1,8} \frac{(M_i - I_i N_i)^2}{M_i + I_i^2 N_i} \quad .$$

After making the leptonic background subtraction of 15% discussed in Section IV.5 to the number of events in each bin, the first hypothesis, for no effect, gave a χ^2 of 8.6 for B > 225 kG. This is reasonable for 8 degrees of freedom whereas the second hypothesis gave a χ^2 of 21.5. The probability for a χ^2 as large as this is only 0.6%. For B > 200 kG, the first hypothesis gave a χ^2 of 9.6 whereas the second gave a χ^2 of 23, the probability for this being only 0.3%. These results are summarized in Table V.1. They show that we were almost certainly not above the critical field required to restore CP symmetry. Over the 100 mms. that were taken to be the high field region, the field drops by about 90% from its value at the centre of the solenoid (see Figure III.8). We conclude therefore that the critical field must be above 21 Tesla.

The field on and field off I(p,d) distributions are shown together in Figure V.5(a) while the field on and expected I(p,d) distribution (for an effect) are shown together in Figure V.5(b), for B > 225 kG. Plots for B > 200 kG are shown in Figure V.6.

The plots show the importance of data at low values of I(p,d) for determining whether an effect was present or not. Although it might have been good to start looking at $K^o \to \pi^+\pi^-$ decays further away from the fringe field, the loss of discriminative power becomes significant. An analysis of the data with cuts for events $\geqslant$ 20 mms. beyond the start of the decay region reduced the statistics for low I(p,d) values giving an 18% probability of an effect for B > 225 kG, and an 11% probability of an effect for B > 200 kG. These results are also shown in Table V.1 and the corresponding I(p,d) distributions for Z $\geqslant$ 20 mms. shown in Figures V.7 and V.8 for B > 225 kG and B > 200 kG respectively.

Finally, to show that a significant drop in the number of events was actually expected if there were an effect, the I(p,d) spectra were integrated from I = 0.3 in steps up to I = 1.1. The results are listed in Table V.2 and the integrated spectra shown in Figure V.9 for B > 225 kG. The slow spill data is also shown normalised to the data received for field on and field off. For Z $\geqslant$ 0 a total of 99 events were found with the field on (after making the 15% background subtraction) against 69 expected for an effect, a difference of 3 std' dev'. For Z $\geqslant$ 20, with less statistics, 85 events were found with field on against 68 expected for an effect which gives $\sim$ 2 std' dev'. For B > 200 kG, Figure V.10, from Z = 0 115 events were found with the field on against 79 expected with an effect, a difference of $3\frac{1}{2}$ std' dev'. From Z $\geqslant$ 20 the difference in the totals is $\sim$ 2 std' dev'. These results support the earlier conclusions, with the χ^2 tests, that we were not above the critical field.

V.2 Conclusions

If Salam and Strathdee are correct in their hypothesis that in a sufficiently high magnetic field CP violation would disappear, the result of our experiment shows that the transition field is almost certainly above 21 Tesla.

The experiment was carried out at the limits of pulsed magnet technology with magnetic fields which were probably well below those required to restore CP symmetry, since fields in the 10^6 gauss range have been quoted as plausible lower limits [4]. However recent work by Chikazumi et al. has produced fields in the megagauss region using non-explosive methods of flux compression[17]. If this work continues to progress then the technique could be used for a further attempt to restore CP symmetry to the K_L^o.

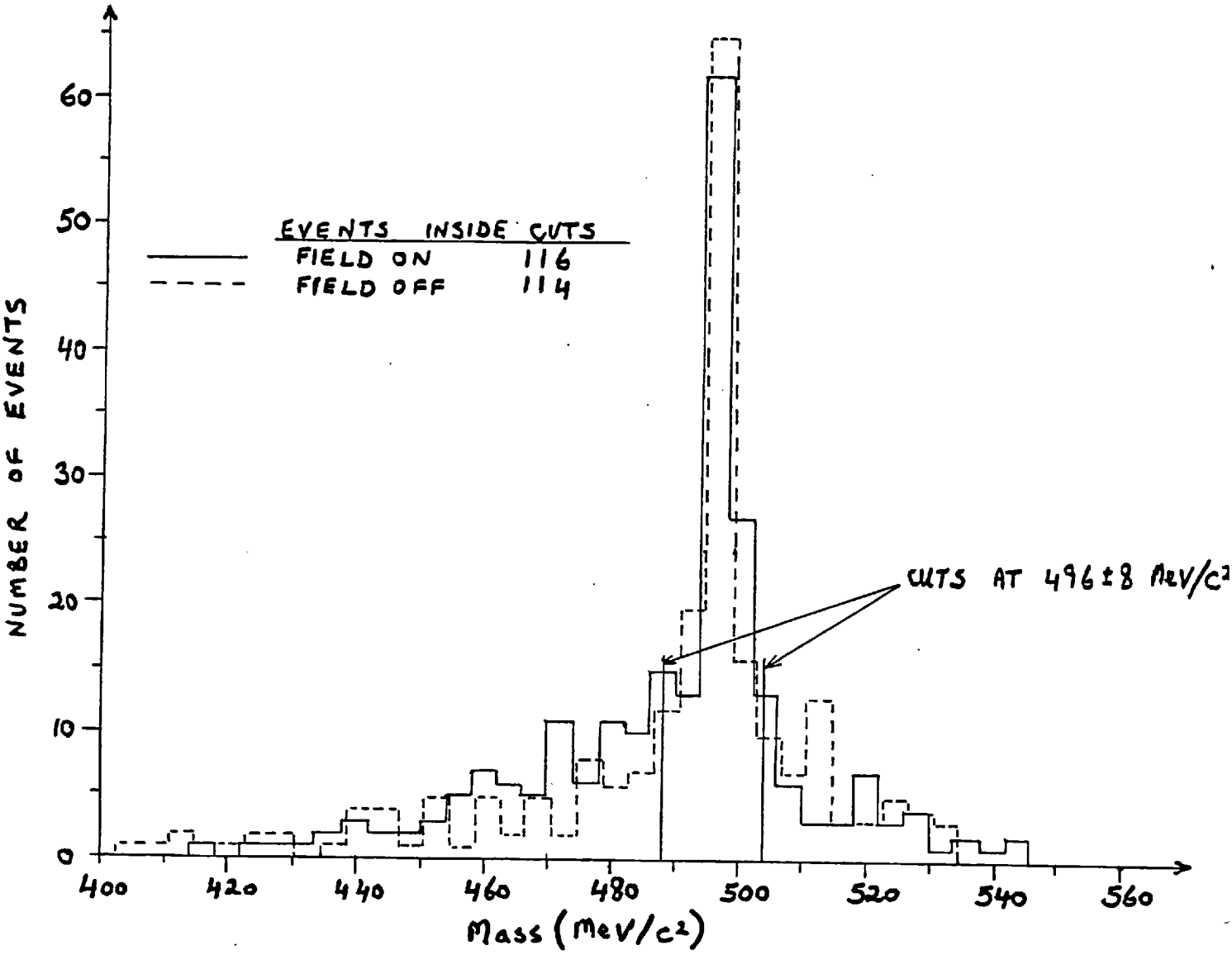

FIG. V.1. EFFECTIVE MASS DISTRIBUTIONS FOR $K^0 \rightarrow \pi^+ \pi^-$ EVENTS IN DECAY REGION, B > 225 KG.

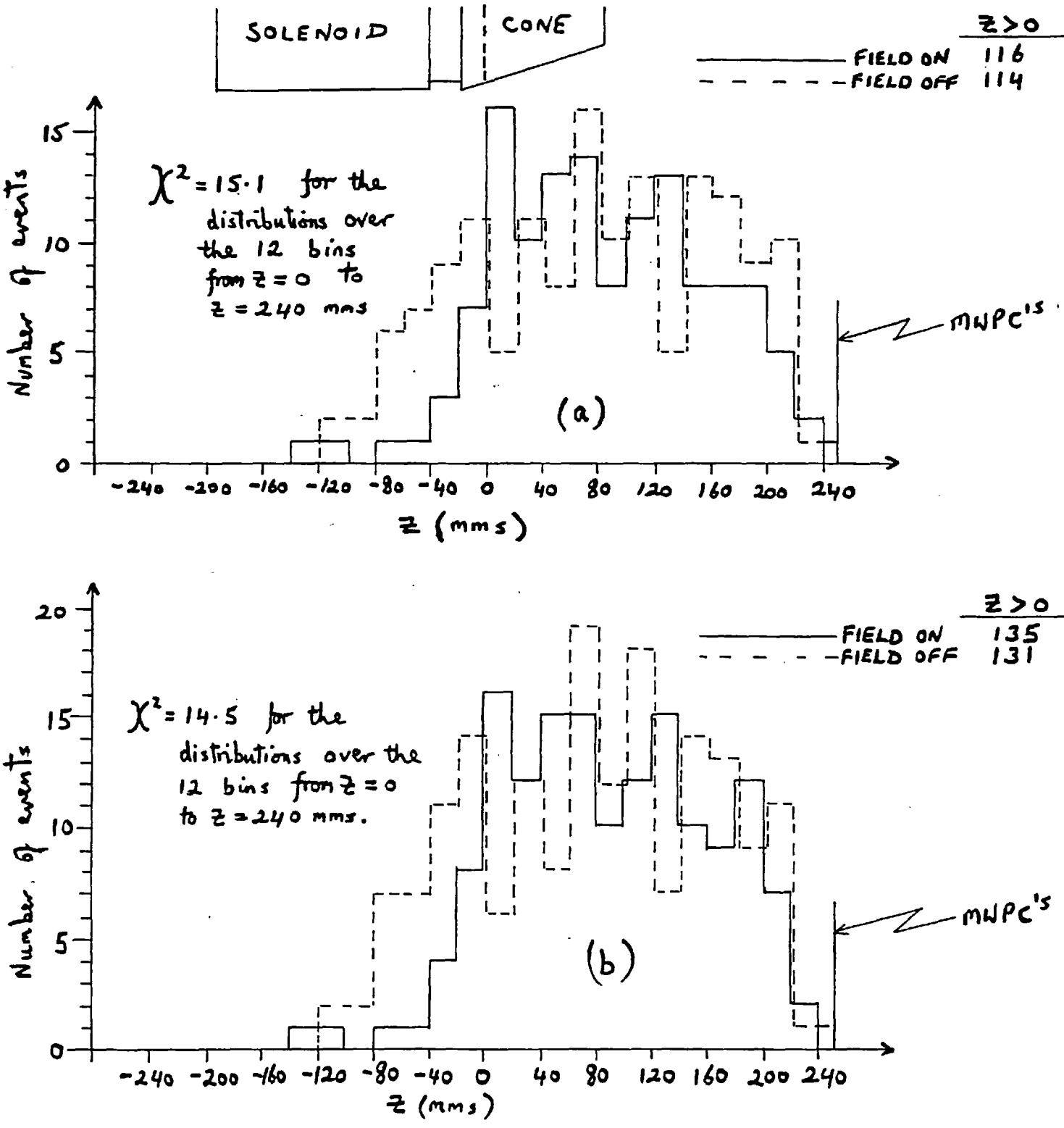

FIG. V.2 (a) and (b). $K^0 \to \pi^+ \pi^-$ DECAYS ALONG z FOR B > 225 KG AND B > 200 KG RESPECTIVELY

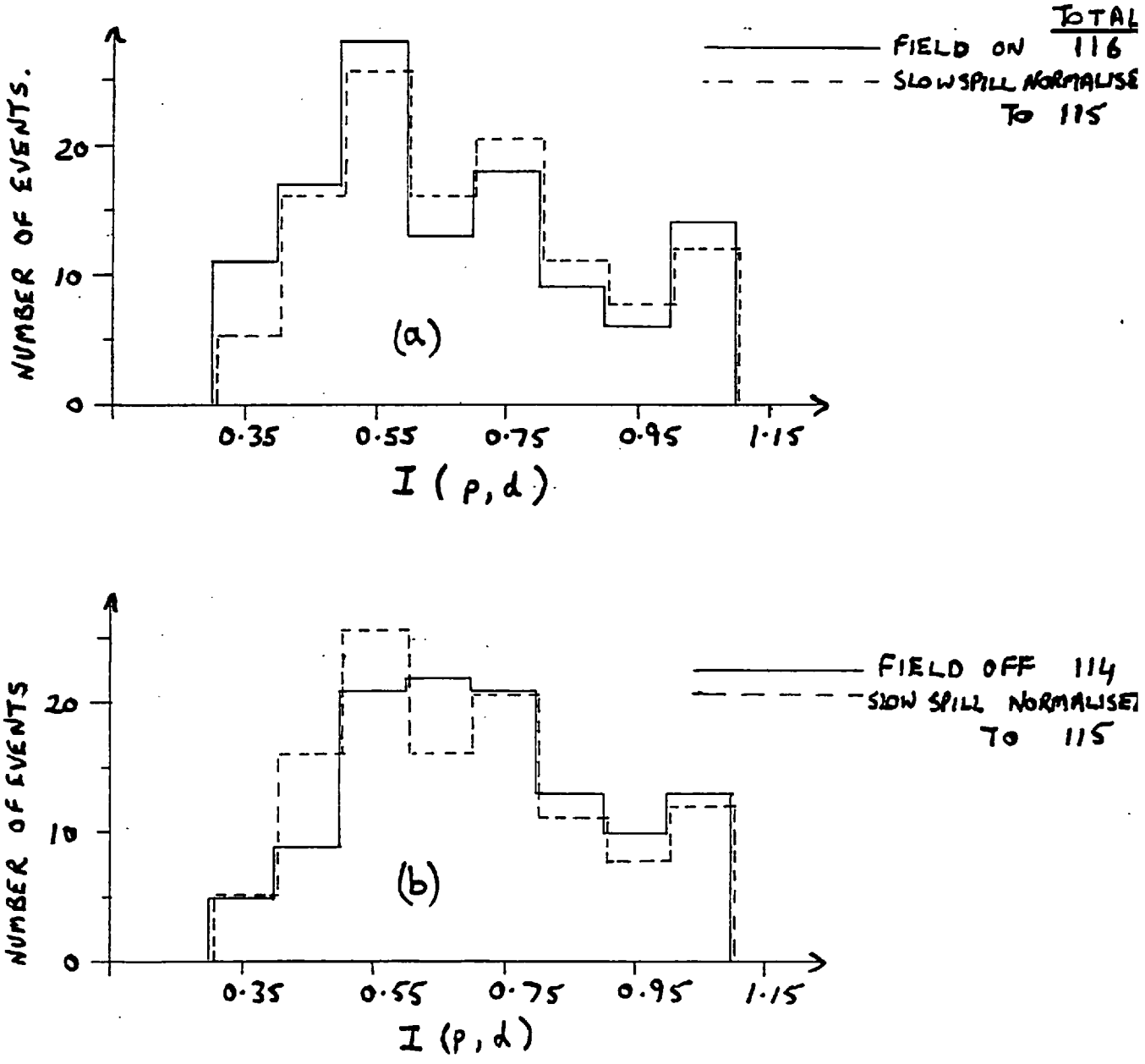

FIG. V·3 (a) and (b). I(p, d) DISTRIBUTIONS FOR FIELD ON AND FIELD OFF RESPECTIVELY, B>225 kg.

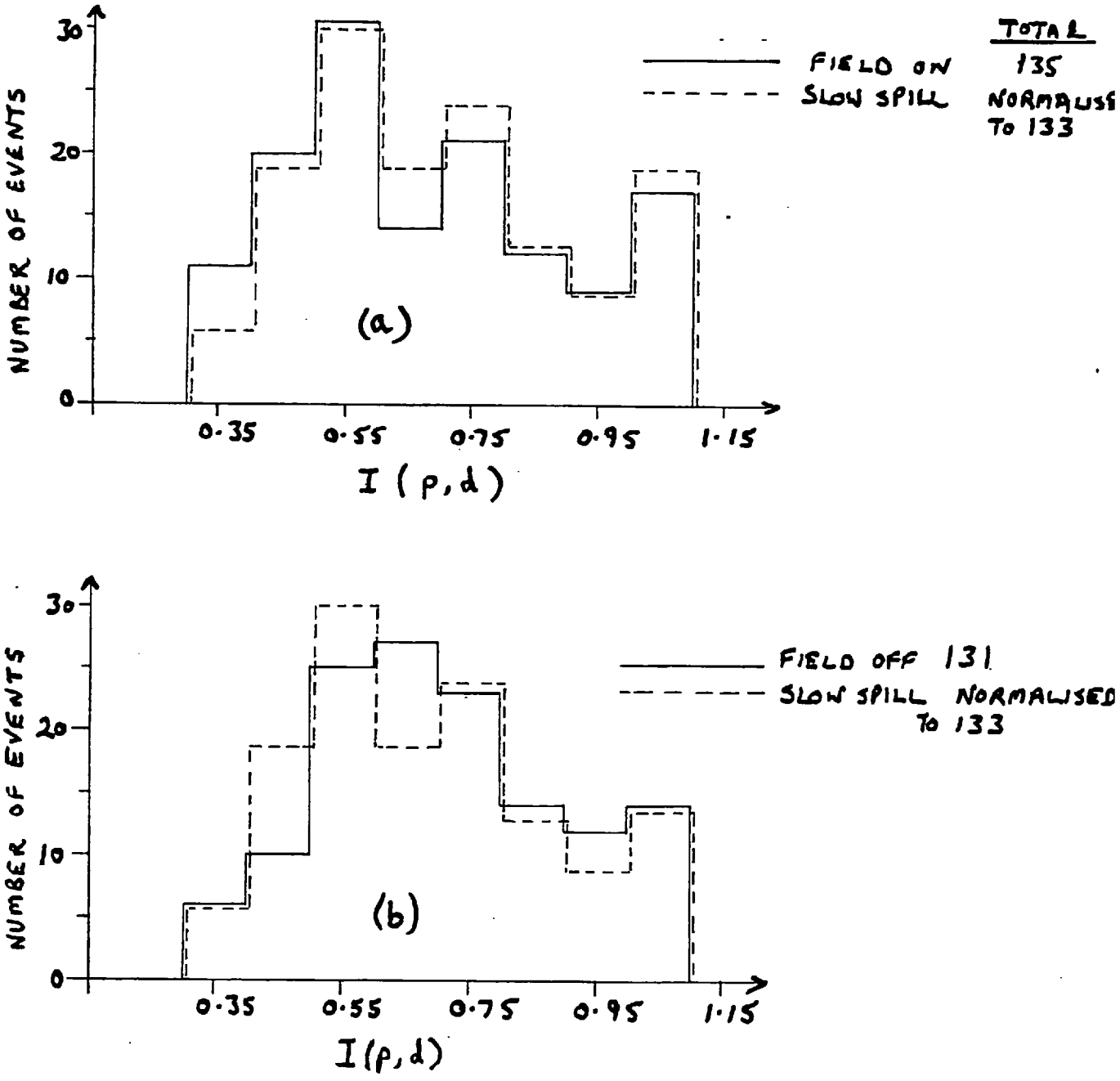

FIG. V·4 (a) and (b). I(p, d) DISTRIBUTIONS FOR FIELD ON AND FIED OFF RESPECTIVELY, B > 200 Kg.

	TOTAL EVENTS	CHISQUARE		CONFIDENCE LEVEL	
		NO EFFECT	EFFECT	NO EFFECT	EFFECT
B > 225 kG	ON 99 OFF 97	8.55	21.51	0.38	0.006
B > 200 kG	ON 115 OFF 111	9.63	23.02	0.29	0.003
B > 225 kG from Z= 20mm	ON 85 OFF 93	5.29	11.35	0.73	0.18
B > 200 kG from Z=20 mm	ON 101 OFF 106	6.74	13.10	0.56	0.11

TABLE V.1

RESULTS OF THE I(p,d) HISTOGRAM

COMPARISONS

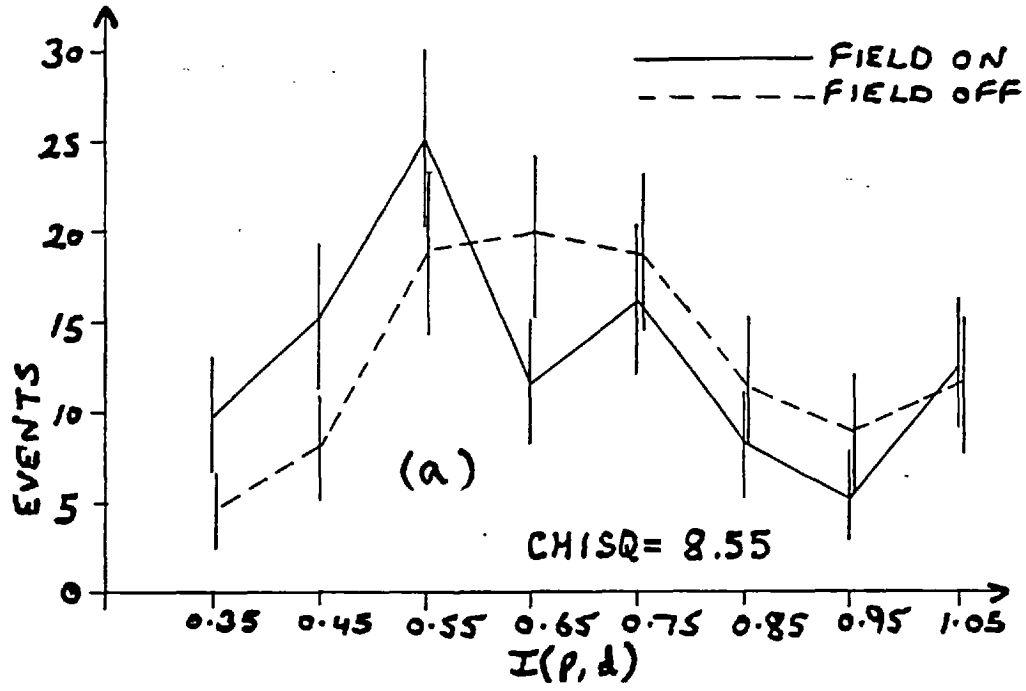

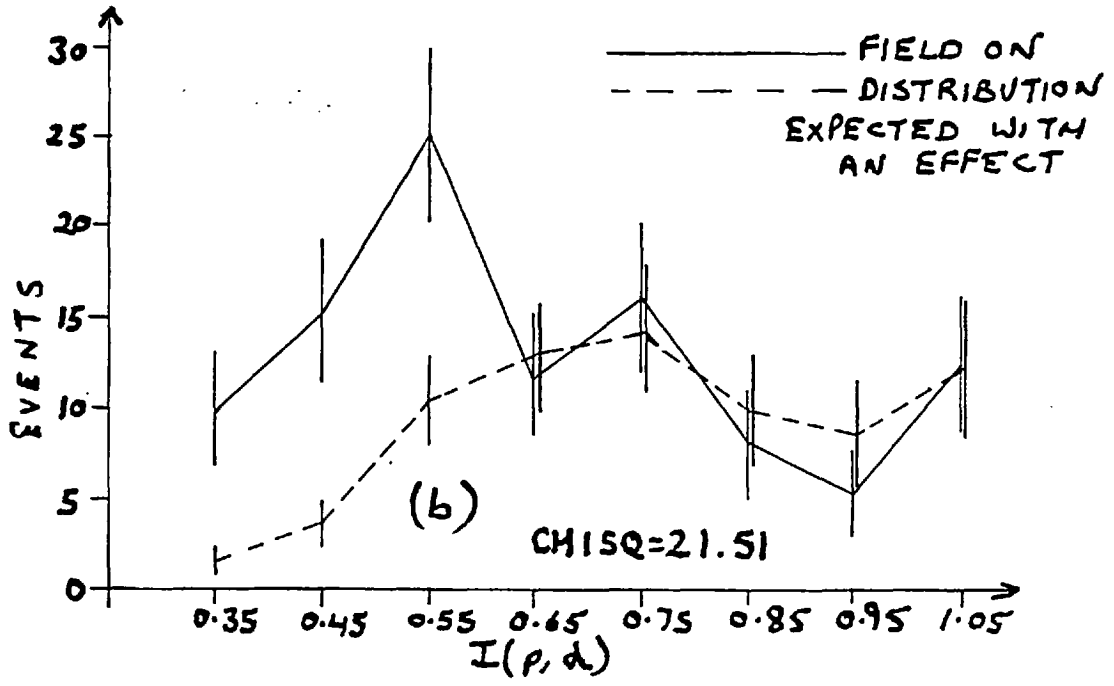

FIG. V·5 (a) and (b). $I(\rho, d)$ COMPARISONS BETWEEN FIELD ON / FIELD OFF AND FIELD ON / EXPECTED, $B > 22.5$ KG

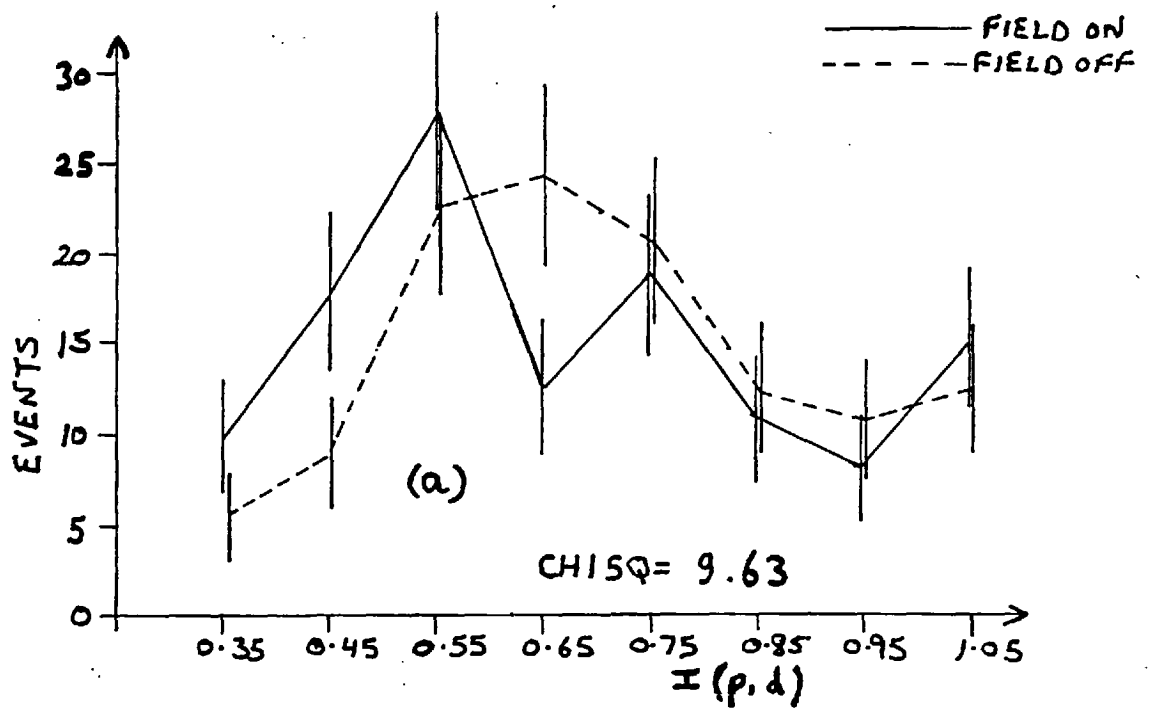

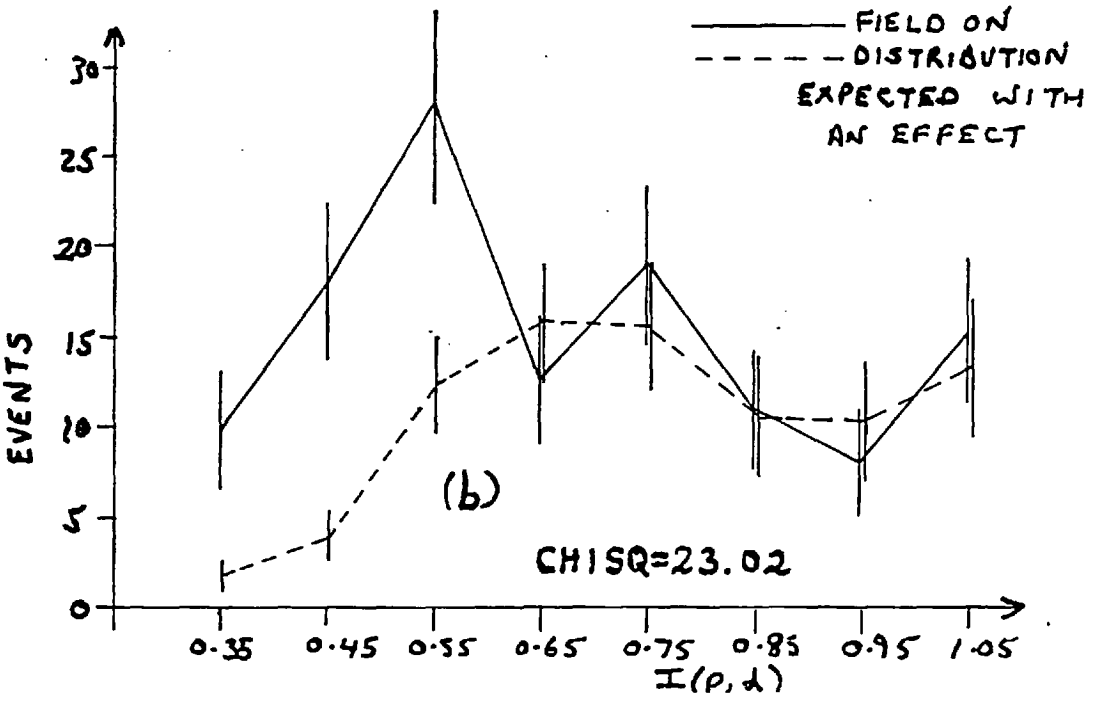

FIG. V·6 (a) and (b). I(p,d) COMPARISONS BETWEEN FIELD ON/FIELD OFF AND FIELD ON/EXPECTED, B > 200 KG.

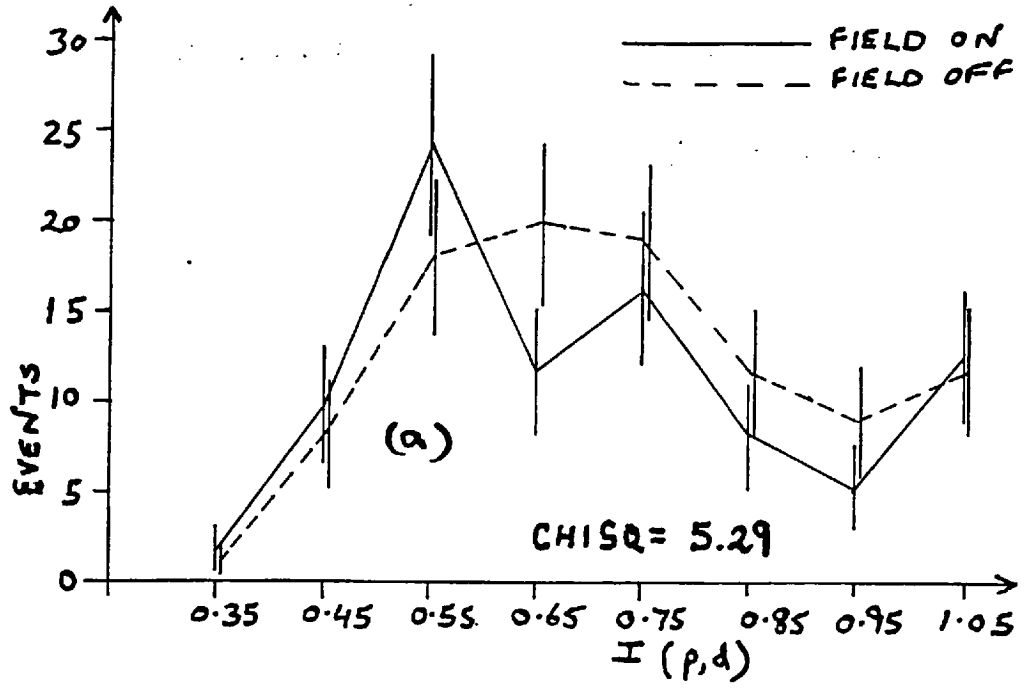

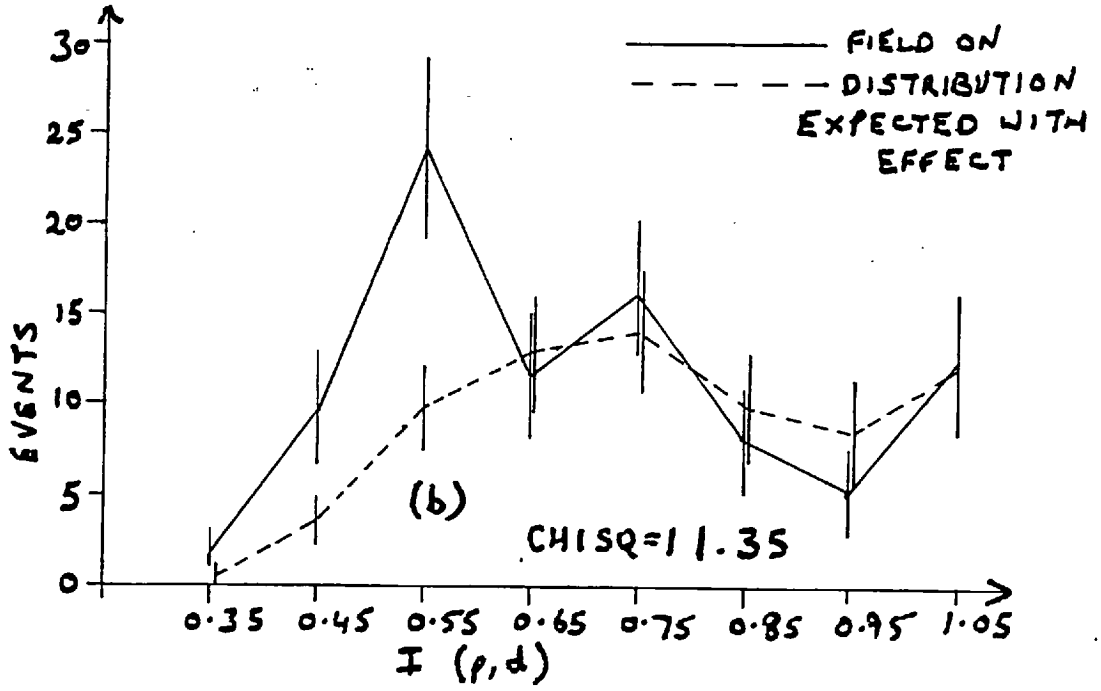

FIG. V·7 (a) and (b) $I(\rho, d)$ comparisons, for events with $z \geq 20$ mms, between FIELD ON/FIELD OFF AND FIELD ON/EXPECTED, $B > 225$ kg.

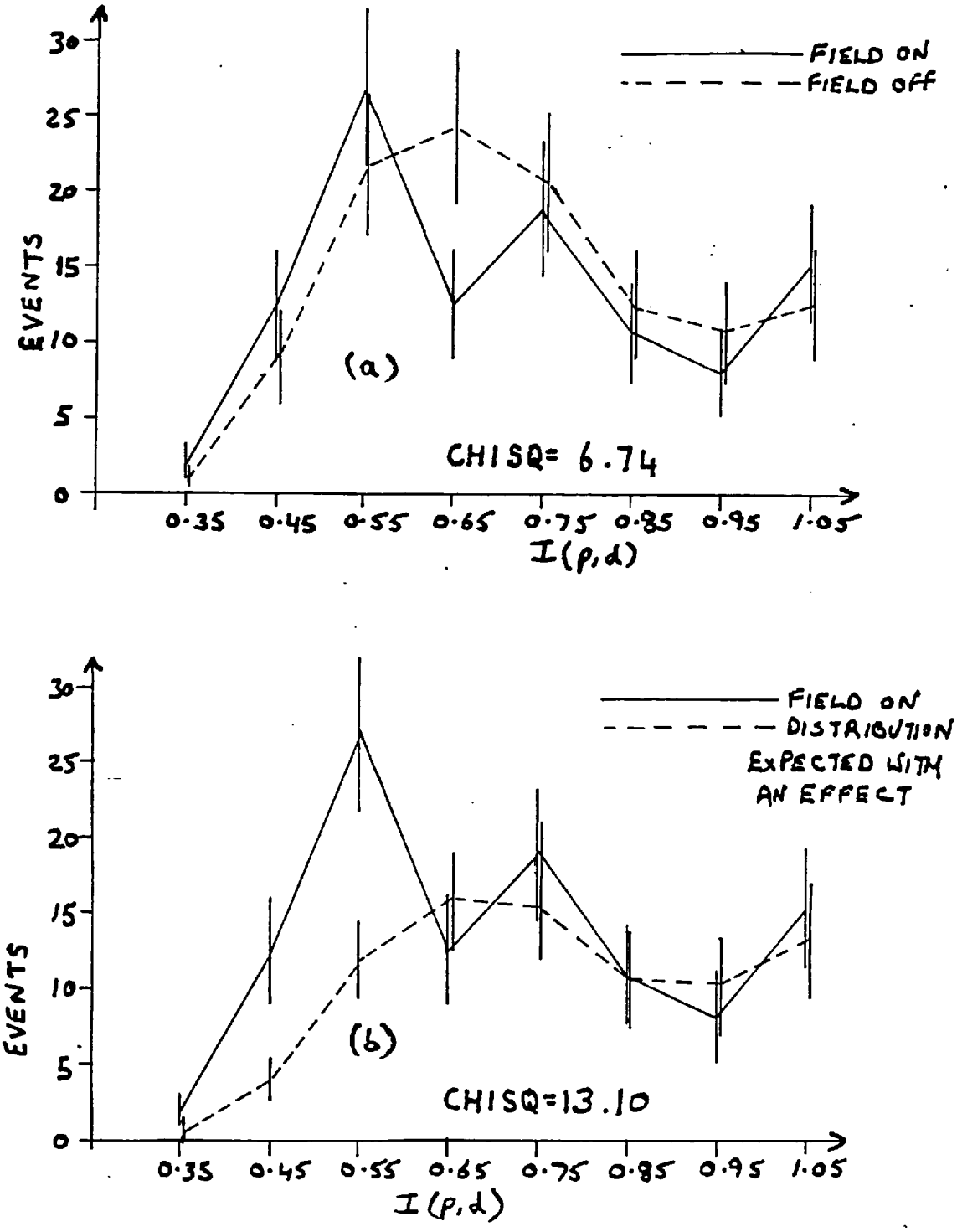

FIG. V.8 (a) and (b) $I(\rho,d)$ COMPARISONS, FOR EVENTS WITH $z \geq 20$ mms, BETWEEN FIELD ON/FIELD OFF AND FIELD ON/EXPECTED RESPECTIVELY, $B > 200$ KG.

	I (p,d)							TOTAL
	0.35	0.45	0.55	0.65	0.75	0.85	0.95	1.05
B > 225kG ON Z > 0mm	9	24	48	59	74	82	87	99
OFF	4	12	30	48	66	77	86	97
'EXPECTED'	2	5	14	27	40	49	58	69
B > 225kG ON Z > 20mm	2	11	34	45	60	68	73	85
OFF	1	9	26	44	62	73	82	93
'EXPECTED'	0	3	13	26	38	48	56	68
B > 200kG ON Z > 0mm	9	26	53	65	82	93	100	115
OFF	5	14	35	58	77	89	99	111
'EXPECTED'	2	6	17	34	47	57	66	79
B > 200kG ON Z > 20mm	2	14	39	51	69	79	87	101
OFF	1	9	30	53	72	84	94	106
'EXPECTED'	0	4	15	31	45	55	65	77

TABLE V.2 INTEGRATION OF I(p,d) SPECTRA

STARTING FROM 0.35, FOR B > 225kG AND B > 200kG

INTEGRATING UP TO I(p,d) = 1.05 GIVES TOTAL NUMBER OF EVENTS.

'EXPECTED' NUMBER , IF THE FIELD RESTORED CP SYMMETRY ,

CALCULATED FROM FIELD OFF DATA.

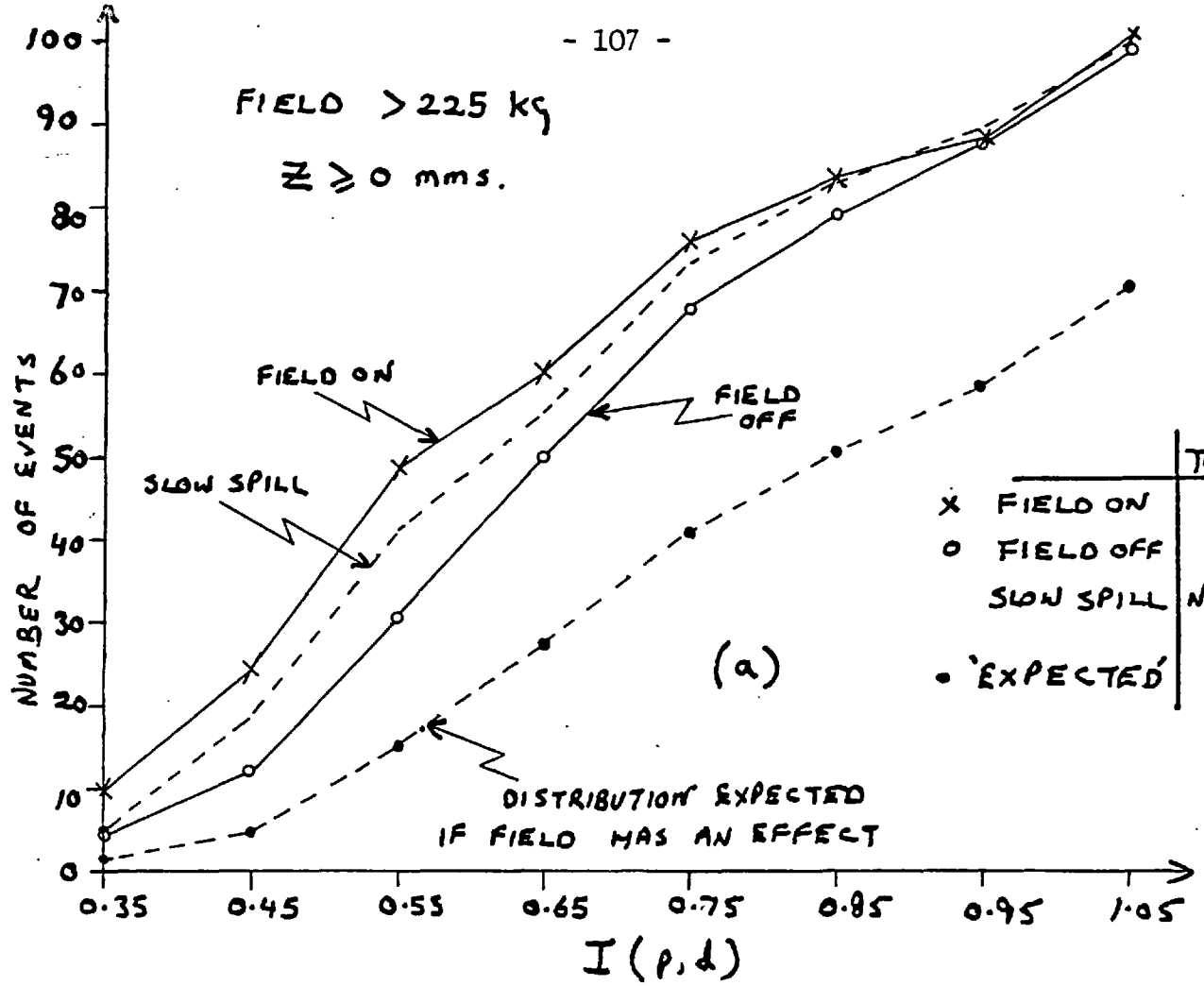

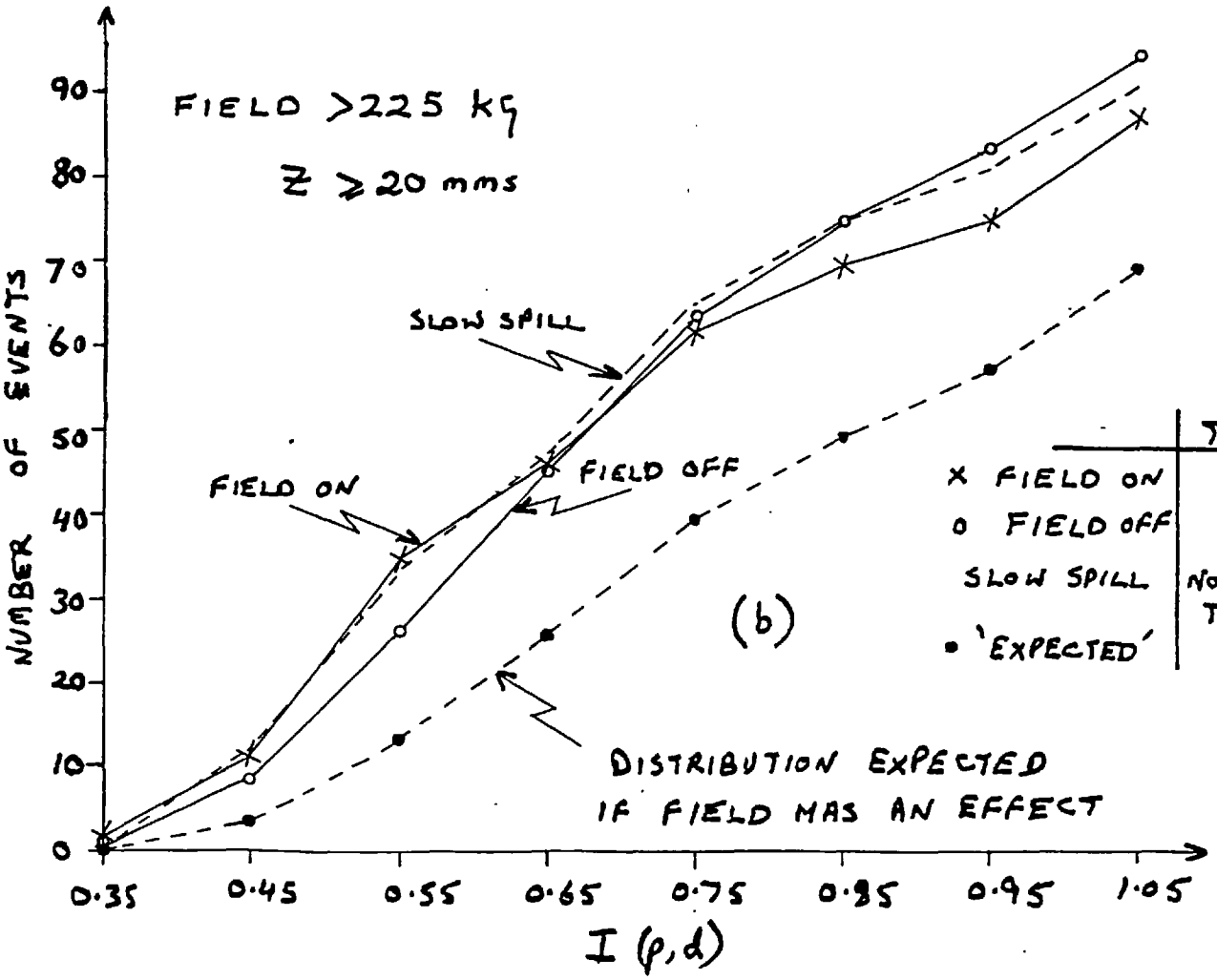

FIG. V.9 (a,b) INTEGRATED SPECTRA FOR B > 225 kg.

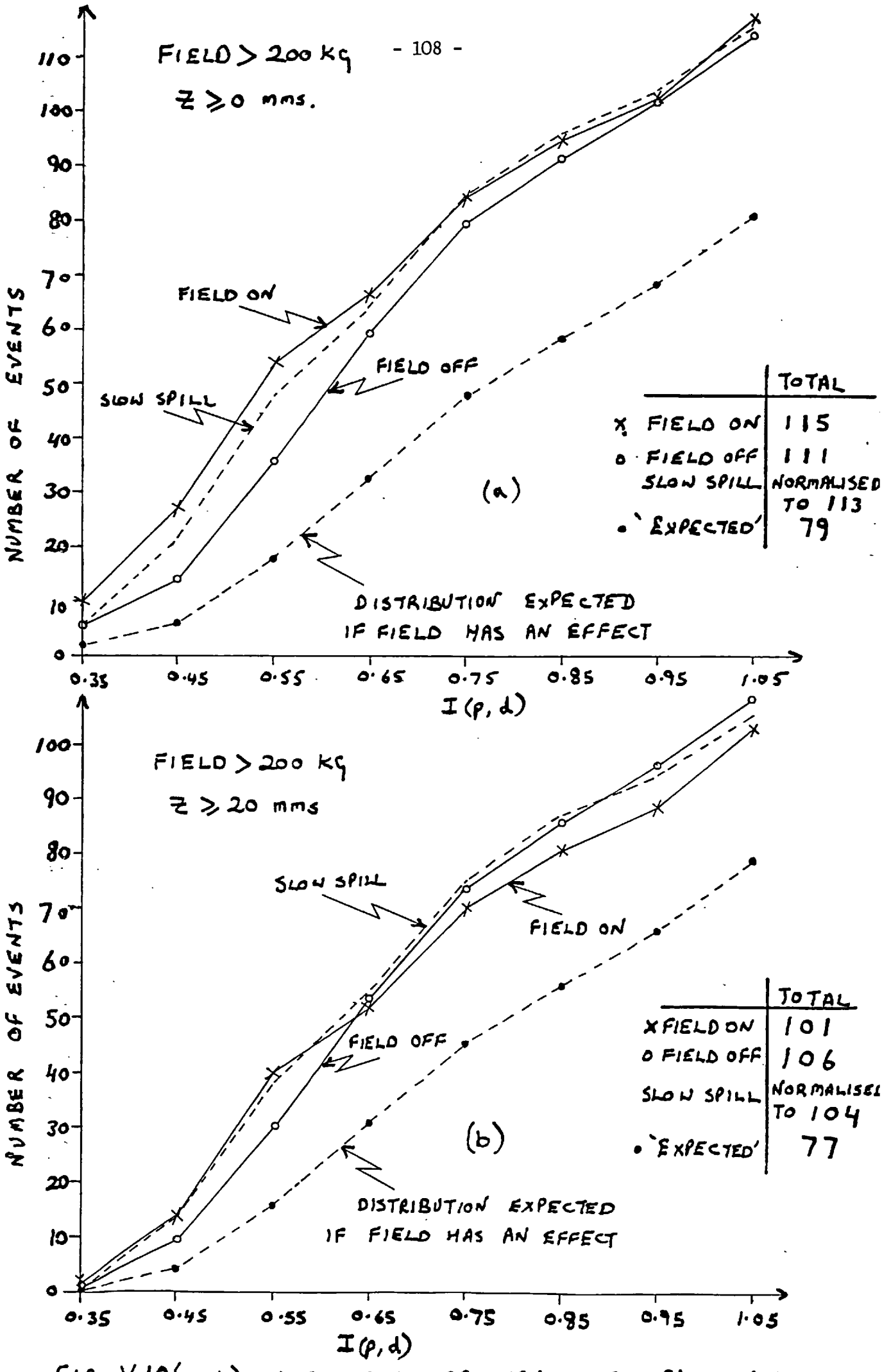

FIG. V.10(a,b) INTEGRATED SPECTRA FOR B>200 KG.

References

1. Abers and Lee, Physics Reports 9C No. 1 p.1 - 141.
2. S. Weinberg, Physical Review 9D , 3357.
3. Kirzhnits and Linde , Physics Letters 42B , 471.
4. Salam and Strathdee, Nature 252 , p.569 , 1974; and also Salam and Strathdee, Nuclear Physics B90 (1975) p. 203 - 220 for the computation of the "loop" graphs involved in estimating the magnetic fields.
5. Bugadov et al., Physical Review D2 , 815, 1970.
6. Suranyi and Hedinger, Physics Letters 56B , 151.
7. Hagberg et al., Nuclear Physics A313 (1979) 276 - 282.
8. Audus et al., Nuovo Cimento 46, 1966.
9. F. Atchison of the Rutherford Laboratory, Oxon, did essentially all the initial estimates of beam flux.
10. The solenoid was initially 10 metres from the target but high radiation background from the X3X beam line forced the experiment to move downstream by 5.5 metres after the K^+ flux measurements.
11. Breskin et al., Nuclear Instruments and Methods, 124 (1975) 189 - 214.
12. This is described further in a paper by Binnie et al. presented to the 6th International Conference on Magnet Technology, Bratislava, August 1977, by R.T. Elliot of the Rutherford Laboratory.

cont.....

13. H. Wind, Momentum analysis by using a quintic spline model for the track, CERN, NP - DHG 73/5.

14. J. Steinberger, K^0 Decay and CP Violation, CERN 70 - 1.

15. Charpak and Gourdin, The K^0 $\bar{K}^0$ system, CERN 67 - 18.

16. J.-M. Gaillard et al., Physical Review Letters vol. 18, p 20, 1967.

17. Chikazumi et al., IEEE Transactions on Magnetics, vol. 14, p 577, No. 5, September 1978.

Acknowledgements

I would like to thank the following:

In particular my supervisor Dr W.G. Jones and my Group Leader Dr D.M. Binnie for all their help and encouragement throughout the experiment. Their assistance has contributed much to the thesis and to my time at Imperial College.

R.T. Elliot, W.M. Evans and P. Flower of the Rutherford Laboratory and Dr J. Carr and D.G. Miller of Imperial College for the tremendous work they accomplished on the solenoid and to whom much credit is due for the success of the experiment.

Dr A. Maki for the considerable work he put into the analysis programme and for the many enjoyable discussions we had during the experiment.

My collaborators Dr T.C. Bacon, Dr D. Quarrie, Dr D. Jones, Dr N.C. Debenham, J. Hiddleston, R. English and W. Razey for the running of the experiment and R. Hobbs and D. Scholes for the machining of the solenoid.

Professor I. Butterworth for the opportunity of working for the High Energy Nuclear Physics Group at Imperial College.

The Science Research Council for their support during the three years of my research and the staff of the Rutherford Laboratory, particularly at the Cosenor's House, for their hospitality during the experiment.

Finally Ms Linda Gold for her excellent typing of this thesis.